ISSN 0038-531X

Russian Original Vol. 54, No. 5, May, 1983

November, 1983

SATEAZ 54(5) 319-388 (1983)

SOVIET ATOMIC ENERGY

АТОМНАЯ ЭНЕРГИЯ
(ATOMNAYA ENERGIYA)

TRANSLATED FROM RUSSIAN

CONSULTANTS BUREAU, NEW YORK

SOVIET ATOMIC ENERGY

Soviet Atomic Energy is abstracted or indexed in *Chemical Abstracts, Chemical Titles, Pollution Abstracts, Science Research Abstracts, Parts A and B, Safety, Science Abstracts Journal, Current Contents, Energy Research Abstracts,* and *Engineering Index.*

Mailed in the USA by Publications Expediting, Inc., 200 Meacham Avenue, Elmont, NY 11003.

POSTMASTER: Send address changes to *Soviet Atomic Energy,* Plenum Publishing Corporation, 233 Spring Street, New York, NY 10013.

Soviet Atomic Energy is a translation of *Atomnaya Energiya,* a publication of the Academy of Sciences of the USSR.

An agreement with the Copyright Agency of the USSR (VAAP) makes available both advance copies of the Russian journal and original glossy photographs and artwork. This serves to decrease the necessary time lag between publication of the original and publication of the translation and helps to improve the quality of the latter. The translation began with the first issue of the Russian journal.

Consultants Bureau journals appear about six months after the publication of the original Russian issue. For bibliographic accuracy, the English issue published by Consultants Bureau carries the same number and date as the original Russian from which it was translated. For example, a Russian issue published in December will appear in a Consultants Bureau English translation about the following June, but the translation issue will carry the December date. When ordering any volume or particular issue of a Consultants Bureau journal, please specify the date and, where applicable, the volume and issue numbers of the original Russian. The material you will receive will be a translation of that Russian volume or issue.

Subscription (2 volumes per year)
Vols. 52 & 53: $440 (domestic); $489 (foreign)
Vols. 54 & 55: $500 (domestic); $555 (foreign)

Single Issue: $100
Single Article: $7.50

CONSULTANTS BUREAU, NEW YORK AND LONDON

c/b
233 Spring Street
New York, New York 10013

Published monthly. Second-class postage paid at Jamaica, New York 11431.

SOVIET ATOMIC ENERGY

A translation of *Atomnaya Énergiya*

November, 1983

Volume 54, Number 5 **May, 1983**

CONTENTS

The Russian press date (podpisano k pechati) of this issue was 4/22/1983. Publication therefore did not occur prior to this date, but must be assumed to have taken place reasonably soon thereafter.

ARTICLES

METEOROLOGICAL ASPECTS OF THE CHOICE OF SITES FOR NUCLEAR POWER PLANTS

N. E. Artemova

UDC 621.039.583:551.5

The radiation safety of nuclear power plants — one of the principal cirteria in site selection — is determined by the radiation action of the plant on the population. The irradiation dosage limit of the population and the amount of radionuclide emissions have been established in the USSR by "Standard Rules for the Design of Nuclear Power Plants" [1], which have been developed on the basis of "NRB-76 Norms of Radiation Safety" [2]. The irradiation dosage limit determines the limiting permissible emissions (LPE) of radionuclides into the atmosphere for normal operation of nuclear power plants. One of the main methods for establishment of LPE is determination of the critical irradiation path, i.e., the most dangerous entry of nuclides into the human organism. With the dosage limits established by the NRB, the coefficients of meteorological dilution for the region of site placement, and also the additional rules, requirements, and recommendations operating in the country with respect to questions of the design of nuclear power units taken into account, one can establish values of the LPE of individual radionuclides and their sum for each nuclear power plant [4].

One of the criteria for the selection of a nuclear power plant site — the safety of the population upon propagation of radionuclides emitted from the stacks of nuclear power plants into the atmosphere, which is determined by the physicogeographical peculiarities of the site, the climatology of the region of placement of the nuclear power plant, and the micrometeorological peculiarities of a given site — is discussed in this paper. In the case in which the region of placement of a nuclear power plant has been determined, it is necessary in the initial selection stage, when evaluating a specific site, to carefully analyze the physicogeographical factors, which produce peculiarities in the dispersal of contaminating materials in the near-surface layer of the atmosphere and affect the coefficient of meteorological dilution of atmospheric emissions. The radiation safety of a nuclear power plant can be correctly estimated only in the case in which the meteorological characteristics used in calculations of the LPE or the assumed dosage loads due to the design emissions are representative for the site of a given nuclear power plant and their makeup corresponds to the computational scheme of the dispersal of atmospheric emissions in a given region.

In order to evaluate the safety of a nuclear power plant in the initial site selection stage from physicogeographical parameters, it is necessary:

to recognize the microclimatic peculiarities of the placement region;

to determine the representatives of the nearest meteorological stations;

to select a reference meteorological station from whose data the characteristics of the climate of the site placement region can be compiled; and

to have a general notion as to the relief of the region on the basis of a visual inspection of the site and to select the locations of control points for the placement of equipment for additional natural investigations if they are necessary. Topographical features within a radius of 15-20 km which are of special interest are valleys, mountain ridges, their heights, and watersheds. One should note the presence of individual obstacles (hills), the nature of the vegetation, large artificial structures, the location of the nearest population centers, and various kinds of potentially dangerous objects.

In estimating the safety of the placement of a nuclear power plant at a specific site in a selected region, the main parameter which permits predicting contamination of the atmosphere and the locality by the design air emissions is the minimum value of the coefficient of meteorological dilution of a radioactive impurity in the atmosphere of the given region caused by its climatic and orographic peculiarities.

Translated from Atomnaya Énergiya, Vol. 54, No. 5, pp. 323-326, May, 1983. Original article submitted April, 16, 1982; revision submitted June 30, 1982.

0038-531X/83/5405-0319$07.50

As is well known, the coefficient of meteorological dilution K_d is the quantity which ties together the emission of contaminating materials Q and the concentration of contaminating materials in the near-surface air c by a relationship of the form

$$Q = K_d (c - c_b),$$

where c_b is the background concentration of the corresponding contaminating material in the region under discussion. The minimum value of the meteorological dilution coefficient serves as a universal characteristic of the dispersing properties of the atmosphere in the region in which the emission source is located. Its value can be obtained by computational means in accordance with any model adopted at present for the dispersal of an impurity which has been constructed for a normal distribution of meteorological parameters in the propagation layer of the emissions and for uniform flat relief of the site.

However, a uniform thermodynamic structure of the atmosphere, as also a flat uniform underlying surface, are seldom observed in nature. In individual so-called anomalous cases there can be significant deviations of the vertical distribution of the wind velocity and temperature from a monotonic one, which are caused by peculiarities in the relief of the locality or the properties of the air masses which form the weather in the region under discussion. A characteristic example of anomalous meteorological conditions, which increase the contamination of the near-surface air layer in comparison with normal conditions, are elevated temperature inversions and calm layers. As analysis of the existing data has shown, one can expect that at a distance of 1-5 km from the source (i.e., in the region of maximum near-surface concentration for sources 100-150 m in height), a single near-surface concentration can temporarily increase by a factor of 1.5-2.5 when an elevated temperature inversion is located directly above the emission level, i.e., for the most dangerous location of the inversion layer. The calculated values of the concentration at a distance of 10-20 km can increase by a factor of 3-6. The development of a calm zone near the surface can, according to the calculations, serve as the cause of an increase in the near-surface concentration by a factor of 1.7-2 upon the emission of an impurity from a source 100-150 m in height.

Unfavorable conditions of accumulation of an impurity in the near-surface layer can also develop in the presence of a fog which encompasses and concentrates the impurity from the superincumbent layers and which increases the near-surface concentration of the radionuclides. Although qualitative estimates of the effect of fog on the impurity concentration are lacking, one should evaluate the repeatability of this factor, which facilitates the creation "haziness" conditions and raising of the near-surface concentration when considering a location for a source of radionuclide emission.

The simultaneous cumulative action of several factors can increase the maximum near-surface concentration by a factor of five; however, the average annual probability of such a combination of unfavorable conditions is small and amounts to approximately several units and fractions of a percent for the entire territory of the Soviet Union according to the existing estimates.

The dislocation of air flows in complex relief (a hilly locality, alternation of mountain ridges and valleys, a coastal region) significantly alters the nature of the motion and the turbulent regime of these flows, which also changes the distribution of the concentration of impurities emitted by a source located in such a region. In order to solve the problem of the nature of diffusion in a complex mountain valley or a coastal site, one should investigate in detail the peculiarities of the air flows with the help of meteorological instruments and indicators (haziness, balanced spheres). Mathematical models are ineffective in this case. When winds of a local nature (mountain valley winds, air blasts, breezes) are present in the region under investigation, it is necessary to make special instrumental meteorological and aerological observations. Analysis of the data obtained will permit characterizing the main distinctive features of the air flows and the conditions of thermodynamic stability in the region of the site and drawing a conclusion as to the degree of its suitability for placement of a source of radionuclide emission.

A preliminary visual inspection of the site by meteorology specialists is especially necessary in order to select and qualitatively compare possible alternative sites and to determine the placement of the control points for additional investigations. If an unfavorable meteorological situation, e.g., a directed flow and unfavorable conditions of atmospheric stability during extended periods, is repeated often at a site, which along with the distribution and density of the population can result in an unacceptable situation in the case of an accident, one should reject the site if the design organization is unable to prove that the possibility exists of guaranteeing safety with the help of engineering solutions.

TABLE 1. System for Evaluation of Physicogeographical Factors in Site Selection According to a Suitability Index

Factor	Good, $\xi = 3$ (class 3)	Satisfactory, $\xi = 2$ (class 2)	Unfavorable, inadmissible, $\xi = 1$ (class 1)	Clearly negative, excluding consideration of the site
Relief	Level with a uniform underlying surface	Level, slightly hilly	Hilly, cut by ravines; side river valley; seacoast	Basin in a mountainous locality; narrow mountain ravine
Wind regime	Average annual wind velocity of 3 m/sec andmore; repeatability of the prevailing wind directions of no more than 25%; repeatability of calms of no more than 20%	Average annual wind velocity of 2.5-2.1 m/sec; repeatability of the prevailing wind directions of 26-40%, repeatability of calms of 21-40%	Average annual wind velocity 1.6-2 m/sec; repeatability of the prevailing wind directions of 41-55%; repeatability of calms of 41-59%	Average annual wind velocity of no more than 1.5 m/sec. A sharply expressed microcirculation is observed — a directed flow in the direction of a populated locality (repeatability of the wind direction or more than 55%). Repeatability of calms of 60% and more
Anomalous stratification (temperature inversion)*	Repeatability of near-surface inversions of no more than 25%; repeatability of elevated inversions of no more than 10%	Repeatability of near-surface inversions of 26-45%; repeatability of elevated inversions of 11-25%	Repeatability of near-surface inversions of no more than 45%; repeatability of elevated inversions of more than 25%	
Location of the population centers	Population centers are located in the wind action direction of least repeatability. The distance from the site to the population centers and the irradiation dosage correspond to those indicated in [2, 3]	There are no population centers in the direction in which the predominant winds act. The distance and dosages indicated in [2, 3] are observed	Small population centers are situated in the action direction of the prevailing winds but beyond the boundaries of the disruption zone (13 km) and there are no higher absolute marks with respect to the absolute mark of the site (by more than 10 m)	Distance to population centers which are indicated in [2, 3] are not observed. The nearest population centers or large city are situated in the action direction of the prevailing winds
Background concentration of toxic or radioactive materials	No more than 0.05 MPC† (DK)	0.1 MPC† (DK)	0.5 MPC† (DK)	Close to MPC† or exceeding it

*Since the height of the radionuclide emission sources does not usually exceed 150 m, and that of toxic emission sources, 200-250 m, one should take account only of elevated inversions with a lower boundary in the 0-300 m layer. If there is no such data, one can (with some margin) use the data for the 0-500 m layer.

†Maximum permissible concentration.

Declassified and Approved For Release 2013/02/06 : CIA-RDP10-02196R000300020005-5

Thus, the evaluation of a site for placement of a nuclear power plant according to the conditions of atmospheric diffusion of radionuclides and the provision of radiation safety of the population is carried out on the basis of the following data, which can be obtained from the reference literature, the archive data of reference meteorological and aerological stations, and special observations at the site, as well as from the organizations of appropriate departments:

1. A complete description of the physicogeographical peculiarities of the site and the region in which it is located, including the topography and relief.

2. The wind velocity in gradations with the corresponding average annual and seasonal repeatability; the repeatability of calm.

3. The average annual repeatability of the wind directions and the average annual wind velocities by points of the compass.

4. The average annual diurnal and average annual (multiyear) maximum air temperature.

5. The average annual repeatability of the categories of atmospheric stability according to Pasquille and the corresponding average wind velocity by categories (with determination of the dilution coefficient by the IAEA method for the sites of foreign nuclear power plants).

6. The average values of the vertical and horizontal dispersion σ_z and σ_y for the different Pasquille stability categories (with refinement of the calculations by the IAEA method for sites in the vicinity of complex relief or with an abrupt change in the nature of the underlying surface). The dispersions σ_z and σ_y can be obtained from the data of trajectory observations behind balanced tetrons (tetragonal tanks) or stereophotogrammetry of smoke flows.

7. Data on the average altitude and the repeatability of elevated and near-surface temperature infersions in the 0-300 or 0-500 m layers.

8. Data on the microclimatic peculiarities of the region (characteristics of the local circulation, the average number of days with fog, the duration of the fog, and peculiarities of the precipitation).

9. Topographic plan diagram of the site placement region to a radius out to 20 km with plotting of the isohypses and an indication of the location and absolute marks of meterological stations of the region, the reference meteorological station, population centers, and their population size.

10. Remoteness of the site from large population centers and the size of their populations; location of the site with respect to rest zones, preserves and health resorts, and the state boundary.

11. Capacity of the nuclear power plant with account taken of the outlook for its expansion and with an indication of the type of reactor facilities.

12. Preferred values of the radionuclide emissions for normal operation of the nuclear power plant and with enhanced short-term emissions.

13. Engineering data on the height of the exhaust stacks adopted in the design, their diameter, the outflow rate of gases, and the volume and temperature of the gas—air mixture emitted into the atmosphere.

14. Data on the location of agricultural lands and farm production carried out in the region.

15. Background concentrations of radionuclides.

It has been proposed in the discussion of nuclear power plant sites according to the five main physicogeographical factors (relief, wind regime, repeatability of anomalous temperature stratification, location of population centers, and the background concentration) to classify sites in accordance with the qualitative and quantitative characteristics of the names factors given in Table 1, which generalizes the experience of the placement and operation of the nuclear power plants operating in the USSR.

Evaluation is performed according to the three-point index ξ, which arbitrarily characterizes the suitability classes of sites. If a factor under consideration includes two or three components (e.g., the wind regime: velocity, wind direction, and repeatability of calms), a complete point in a class is distributed evenly among the components: each of the compo-

nent factors is evaluated for the actual site in fractions of a total point in that class to which it most closely belongs according to qualitative and quantitative characteristics. For example, each of the three components of the wind regime in class 3 has a limit of one point, in class 2, a limit of 2/3 point, and in class 1, a limit of 1/3 point. In accordance with the system proposed in Table 1 for the evaluation of sites according to physicogeographical conditions, the greatest total number of points is 15, and the least is 5. Thus, the competitiveness of alternative sites for construction of a nuclear power plant is determined within the limits of these values, depending upon the total number of points obtained by each site.

The complete evaluation of a site with respect to a set of complex criteria, one of which are physicogeographical conditions considered here, can be performed by summing up the evaluations of all the complex criteria with account taken of their normalization and the weighted contribution of each criterion to the overall system.

LITERATURE CITED

1. Health Rules for the Design and Construction of Nuclear Power Plants of SP AÉS-70 [in Russian], Énergoizdat, Moscow (1981).
2. NRB-76 Norms of Radiation Safety [in Russian], Atomizdat, Moscow (1978).
3. "Requirements for placement of nuclear heat supply plants and nuclear heat and power plants according to radiation safety conditions," At. Energ., 49, No. 2, 150 (1980).
4. N. E. Artemova et al., Permissible Emissions of Radioactive and Harmful Chemical Materials into the Near-Surface Layer of the Atmosphere [in Russian], Atomizdat, Moscow (1980).

RADIATION ENVIRONMENT AND ACTIVITY OF THE PRINCIPAL TECHNOLOGICAL SURROUNDS OF THE BN-600

L. E. Gnedkov, Yu. L. Gushchin, A. S. Zhilkin, E. I. Inyutin, A. I. Kiryushin, I. I. Koltik, N. F. Korshunov, E. S. Lisitsyn, S. L. Osipov, O. B. Samoilov, V. A. Sergeev, M. F. Troyanov, A. G. Tsikunov, and V. N. Shiryaev

UDC 621.039.526:621.039.538

During the physics and power generation startup, and during operation of the BN-600 at a power of 80% of nominal in 1979-1980, experimental investigations were carried out on the radiation shielding and activity of the technological surrounds of the primary and secondary circuits. The radiation measurements on the reactor were conducted according to a program developed by taking into account the experience in the organization and investigations into the radiation environment of the BN-350 [1], namely: the radiation environment in the station buildings and the radioactivity of the technological surrounds of the reactor were measured; the efficiency of the reactor biological shield and the compartments of the primary circuit were studied, and also the intravessel shielding of the reactor; and the effect of radiation on the structural components of the reactor was determined.

Design of the BN-600 Shielding. The principal plant of the primary circuit is installed in a common tank — the reactor vessel, filled with sodium. The construction of the reactor shield (Figs. 1, 2) [2] includes the intravessel shield, the biological shield of the compartments, and the transport-technological channel shielding.

The intravessel shield, surrounding the core, performs the functions of a radiation and thermal shield. Its structural features are determined by the necessity of shielding the intermediate heat exchangers (IHE) in order to reduce the induced activity of the coolant of the secondary circuit to an acceptable level. The principal role of the counter-activation shield is played by the lateral neuron shield (Fig. 1), consisting of an assembly of steel plates in the inner part and steel tubes filled with graphite and borated graphite in the outer part. The total thickness of the shield at the level of the center of the core is ∿2 m. Upwards, at the section of the collant entry into the heat exchangers, the shield has a

Translated from Atomnaya Énergiya, Vol. 54, No. 5, pp. 326-330, May, 1983. Original article submitted November 22, 1982.

0038-531X/83/5405-0323$07.50

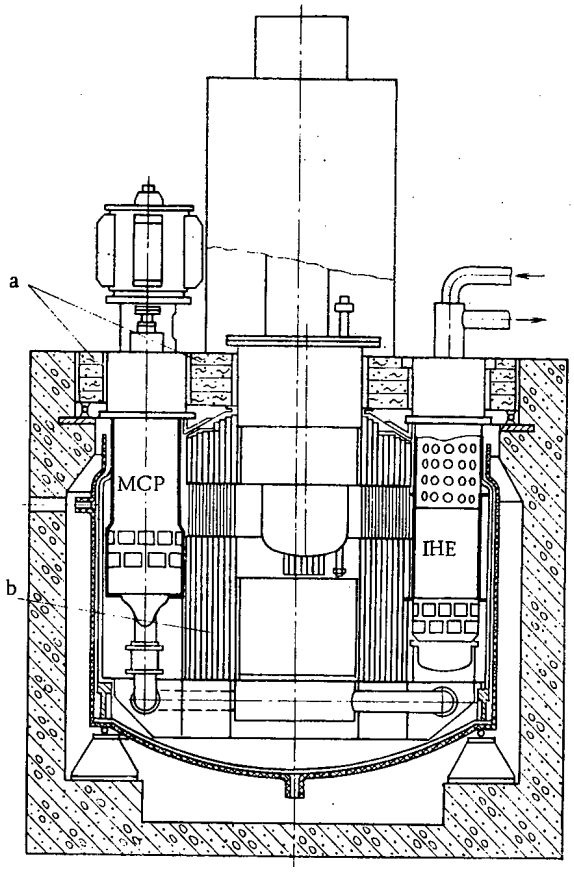

Fig. 1

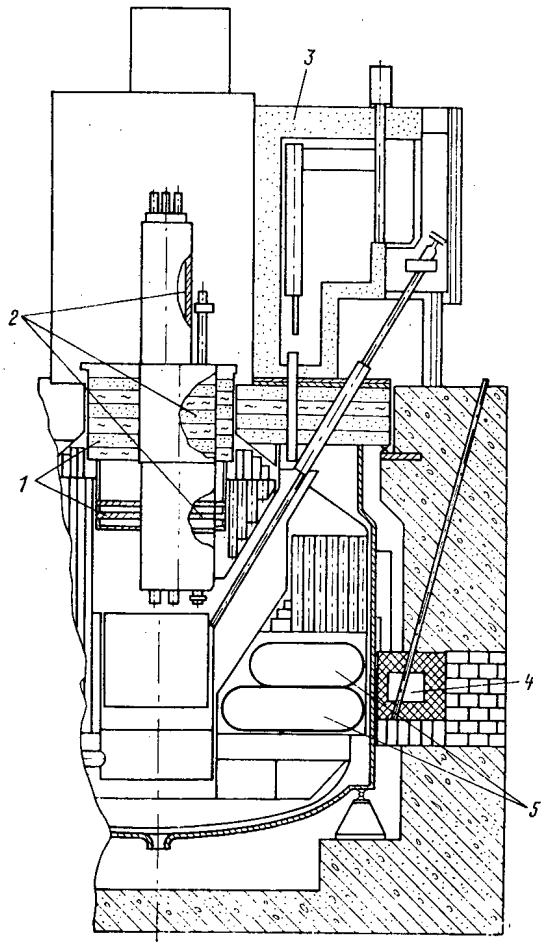

Fig. 2

Fig. 1. Longitudinal section of the reactor through the main circulatory pump and the intermediate heat exchanger: a) upper fixed shield; b) lateral neutron shield.

Fig. 2. Longitudinal section of the reactor through the elevators and the ionization chamber unit: 1-3) shield in the large rotatable plug, in the central column of the recharging unit; 4) ionization chamber unit (ICU); 5) neutron tubes.

similar constitution, and structurally it is made so as to provide a passage for the coolant from the core to the heat exchangers. Higher, directly above the zone of entry of the coolant into the heat exchangers, the lateral shield is closed by an assembly of steel plates, fixed to the rotatable plug and in the central column. Below, the lateral shield is closed by the pressure chamber and, surrounding it, by an assembly of steel plates. In the region of the elevators, a number of detachable steel bars is installed.

Part of the lateral intravessel shield is cut out for positioning the fuel element assembly (FEA) charging and recharging elevators, and also for positioning the cavities of the so-called neutron guides (see Fig. 2). A graphite recess, with an ionization chamber unit (ICU) installed in it for monitoring the reactor power, adjoins the neutron guides from the side of the reactor shaft. In order to reduce the outflow of neutrons and to reduce activation of the secondary circuit coolant, the neutron guides and elevators are surrounded by a steel–graphite shield. In the region of the neutron guides in the "insurance" vessel, a П-shaped shield of steel tubes with graphite (Fig. 3) is mounted. It surrounds the shield of the reactor shart, made of serpentinite concrete (upper) and iron oxide (lateral), which are enclosed in steel housings.

For the biological protection of the compartments located behind the reactor vessel, normal concrete is used with a thickness of 1-4 m, and for the rooms of the central hall, a rotatable plug with alternate layers of steel and graphite, with an overall thickness of ∿1.9 m, and a circular fixed shield of an assembly of steel and serpentinite concrete with an overall

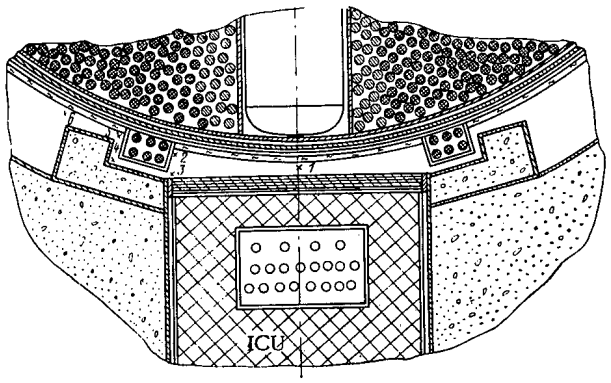

Fig. 3. Horizontal section in the region of the ICU (× indicates measurement points).

thickness of ∿1.4 m, which covers the reactor shaft, are used. In the upper parts of the plant, at the level of the fixed shields, a steel–graphite shield is located.

Transportation of the fuel element assemblies (FEA) from the reactor to the spent assembly drum and into the cooling pond is effected by a special transfer channel. The thickness of the shielding of cast iron shot of the transfer and wash-down boxes is equal to 0.95 m.

Extent of the Radiation Investigations and Equipment Used. Radiation investigations on the BN-600 were conducted at all stages of the physics and power startups. In the prestartup period, the background values of the γ and neutron radiation levels and the activity of the technological surrounds were determined, and the shielding of the transfer-technological channel was checked by means of a startup source. During the physics startup and during operation of the reactor at a power of approximately up to 5 MW, the γ and neutron radiation level in the reactor vessel, in the primary circuit compartments, and in the ICU channel were measured, and intrareactor experiments were carried out on the irradiation of indicators.

In the case of the radiation measurements during the power startup of the reactor (combined testing of the plant at approximately 30% of power), the efficiency of the reactor biological shield was checked, the activity and radionuclide composition of the sodium coolant and of the protective gas of the primary circuit were measured, and the monitoring system for the leak-tightness of the fuel element cans for gas and delayed neutrons was tested.

Monitoring of the radiation environment and technological monitoring of the radioactive parameters was carried out by stationary remote control, and local and portable instruments. The activity of the technological surrounds was measured by a sampling method and by the method of γ spectrometry with semiconductor detectors in the plant of the radioactive systems and on special measurement sections. The operative data of the regular radiation monitoring systems were centralized at the dosimetric monitoring panel and at the reactor control modular panel. The radiation parameters monitored are the level of the γ and neutron radiation in the reactor compartments, the concentration of radioactive gases in the reactor compartments and the aerosols in the air of the working compartments and ventilation systems, the radioactive contamination of the coolant and gas of the primary circuit, the hermiticity of the fuel element cans with respect to delayed neutrons in the coolant of the primary circuit and the total activity of the noble radioactive gases in the reactor cushion, the hermeticity of the system and plant of the primary circuit, and the operating efficiency of the purification system [3, 4], etc.

Radiation Measurements during the Physics Startup of the Reactor. The neutron flux density distribution and the γ radiation dose intensity behind the pressure vessel in the reactor shaft were investigated at a power level of up to 5 MW. For access to the pressure vessel, the upper manhole and the temporarily opened lower maintenance manhole in the shift were used. The measurements were made from the instant of installation of the neutron source in the core.

Particular attention was paid to measurements in the region of the Π-shaped shield (see Fig. 3 and Table 1). A comparison of the values of the neutron flux density inside the Π-shaped shield and behind it show its high efficiency.

For the purpose of forecasting the radiation environment in the compartments with sodium systems of the primary circuit, the γ radiation dose intensity was measured, in the vicinity

TABLE 1. Neutron Radiation Level in the Region of the Π-Shaped Shield, Measured at a Reactor Power of 0.36 kW

Number of measurement points (see Fig. 3)	Neutron flux density 10^{14} neutrons/(m^2·sec)	
	thermal	intermediate
1	400	2000
2	54	300
3	42	—
4	3,3	—
5	1,3	4
6	0,1	1,2

TABLE 2. Neutron Flux Density φ at Certain Measurement Points (Fig. 4), neutron/(m^2·sec)

Number of measurement points	φ	Number of measurement points	φ	Number of measurement points	φ
1	10^{14}	9	10^8	14	$4\cdot10^7$
2	$1{,}5\cdot10^{13}$	10	$1{,}5\cdot10^7$	15	$5\cdot10^6$
6	$5{,}3\cdot10^{10}$	11	$4\cdot10^6$	16	$1{,}4\cdot10^8$
7	$9{,}5\cdot10^9$	12	$3{,}5\cdot10^{12}$	17	$2{,}6\cdot10^9$
8	$1{,}3\cdot10^9$	13	$6\cdot10^8$	18	$4{,}8\cdot10^{10}$

of different plant of the primary circuit. The γ-radiation dose intensity in the compartments of the primary circuit during operation of the reactor at nominal power is shown below, R/sec (1 R = $2.58\cdot10^{-4}$ C/kg):

Reactor shaft:	
reactor bottom and pressure vessel	1.7-2.3
roller supports of the reactor	0.08-0.46
Primary circuit auxiliary sodium pipeline compartment	
at the inlet to the compartment	0.2
at the surface of the pipeline thermoinsulation	2.3
at the surface of the can hermiticity monitoring (CHM) thermoinsulation	3.5

Radiation Environment in the Reactor Compartments. This was investigated mainly during operation of the reactor at 60-80% power. During the measurement in the servicing compartments adjacent to the reactor shaft and to the compartments with the sodium and gas systems of the primary circuit, it was established that the level of ionizing radiation in these compartments is determined by the γ radiation from the primary circuit coolant and does not exceed 0.2 μR/sec. The neutron radiation contribution is less than 1%.

The level of the neutron radiation below the bottom and behind the lateral surface of the reactor vessel is determined by the passage of neutrons through the hollow neutron guides and below the Π-shaped shield. When converted to nominal reactor power, the total neutron flux density inside the Π-shaped shield opposite the neutron guides amounts to 10^{14} neutrons/(m^2·sec), below the Π-shaped shield, to $3.5\cdot10^{12}$ neutrons/(m^2·sec); at the lateral surface of the reactor vessel in the region of the intermediate heat exchanger and near to the ICU (at the level of the neutron guides), to $9.5\cdot10^9$ neutrons/(m^2·sec), and at the lateral surface of the reactor vessel in the region of the main circulatory pumps (MCP), the most distant from the ICU, to $4.0\cdot10^6$ neutrons/(m^2·sec). The thermal neutron flux density in the ICU channels, when scaled to nominal reactor power, for the second row of channels amounted to $4.9\cdot10^{12}$ neutrons/(m^2·sec) [by design, $6\cdot10^{12}$ neutrons/(m^2·sec)].

The γ radiation dose intensity in the reactor shaft is determined by the activation γ emission of the primary circuit coolant, and, when scaled to nominal reactor power, at the lateral surface and below the bottom of the reactor vessel it is equal to 1.7-2.3 R/sec, and at the cap of the reactor vessel it does not exceed 0.6 R/sec. An exception is the section opposite the neutron guides inside the Π-shaped shield, where the γ-radiation dose intensity is determined by the captured γ emission in the reactor vessel and, when scaled to nominal reactor power, it is equal to 9.7 R/sec. The γ shield of the ICU channels reduces the γ-radiation dose intensity to 0.6 R/sec.

When measuring the level of radiation at the cap of the reactor vessel, a significant nonuniformity of the neutron flux density is observed around the perimeter of the cap (Table 2). The neutron flux density in the region of the elevator connecting pipe, when scaled to nominal reactor power, is equal to $6\cdot10^8$ neutrons/(m^2·sec) and between the tubes of the intermediate heat exchanger and the MCP closest to the elevator it is equal to $4\cdot10^7$ neutrons/(m^2·sec); between the tubes of the MCP and the next intermediate heat exchanger it is $5\cdot10^6$ neutrons/(m^2·sec).

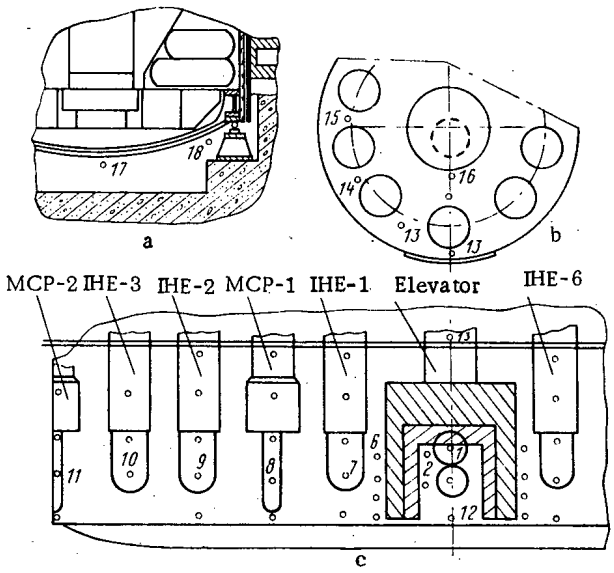

Fig. 4. Recorder chart of the neutron flux density measurement points (see Table 2): a) cross section of the reactor; b) view of the cap of the reactor vessel; c) projection of plant on the lateral surface of the reactor vessel.

The level of the γ and neutron radiation in the semiattended compartments above the reactor shield (below the dome of the reactor, in the compartments of the intermediate heat exchangers and the MCP of the primary circuit) was measured in the greatest detail. This was necessary because of the presence in the upper shield of a large number of structural and technological slits and gaps, typical for this reactor layout. According to the measurement results, no appreciable effect was noted on the radiation environment of the structural nonuniformities in the upper shield. The level of ionizing radiation in the compartments, caused by the γ emission of the primary circuit coolant, amounts to 0.02 μR/sec. The neutron emission contribution did not exceed 10-25%, with the exception of the section above the shield plug where, in the maintenance hatch, temporary startup neutron probes were installed. At the surface of the plug, the radiation dose at 80% reactor power level was determined by the neutron radiation and did not exceed 0.2 μrem/sec (1 rem = 10^{-2} eV).

Activity of the Primary and Secondary Circuit Coolant and the Gas Cavity of the Reactor. The activity of the coolant of the primary and secondary circuits was measured mainly by a nonsampling method. During operation of the reactor, measurements were made on the spectrometric section of the sodium loop of the can hermieticity monitoring and in the sodium pipelines of the secondary circuit, and during periods of reactor shutdown, in the pipelines of the supplementary sodium system of the primary circuit.

The specific activity of ^{24}Na in the primary and secondary circuit coolant, scaled to nominal reactor power, amounted to $6.8 \cdot 10^5$ MBq/kg* (according to design, $7.8 \cdot 10^5$ MBq/kg), and the specific ^{22}Na activity over 63 effective days of reactor operation attained 2.8 MBq/kg, which scaled to equilibrium value, amounts to 60 MBq/kg (by design, $1.5 \cdot 10^2$ MBq/kg).

In order to measure the activity of the primary circuit gas, samples were taken from the reactor gas cavity. The activity of the reactor gas cavity, determined by ^{41}Ar, when scaled to nominal reactor power, amounted to $6.3 \cdot 10^3$ MBq/m^3 (by design, $7.4 \cdot 10^3$ MBq/m^3). During the γ spectrometric analysis of the gas samples, radionuclides of xenon and krypton were detected in the reactor gas cavity. The total specific fission product activity, due to the initial contaminated fuel of the fuel elements, when operating the reactor at 80% power, amounted to $3 \cdot 10^2$ MBq/m^3. In these conditions, the gas—aerosol radioactive effluents of the BN-600 are more than two orders less than the values assigned by health standards, and are found at the limit of the threshold of sensitivity of the recording equipment.

The activity of the secondary circuit sodium was measured in two ways: in the first, the internal reactor storage vault was filled with simulated fuel element assemblies, and in the second, with spent fuel element assemblies. The activity of the secondary circuit coolant in loops 4 and 6, adjacent to the elevators, was almost unchanged with change of composition of the internal reactor storage vault and, when scaled to nominal reactor power, was equal to $(4.4\text{-}5.5) \cdot 10^2$ Bq/kg. The activity of the secondary circuit coolant in loop 5 opposite to the elevator, when scaled to nominal power, amounts to $8.1 \cdot 10^1$ Bq/kg if the internal storage vault

*1 Ci = $3.7 \cdot 10^{10}$ Bq = $3.7 \cdot 10^4$ MBq.

is filled with simulated fuel element assemblies, and $3 \cdot 10^2$ Bq/kg if the storage vault is filled with spent fuel element assemblies. These results confirm that the effect of neutron multiplication in the fuel element assemblies of the internal storage vault on the activation of the secondary circuit coolant in loops 4 and 6 almost did not appear in these experiments on the activation background by neutrons leaking through the neutron guides; however, it is significantly noticeable in loop 5, which is located far from the neutron guides.

CONCLUSIONS

The results of measurements of the radiation environment and the activity of the technological surrounds correspond in the main to the design values. The level of radiation in the servicing and semiservicing compartments of the reactor does not exceed the regulation values and is determined by the γ activity of the primary and secondary circuit coolants. The intravessel shield of the intermediate heat exchangers effectively attenuates the neutron radiation, which reduces the activity of the coolant in them and ensures free servicing of the secondary circuit plant. The experimental data obtained could be used for designing the radiation shielding of fast sodium reactors and for testing numerical methods and programs.

LITERATURE CITED

1. D. S. Yurchenko et al., At. Energ., 36, 2, 107 (1974).
2. V. M. Budov et al., BN-600 Fast Neutron Nuclear Reactor — a Facility for Power Generation of the Near Future [in Russian], NUCLEX-75, Basle (1975).
3. Health Regulations for the Design and Construction of Nuclear Power Stations [in Russian2, Énergoizdat, Moscow, SP AES-79 (1981).
4. Principal Health Regulations for Working with Radioactive Substances and other Ionizing Radiation Sources [in Russian], Átomizdat, Moscow (OSP-72) (1973).

TEMPERATURE PULSATIONS IN THE HEAT-TRANSMITTING WALL OF A STEAM GENERATOR MODEL WITH HEATED SODIUM

P. L. Kirillov, N. M. Turchin,
N. S. Grachev, V. V. Khudasko,*
I. Shneller, I. Bitsa, and I. Khum†

UDC 621.181.021

Reservations have recently been advanced that temperature oscillations of the tube wall of a steam generator and the variable thermal stresses which arise as a result of this can affect the longevity of the tubes. In this connection, data are necessary on the strength of the temperature pulsations, their spectral density on the surfaces of a heat-transmitting wall, and the autocorrelation function and equivalent frequencies.

Temperature oscillations in the heat-transmitting wall of a sodium—water single-pass steam generator can be produced by various causes. Temperature pulsations associated with the appearance of a heat exchange crisis are of special interest. According to contemporary notions, they are caused by the alternate washing of a heat-transmitting wall with water and steam. References [1-3] are devoted to investigations of temperature pulsations in the heat-transmitting walls of steam generators having the parameters of the operating conditions of contemporary nuclear power plants with fast reactors.

The statistical characteristics of temperature pulsations (dispersion, spectral density—autocorrelation function, and the probability distribution function) in the heat-transmitting wall of a single-tube model of a stream generator were investigated at a pressure p = 13.7 MPa and a mass velocity ρw = 350-1000 kg/m^2·sec, and at p = 9.8 MPa and ρw = 700 kg/m^2·sec [1]. The extent of the temperature oscillation zone in the heat-exchange crisis region was 30-60 mm in tests. Oscillations at a frequency less than 1 Hz make the greatest contribution to the values of the pulsation intensity, and the maximum intensity in scaling to the inner surface of the heat-transmitting wall was 10°K.

*USSR.
†Czechoslovakia.

Translated from Atomnaya Énergiya, Vol. 54, No. 5, pp. 330-333, May, 1983. Original article submitted March 15, 1982.

 0038-531X/83/5405-0328$07.50

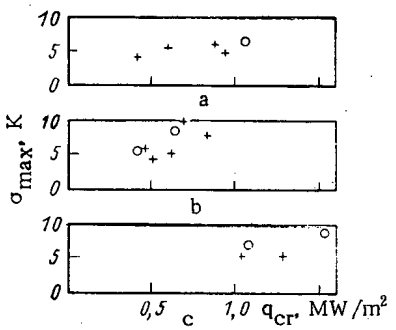

Fig. 1. Dependence of the maximum standard deviations of pulsations of the wall temperature on the critical thermal flux for (a) p = 13.7 MPa and ρw = 700 kg/m²·sec, (b) 13.7 MPa and 350 kg/m²·sec, and (c) 9.8 MPa and 700 kg/m²·sec; ○ and + denote the data of this paper and of [1], respectively.

According to the results of the investigation [2], the pulsation intensity for ρw = 400-850 kg/m²·sec is 6°K in the frequency band from 0.01 to 2 Hz, and the heat-exchange crisis region is restricted to 0.2 m in length. Inappreciable oscillations of the flow rate (∿1%) have resulted in temperature pulsations with doubled amplitude to 20-30°K.

Two types of temperature pulsations have been noted in [3] with p = 8-14 MPa and ρw = 300-550 kg/m²·sec: with periods of 10-30 sec and 1-4 sec. Evidently, the first type of pulsations is caused by oscillations of the water flow rate, and the second one is caused by drying up of the liquid film in the crisis zone. The authors of [3] have restricted themselves to an investigation of the effect of the mass velocity and pressure on the maximum value of the temperature pulsations. Other statistical characteristics of the temperature pulsations are not given.

In connection with the fact that the range of investigations with regard to pressure and mass velocity in [1-3] is limited and does not encompass the operating regions of contemporary nuclear power plants, we have investigated the temperature pulsations of a heat-transmitting wall at p = 7.8-13.7 MPa and ρw = 340-1000 kg/m²·sec. The tests were conducted on a single-tube model of a "tube in a tube" steam generator, whose construction has been described in [4]. Fifteen Chromel–Alumel microthermocouples each were mounted with a 10-mm spacing on a heat-transmitting wall of the geam generator model in two regions at a distance of ∿1 m from the entrance and exit of water (steam) in slots 1 × 1 mm in cross section. The thermocouple junctions were located in the heat-transmitting wall at a distance of 0.5 mm from the heated side. Signals from the thermocouples were fed through amplifiers to a magnetic recorder, and then with the help of a converter they were translated into digital form and communicated to a computer. Signals from six thermocouples were recorded simultaneously. Filters were provided in a measuring system which eliminate noise with frequencies <0.01 and >5 Hz. The duration of a record of the process is ∿0.15 m. These measurements permitted determining the characteristics necessary for the subsequent calculations:

standard deviation

$$\sigma_x = \sqrt{\frac{1}{N-1}\sum_{i=1}^{N}(t_i - t)^2}; \tag{1}$$

normalized autocorrelation function

$$R(\tau) = \left\{\frac{1}{N-1}\sum_{i=1}^{N-r}(t_i - \bar{t})(t_{i+r} - \bar{t})\right\}\sigma_x^{-2}; \tag{2}$$

and normalized spectral density

$$S_x(f) = 2\Delta\tau\left\{R(0) + 2\sum_{r=1}^{m-1} R(r,\ \Delta\tau)\cos\frac{\pi kr}{m} + (-1)^k R(m,\ \Delta\tau)\right\}, \tag{3}$$

where $\bar{t}$ is the average temperature, N is the number of measurements, f = kΔf (k = 1, 2, 3, ...), Δf = $(2m\Delta\tau)^{-1}$ is the frequency spacing, Δτ is the time spacing, τ = rΔτ (r = 1, 2, 3, ...), and m is the number of points of the correlation function.

Scaling of the values of the standard deviation σ_X and the normalized spectral density $S_X(f)$ at the embedding site of a thermocouple to their corresponding values on the inner sur-

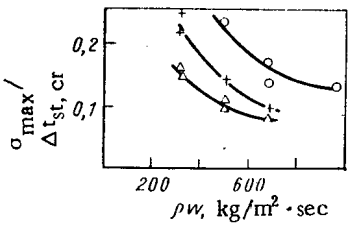

Fig. 2

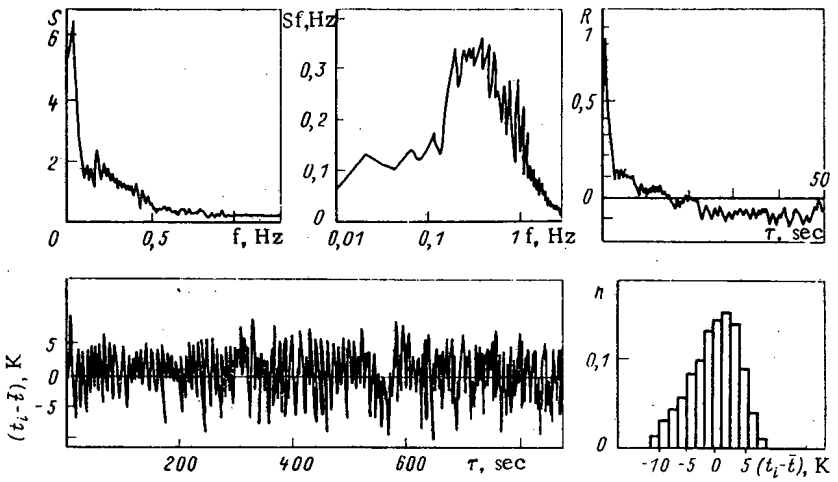

Fig. 3

Fig. 2. Dependence of $\sigma_{max}/\Delta t_{st,cr}$ on the mass velocity ρw for pressures of 7.9 (Δ), 9.8 (○), and 13.7 MPa (+), respectively.

Fig. 3. Statistical characteristics of the temperature pulsations for p = 9.9 MPa, ρw = 500 kg/m²·sec, and σ = 9.3°K.

face σ and S(f) was carried out in combination with the procedure of [1]. The equivalent frequency was determined from the relationship

$$f\bar{l} = \int_0^{f_0} Sf^2\,df \Big/ \int_0^{f_0} S\,df, \tag{4}$$

where f_0 is the frequency satisfying the relationship

$$\int_0^{f_0} S\,df = 0.95. \tag{5}$$

The maximum values σ_{max} on the inner surface of a tube in the heat exchange crisis zone are of special interest. The values of σ_{max} depend on the pressure, mass velocity of the steam–water flow, and critical density of the thermal flux. The values of σ_{max} obtained in this paper and in [1] are compared in Fig. 1. Good agreement of these data is observed. The dependences of $\sigma_{max}/\Delta t_{st,cr}$ on the mass velocity are presented in Fig. 2. The value of $\Delta t_{st,cr}$ is determined by the relationship

$$\Delta t_{st,cr} = \frac{q_2}{\alpha_2} - \frac{q_1}{\alpha_1}, \tag{6}$$

where q is the thermal flux and α is the heat transfer coefficient. The subscripts "1" and "2" refer, respectively, to the start and end of the heat exchange crisis zone. It follows from Fig. 2 that $\sigma_{max}/\Delta t_{st,cr}$ increases as ρw decreases for a fixed pressure. For a constant mass velocity, $\sigma_{max}/\Delta t_{st,cr}$ has its largest value at a pressure of ∿10 MPa.

An example of a record of the values of the wall temperature and the results of its statistical analysis are given in Fig. 3. In addition to the spectral density S(f) and the function fS(f), the normalized autocorrelation function R(τ) and the probability distribution function of the repeatability of the temperature pulsations $n(t - \bar{t})$ are also given. It follows from consideration of the function fS(f) that the band of recorded frequencies is practically limited by the value of 2 Hz, and no predominant frequency of any kind has been detected in it. The spectral density curve has a maximum af f ≤ 0.1 Hz, which is probably associated with the effect of common loop instabilities – oscillations in the sodium and water temperatures (Figs. 4 and 5).

The values of the equivalent frequencies are 0.3–0.55 Hz for pressures of p = 9.8 and 13 MPa and 0.95 Hz for p = 7.9 MPa. The experimental data of the statistical characteristics

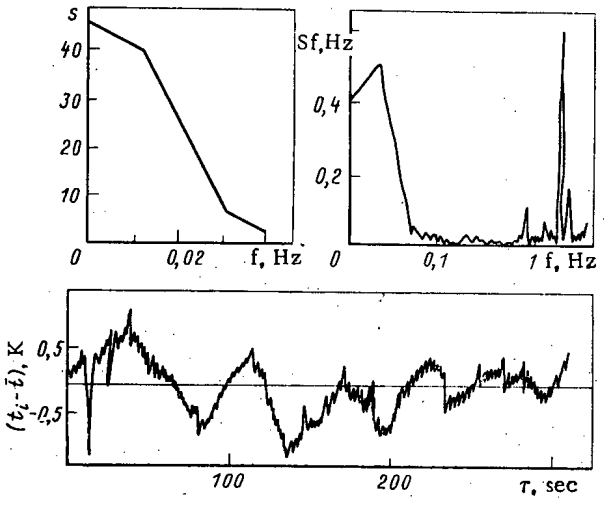

Fig. 4

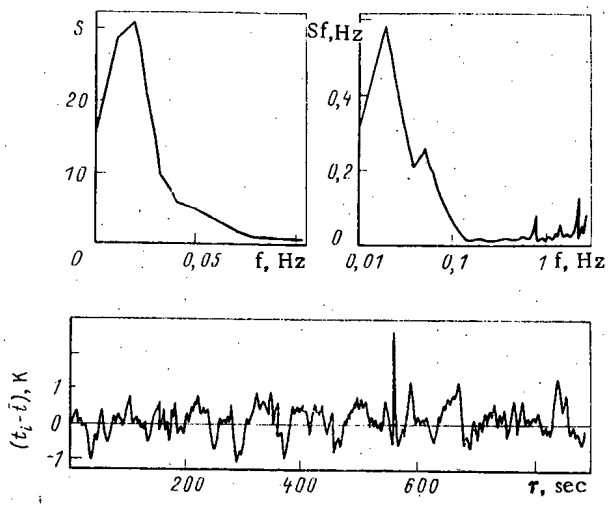

Fig. 5

Fig. 4. Statistical characteristics of the temperature pulsations of sodium at the entrance for a water pressure of 7.9 MPa and ρw = 340 kg/m^2·sec.

Fig. 5. Statistical characteristics of the temperature pulsations of water at the entrance for p = 9.8 MPa and ρw = 960 kg/m^2·sec.

of temperature pulsations in the heat-transmitting wall of a sodium–water steam generator in the heat exchange crisis zone for ρw = 340–1000 kg/m^2·sec, p = 8–14 MPa, and q = 0.4–2 MW/m^2 can be used to calculate the longevity of a steam-generating tube in a sodium–water steam generator. In the investigated range of parameters the greatest temperature pulsations (σ_{max} = 15°K) are recorded at a pressure of 10 MPa.

One can draw the following conclusions from the results of this paper:

the frequency spectrum of wall temperature pulsations in the heat exchange crisis zone is of the nature of a random process;

the equivalent frequencies for p = 10–14 MPa are found in the 0.3–0.55 Hz range; and

the mean-square values of the wall temperature pulsations decrease practically linearly as the mass velocity increases.

LITERATURE CITED

1. V. A. Vorob'ev et al., in: Seminar TF-74 "Investigations of the Critical Thermal Fluxes in Bunches of Rod" [in Russian], Izd. SEV, Moscow (1974), p. 267.
2. B. V. Kebadze et al., At. Énerg., 39, No. 4, 250 (1975).
3. K. Roko et al., in: Proc. 6th Int. Heat Transfer Conf., Vol. 1, Toronto (1978), p. 429.
4. N. S. Grachev and V. V. Khudasko, Teplofiz. Vys. Temp., No. 4, 334 (1978).

ACCUMULATION OF ^{232}U IN THE CYCLIC UTILIZATION OF FUEL IN THE VVÉR-440

T. S. Zaritskaya, L. V. Matveev,
A. P. Rudik, and É. M. Tsenter

UDC 621.039.516.22

The growth of nuclear power inevitably leads to the reuse of nuclear fuel. This may involve the direct use of depleted fuel from reactors of one type in reactors of another type [1], or the reenrichment of spent fuel and its use in a reactor of the same type. The present article is devoted to an analysis of certain aspects of this problem as applied to the VVÉR-440.

Earlier papers [2-4] took account of the fact that a certain amount of ^{232}U is accumulated in the irradiation of nuclear fuel in a reactor. This nuclide can complicate the reuse of reprocessed uranium by worsening the radiation environment at various stages of the fuel cycle [3]. ^{232}U is formed in nuclear fuel in the following transformation chains:

1. $^{238}U(n, 2n)^{237}U(\beta^-)^{237}Np(n, 2n)^{236}Np\ (50\%, \beta^-)^{236}Pu\ (\alpha)^{232}U.$
2. $^{235}U\ (n, \gamma)\ ^{236}U\ (n, \gamma)\ ^{237}U\ (\beta^-)\ ^{237}Np\ (n, 2n)^{236}Np\ (50\%, \beta^-)^{236}Pu\ (\alpha)^{232}U.$
3. $^{234}U\ (\alpha)\ ^{230}Th\ (n, \gamma)^{231}\ Th\ (\beta^-)\ ^{231}Pa\ (n, \gamma)^{232}\ Pa\ (\beta^-)^{232}U.$
4. $^{235}U\ (\alpha)\ ^{231}Th\ (\beta^-)\ ^{231}Pa\ (n, \gamma)\ ^{232}Pa\ (\beta^-)\ ^{232}U.$
5. $^{234}U\ (n, 3n)\ ^{232}U.$
6. $^{236}U\ (n, \gamma)\ ^{237}U\ (\beta^-)\ ^{237}Np\ (n, 2n)\ ^{236}Np(50\%, \beta^-)^{236}Pu\ (\alpha)\ ^{232}U.$
7. $^{230}Th\ (n, \gamma)\ ^{231}Th\ (\beta^-)^{231}Pa\ (n, \gamma)\ ^{232}Pa\ (\beta^-)\ ^{232}U.$
8. $^{231}Pa\ (n, \gamma)\ ^{232}Pa\ (\beta^-)\ ^{232}U.$
9. $^{237}Np\ (n, 2n)\ ^{236}Np\ (50\%, \beta^-)\ ^{236}Pu\ (\alpha)\ ^{232}U.$

Using the combination–iteration method [5], we calculated the accumulation of ^{232}U with sufficient accuracy by limiting ourselves to a once-through solution of the space-energy problem. The method employs a two-component representation of the reaction rate [6], and both the effective thermal neutron flux φ_T, and the effective hardness of the spectrum (γ_S) (a factor characterizing the ratio of the resonance and thermal fluxes) determined by the TRIFON program [7] in a 26-group approximation are varied with a change of the concentration of all fissionable nuclides in the reactor. The physical characteristics of the nuclides taking part in the accumulation of ^{232}U are listed in Table 1. Since the product of the hardness

TABLE 1. Physical Characteristics of Nuclides

Nuclide	$T_{1/2}$	Reaction	σ, b	I, b
^{230}Th *	$8{,}0\cdot10^4$ yrs	n, γ	23,2	505,0
^{231}Th	25,52 h	β^-	—	—
^{231}Pa	$3{,}28\cdot10^4$ yrs	n, γ	210	750
^{232}Pa	1,31 days	β^-	—	—
^{232}U *	72 yrs	$n, \gamma+f$	148,3	300
^{234}U *	$2{,}45\cdot10^5$ yrs	n, γ	100	315
^{235}U	$7{,}038\cdot10^8$ yrs	n, γ	98,5	58,1
		f	529,1	119,6
^{236}U	$2{,}342\cdot10^7$ yrs	n, γ	5,2	125,6
^{237}U	6,75 days	β^-	—	—
^{238}U	$4{,}468\cdot10^9$ yrs	n, γ	2,8	10,64
		f	0	1,44
^{236}Np	22,5 h	50% β^-, 50% ε	—	—
^{237}Np	$2{,}14\cdot10^6$ yrs	n, γ	195,1	218,2
^{236}Pu *	2,85 yrs	n, γ	33	100
		f	165	478,5

Translated from Atomnaya Énergiya, Vol. 54, No. 5, pp. 333-336, May, 1983. Original article submitted February 22, 1982.

 0038-531X/83/5405-0332$07.50

TABLE 2. Accumulation of ^{236}Pu and ^{232}U in Depleted Fuel as a Function of Burnup

Chain	Burnup, kg/ton				
	7,45	14,9	22,4	29,8	37,2
1. $^{238}U(n, 2n)$ . . . ^{236}Pu	$4,22\cdot10^{-12}$	$1,49\cdot10^{-11}$	$2,92\cdot10^{-11}$	$4,52\cdot10^{-11}$	$6,10\cdot10^{-11}$
^{232}U	$2,10\cdot10^{-13}$	$1,45\cdot10^{-12}$	$4,24\cdot10^{-12}$	$8,74\cdot10^{-12}$	$1,47\cdot10^{-11}$
2. $^{235}U(n, \gamma)$ . . . ^{236}Pu	$9,54\cdot10^{-12}$	$6,58\cdot10^{-11}$	$1,90\cdot10^{-10}$	$3,84\cdot10^{-10}$	$6,34\cdot10^{-10}$
^{232}U	$3,48\cdot10^{-13}$	$4,84\cdot10^{-12}$	$2,10\cdot10^{-11}$	$5,70\cdot10^{-11}$	$1,17\cdot10^{-10}$
3. $^{234}U(\alpha)$ . . . ^{232}U	$3,43\cdot10^{-12}$	$2,40\cdot10^{-11}$	$7,05\cdot10^{-11}$	$1,44\cdot10^{-10}$	$2,42\cdot10^{-10}$
4. $^{235}U(\alpha)$ . . . ^{232}U	$2,54\cdot10^{-12}$	$8,31\cdot10^{-12}$	$1,52\cdot10^{-11}$	$2,19\cdot10^{-11}$	$2,73\cdot10^{-11}$
5. $^{234}U(n, 3n)$ ^{232}U	$1,05\cdot10^{-11}$	$1,88\cdot10^{-11}$	$2,49\cdot10^{-11}$	$2,92\cdot10^{-11}$	$3,14\cdot10^{-11}$
^{236}Pu	$1,38\cdot10^{-11}$	$8,10\cdot10^{-11}$	$2,18\cdot10^{-10}$	$4,30\cdot10^{-10}$	$6,85\cdot10^{-10}$
Total for chains 1—5					
^{232}U	$1,70\cdot10^{-11}$	$5,74\cdot10^{-11}$	$1,35\cdot10^{-10}$	$2,61\cdot10^{-10}$	$4,32\cdot10^{-10}$
7. $^{230}Th(n, \gamma)$ . . . ^{232}U	$1,67\cdot10^{-11}$	$5,71\cdot10^{-11}$	$1,08\cdot10^{-10}$	$1,62\cdot10^{-10}$	$2,13\cdot10^{-10}$
8. $^{231}Pa(n, \gamma)$ . . . ^{232}U	$8,46\cdot10^{-12}$	$1,40\cdot10^{-11}$	$1,71\cdot10^{-11}$	$1,87\cdot10^{-10}$	$1,87\cdot10^{-11}$
Total ^{232}U	$4,22\cdot10^{-11}$	$1,28\cdot10^{-10}$	$2,61\cdot10^{-10}$	$4,42\cdot10^{-10}$	$6,64\cdot10^{-10}$

of the spectrum and the resonance integral (γ_S, I) is determined directly in the TRIFON program, and not each quantity separately, it is possible to take $\gamma_S(0) = 1$ in the kinetic equations. The values of σ and $\gamma_S I$ marked with an asterisk in Table 1 were not determined by the TRIFON program. In these cases the cross sections were taken from [8]. The actual physical value $(\gamma_S)_{phys} = 0.5$ can be found by comparing the values of $(\gamma_S I)_{TRIFON}$ for ^{235}U with the tabulated value of the resonance integral:

$$(\gamma_s I)_{\text{TRIFON}} = (\gamma_s)_{\text{phy}} I_{\text{tab}}. \quad (1)$$

Therefore, the values of the resonance integrals in Table 1 marked with an asterisk are half as large as the conventional values of I. The thermal cross sections for these nuclides were taken at 0.0253 eV, whereas in the TRIFON program they were averaged over the energy spectrum in groups 25 and 26. The half-lives listed in Table 1 were taken from [9]. The initial thermal flux was $1.6\cdot10^{13}$ neutrons/cm^2·sec, which corresponds to a specific power W = 84.5 MW/ton [10].

Most processes leading to the formation of ^{232}U involve the threshold reactions (n, 2n) or (n, 3n) for ^{234}U with threshold energies of 6-7 and 12.6 MeV, respectively. These reactions were taken into account by introducing [5] the effective resonance integral I^{ef}:

$$I^{ef}_{n,2n} = \langle\sigma_{n,2n}\rangle \frac{\xi\sum_s}{\sum_{tot}} P, \quad (2)$$

where $\langle\sigma_{n,2n}\rangle$ is the microscopic cross section for the (n, 2n) reaction averaged over the fission spectrum; $\xi\Sigma_S$, slowing-down power; Σ_{tot}, macroscopic cross section for the interaction of neutrons with energies ~8 MeV with the fuel element material; and P, probability that a fission neutron interacts in some fuel element before its energy falls below the reaction threshold. The calculated values of $I^{ef}_{n,2n}$ in mb for the VVÉR-440 are as follows (for ^{234}U $I^{ef}_{n,3n}$): ^{234}U, 0.13; ^{238}U, 33; ^{237}Np, 6.6. These values of $I^{ef}_{n,2n}$ enter the kinetics equations for $\gamma_S(0) = 1$.

Table 2 lists the calculated values of the accumlation of ^{236}Pu and ^{232}U in depleted VVÉR-440 fuel with an initial ^{235}U content of 3.6% for various values of the fuel burnup (kilograms of fission products per ton of initial mixture of ^{238}U and ^{235}U). The calculations were performed for fuel elements on the periphery of an assembly. Figure 1 shows the accumulation of ^{232}U and ^{236}U in uranium from the various transformation chains (at the instant of unloading from the reactor) as a function of fuel burnup. It was assumed that before the beginning of irradiation the fuel contained 0.03% ^{234}U, $8.5\cdot10^{-8}$% ^{230}Th, and $3.5\cdot10^{-9}$% ^{231}Pa (the ^{230}Th and ^{231}Pa contents correspond to the amounts accumulated in fuel per year as a result of the alpha decay of ^{234}U and ^{235}U, respectively). The ^{232}U content in reprocessed uranium has a substantial effect on the cooling time of depleted fuel before chemical reprocessing, during which time part of the ^{236}Pu accumulated in the fuel is transformed into ^{232}U as a result of alpha decay with a half-life of 2.85 yrs. In addition, it should be emphasized that there is an appreciable contribution to the total accumulation of ^{232}U from chains beginning with ^{231}Pa, and particularly ^{230}Th. The amounts of ^{232}U and ^{236}Pu accumulated in chain 9 in the second and subsequent irradiation cycles are determined by the completeness of the chemical removal of neptunium from the reprocessed uranium. For a 10^{-3}% ^{237}Np content in the fuel before the

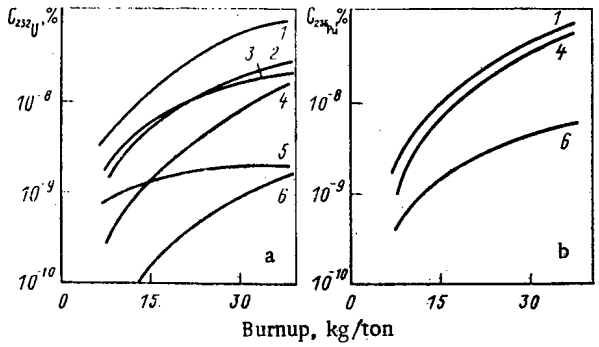

Fig. 1. Dependence of accumulation of (a) ^{232}U and (b) ^{236}Pu on fuel burnup: 1) total accumulation ^{232}U (a) and ^{236}Pu (b); 2) accumulation of ^{234}U; 3) ^{230}Th; 4) ^{235}U; 5) ^{231}Pa; 6) ^{238}U.

start of irradiation, the contribution of this chain to the total accumulation of ^{232}U is less than 4%. Chain 9 was not taken into account in further calculations.

As a result of chemical reprocessing, uranium with an isotopic composition different from that of unirradiated uranium may be extracted from spent fuel. The reprocessed uranium contains ^{236}U and ^{232}U, which were not present in unirradiated fuel made of natural uranium. The concentrations of ^{234}U and ^{235}U in reprocessed uranium decrease as a result of their burnup in the reactor. To reuse the reprocessed uranium the ^{235}U content must be increased to 3.6%.

The isotopic composition of uranium obtained as a result of enrichment depends on the ratio of natural and reprocessed uranium entering the separation plant. Two versions were considered: a simple transformation and breeding. In the first version it was assumed that the reprocessed uranium is mixed with natural uranium in such a ratio that the amount of enriched uranium obtained is exactly equal to the amount of uranium put into the VVÉR-440 before the start of the preceding irradiation cycle. In the second version it was assumed that the amount of enriched uranium obtained is twice as large as in the preceding irradiation cycle. The length of one cycle is 7 yrs: 3 yrs irradiation of the fuel in the reactor, 3 yrs cooling of the depleted fuel before chemical reprocessing, and 1 yr for the manufacture of new fuel.

In the first cycle, fuel made of natural fertile material was loaded into the reactor. Uranium reprocessed from depleted fuel with a burnup of 30 kg/ton entered the separation plant, where it was enriched to 3.6%, after which new fuel for the VVÉR-440 was manufactured from it. The change in isotopic composition of the uranium during its enrichment was calculated by the method described in [11, 12]. Before the start of the second irradiation cycle the fuel contains a certain amount of ^{236}U and ^{232}U. Because ^{236}U is present, chain 6 will operate in the second irradiation cycle, and large amounts of ^{232}U and ^{236}Pu will be accumulated. Part of the ^{232}U present in the fuel before the start of irradiation burns up in the reactor, and the rest contributes to the accumulation of ^{232}U in the second cycle. The reprocessed uranium is again sent to the separation plant, etc. The concentration of ^{232}U in uranium increases from cycle to cycle until the following conditions are satisfied:

1. The ^{236}U content in the fuel comes to equilibrium (the accumulation of ^{236}U per irradiation cycle is compensated by the dilution of reprocessed uranium by natural fertile material);

2. The ^{234}U content in the fuel comes to equilibrium (the increase in the ^{234}U concentration after leaving the separation plant is compensated by its burnup in the reactor);

3. The amount of ^{232}U newly formed per irradiation cycle in the reactor is compensated by its decrease due to burnup, decay, and dilution by natural fertile material during enrichment.

In the calculations we did not take account of the change of the physical characteristics (σ and $\gamma_S I$) resulting from the increase of the ^{236}U content in the fuel during recycling. All the conditions are satisfied after 14-15 irradiation cycles for simple conversion, and after 6-7 cycles for the breeding version. However, 90% of the equilibrium content of ^{232}U in uranium is reached much earlier; after 7-8 and 3 irradiation cycles, respectively.

The change in the relative content (K) of ^{234}U and ^{236}U in reprocessed uranium during recycling is shown in Fig. 2. The content of these isotopes in reprocessed uranium after the first irradiation cycle, 0.018 and 0.43%, respectively, was taken as a unit. Figure 3 shows

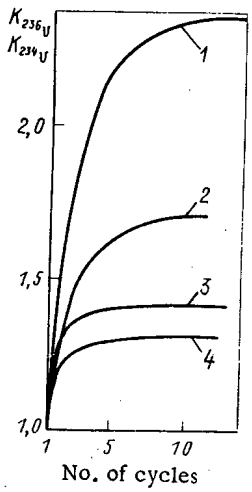

Fig. 2

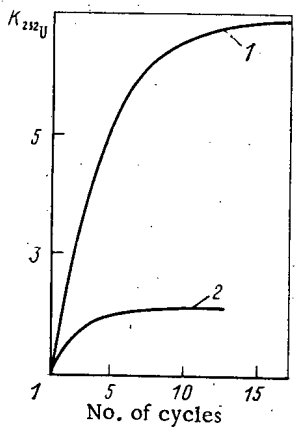

Fig. 3

Fig. 2. Change of the relative content of ^{236}U (1, 3) and ^{234}U (2, 4) in reprocessing uranium during recycling 1, 2 and 3, 4 are for simple conversion and breeding, respectively.

Fig. 3. Change of relative ^{232}U content in reprocessing uranium during recycling for: 1) simple transformation; 2) breeding.

the change of the relative content of ^{232}U in reprocessed uranium calculated by assuming that the fuel had been stored for 1 yr from the time of the last chemical purification from thorium and protactinium up to the start of irradiation in the reactor, and a 3 yr cooling of depleted fuel before chemical reprocessing. The ^{232}U content in uranium reprocessed after the first irradiation cycle is $6.9 \cdot 10^{-8}$%.

In conclusion, we note that the uncertainty in the effective reaction cross sections for the formation of ^{232}U, particularly the (n, 2n) and (n, 3n) reactions, can lead to a change in the calculated ^{232}U content in reprocessed uranium by about a factor of two, but this uncertainty has little effect on the values obtained for the equilibrium content of ^{232}U.

LITERATURE CITED

1. T. S. Zaritskaya, A. K. Kruglov, and A. P. Rudik, At. Energ., 46, 183 (1979).
2. T. S. Zaritskaya et al., At. Energ., 48, 67 (1980).
3. L. V. Matveev and É. M. Tsenter, At. Tekh. Rubezhom, No. 4, 10 (1980).
4. Yu. G. Bobkov et al., At. Energ., 48, 395 (1980).
5. T. S. Zaritskaya and A. P. Rudik, "Combination-iteration method for calculating fuel burnup in nuclear reactors (I. Single-Stage Kinetics)," Preprint ITÉF-122, Moscow (1980).
6. A. K. Kruglov and A. P. Rudik, Artificial Isotopes and a Procedure for Calculating Their Formation in Nuclear Reactors [in Russian], Atomizdat, Moscow (1977).
7. A. Ya. Burmistrov and B. P. Kochurov, "Space-energy distribution of neutrons in a cylindrical cell of a reactor (TRIFON Program)," Preprint ITÉF-107, Moscow (1978).
8. Neutron Cross Sections, BNL-325 (1973).
9. C. Lederer and V. Shirley, Tables of Isotopes, Seventh Edition, Wiley, New York (1978).
10. V. V. Semenov, "Basic physicotechnical characteristics of VVÉR reactor installations," Preprint IAÉ-3104, Moscow (1979).
11. A. de la Garza, Nucl. Technol. 32, 176 (1977).
12. A. de la Garza, G. Garrett, and J. Murphy, Chem. Eng. Sci., 15, 188 (1961).

MORPHOLOGY AND STRUCTURE OF THE OXIDE FILMS FORMED ON OKh16N15M3B STEEL IN DISSOCIATING N_2O_4 AT 1170-1370°K

V. N. Vechkanov, A. N. Khodan, A. P. Zakharov,
V. P. Isakov, A. A. Antonov, and A. S. Chernikov

UDC 621.039.548.535

There are prospects for using nitrogen tetroxide and mixtures based on it as coolants for fast reactors [1], so it was necessary to examine the reactions of OKh16N15M3B austenitic stainless steel with dissociating N_2O_4 in the range 1170-1370°K at a pressure of 0.1 MPa.

The tests at 1170-1370°K were performed in a medium represented by a mixture of NO, O_2, and NO_2, formed by thermal dissociation:

$$N_2O_4 \rightleftharpoons 2NO_2 \rightleftharpoons 2NO + O_2.$$

At 1170°C, the medium had the following equilibrium composition: NO 66 mass %, O_2 33 mass %, and NO_2 1 mass %. On raising the temperature to 1370°K, the NO_2 content fell to a fraction of a percent.

Specimens were made from tubes of OKh16N15M3B steel of diameter 6 mm, height 10 mm, and wall thickness 0.4 mm, which were quenched in air after annealing at 1320°K. The surfaces of the tubes were polished electrolytically after quenching. The specimens were preheated to a given temperature in argon. The times spent in the coolant ranged from 1 to 30 h at 1170, 1270, and 1370°K, as measured with a Chromel–Alumel thermocouple and maintained constant to ±20°C. After oxidation, the specimens were cooled in air and stored in a desiccator. The masses of the specimens were measured by weighing periodically with an error of ±0.05 mg. The morphology and composition of the oxide films were examined by scanning electron microscopy and with a Camebax MBX 100 microprobe.

The oxidized specimens were pressed at 420°K under a pressure of 0.3 MPa in a mixture of bakelite and pyrographite powders taken in the ratio 2:1, were ground with emergy paper, and were polished with diamond powders of particle sizes 10/7, 5/3, and 1/0 μm. Electron micrographs of the oxidized surfaces were taken without any special preparation.

Tests at 1170°K. In the initial stages of oxidation up to 10 h, there was active growth of deposits along the scratches (Fig. 1a). The formation of these deposits is associated with detachment of the initial oxide layer at the edges of the scratches on account of the increase in the stresses on oxidation. As a result, cracks form on these parts earlier than on the smooth surface. The thicknesses of the oxide layer at the grain boundaries become appreciably less than on the rest of the surface. Subsequently, these boundaries gradually expand. The disruption of the protection by the oxide film over much of the area becomes appreciable after about 30 h. Characteristic domed areas are formed, which are produced by crystals of size about 0.5-1.5 μm.

Tests at 1270°K. The effects of the grain boundaries became apparent in oxidation for less than 2 h (Fig. 1b). After 5 h, there were complex formations of area 300-400 μm containing crystals about three times larger than those on the rest of the surface.

Tests at 1370°K. Preferential grain-boundary oxidation was not observed even during the first hour of test. After 10 h, the surface was covered with domes of diameter 230 μm, with the bases covered by networks of cracks. The cracks may be due to a difference in the coefficients of thermal expansion between the oxide film and the steel or to growth of the oxide film. The number of cracks and the extent of them increase with the oxidation time (Fig. 1c). After 5 h, the crystals acquired a rounded form. On examining the inner surface of film removed from the alloy, it was found that the facets of the crystals were preserved. The average crystal sizes in the outer layer of the oxide after 30 h of test at 1170, 1270, and 1370°K were about 0.6, 1.3, and 4 μm, correspondingly.

Translated from Atomnaya Énergiya, Vol. 54, No. 5, pp. 336-339, May, 1983. Original article submitted May 12, 1982.

 0038-531X/83/5405-0336$07.50

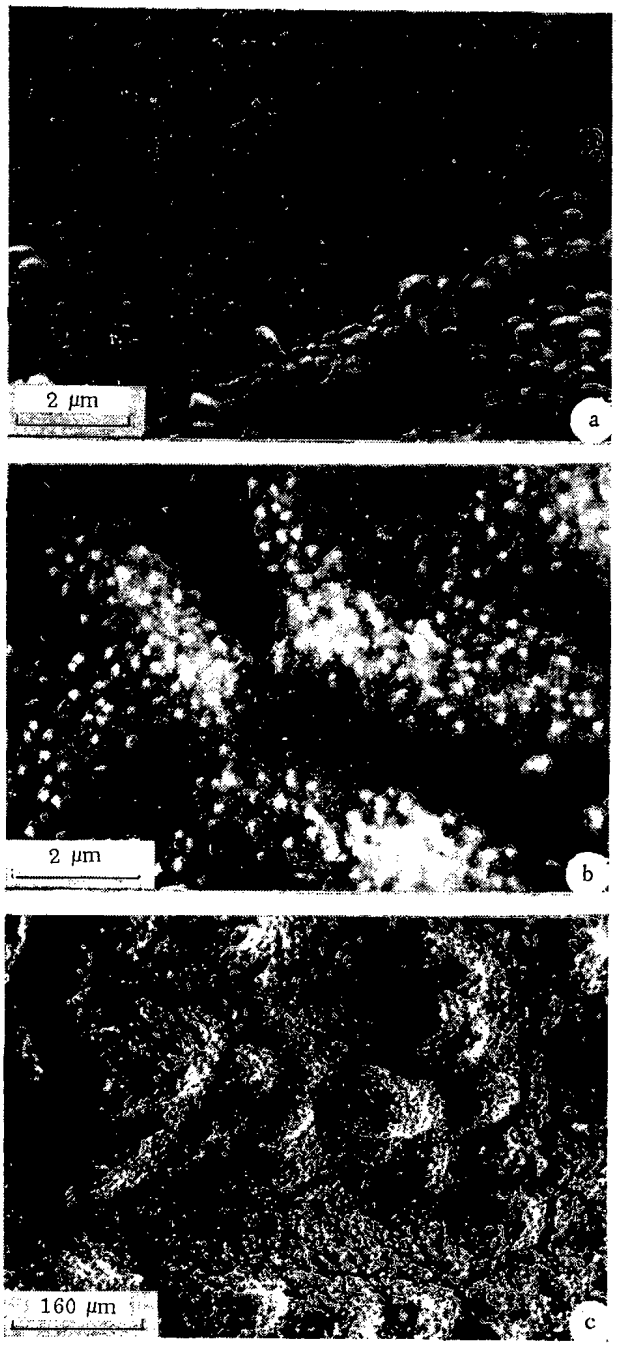

Fig. 1

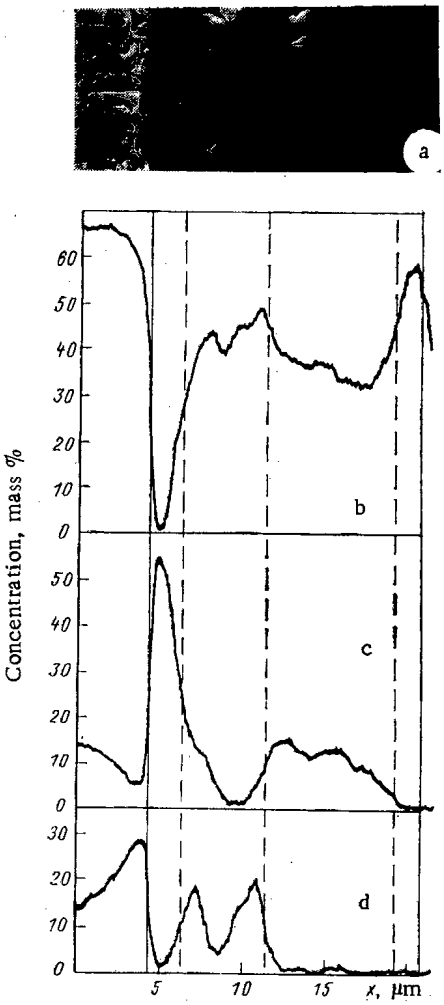

Fig. 2

Fig. 1. Surface of OKh16N15M3B steel after testing in N_2O_4 at 1170°K for 1 h (a); 1270°K, 1 h (b); 1370°K, 30 h (c).

Fig. 2. Microanalysis of a cross section of a specimen tested at 1370°K for 1 h: a) secondary electron image; b-d) distributions of Fe, Cr, and Ni, correspondingly.

Microprobe analysis gave the relative contents of Fe, Ni, and Cr in 10-15 different parts of the oxide film of size 25 × 25 μm. There was a reduction in the Cr/Fe ratio on the undamaged surface of the film after about 5 h at 1170°K, and after 2 h at 1270°K or 1 h at 1370°K. However, the chromium content was increased by a factor of 5-12 in the exfoliated parts of the film.

Microanalysis of cross sections showed that the distributions of the major elements in the oxide film were not qualitatively altered. The layer adjoining the oxide film was depleted in chromium. After 30 h, the chromium content at the steel–oxide boundary was about

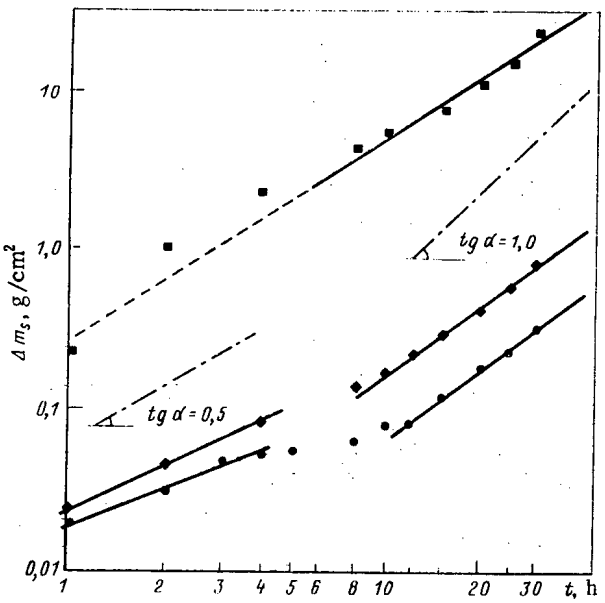

Fig. 3. Oxidation kinetics of steel OKh16N15M3B in N_2O_4 at 1170 (●), 1270 (◆), and 1370°K (■).

3.7% at 1370°K, about 5.5% at 1270°K, and about 6.8% at 1170°K, with the iron content somewhat reduced and the nickel content increasing, the latter attaining 29% at 1170°K. A three layer structure was found (Fig. 2) for oxide films of thickness more than 2-3 μm. The layer nearest the steel consisted of Cr_2O_3 with small amounts of Fe and Ni. The outer layer was formed by Fe_2O_3. Within these layers was a heterophase region formed evidently by two spinel structures: $(Ni_xFe_{1-x})\,Cr_2O_4$ and $(Fe_3O_4)_y\,(FeCr_2O_4)_{1-y}$. The value of x did not exceed 0.1, whereas y can attain values close to 1, as it increases the temperature and oxidation time. For example, y = 0.93 and 0.75 for specimens oxidized for 10 h at 1270°K and 1 h at 1370°K, correspondingly.

Figure 3 shows the gain in weight during oxidation. The oxidation begins during the preliminary heating in argon, which contains traces of oxygen and water, and results in the formation of a thin layer of Cr_2O_3, whose outer part acquires the spinel structure on the basis of solid solutions of Fe_3O_4 and $FeCr_2O_4$ [2, 3], so the increase in weight was measured after oxidation for 1 h after admitting the coolant. The absence of an inflection on the curve of 1370°K may be due to changes in the properties of the protective Cr_2O_3 layer, since the Cr/Fe ratio changes only slightly. In the case of pure Cr_2O_3 in an oxygen atmosphere, the transition to inherent ionic conduction occurs at 1400-1600°K [4]. The addition of Fe_2O_3 reduces the conductivity, but the change in the ionic transport mechanism occurs at a lower temperature (1000-1100°K). As the iron content in the Cr_2O_3 film was not more than 1%, the marked increase in the oxidation rate on raising the temperature may be associated with the change in conductivity of the Cr_2O_3. However, this may not be the only effect.

As the chromium is selectively oxidized and the layer based on Cr_2O_3 accumulates, the surface of the steel becomes depleted in chromium. In the case of Fe–Cr binary alloys, their oxidation at 1270-1570°K is accompanied by a reduction in the chromium content at the alloy–oxide boundary by a factor of 2-3 [5]. When the oxide film has exfoliated, the chromium-depleted alloy begins to oxidize. If the chromium content is less than 13%, a layer of the spinel $FeCr_2O_4$ is formed, whose protective properties are worse than those of Cr_2O_3 [6], which may lead to catastrophic oxidation of the alloy. Estimates indicates that the reduction in the surface chromium concentration at a depth of 2 μm at 1170°K occurs in about 10 h, as against about 2 h at 1270°K and about 0.5 h at 1370°K, and the chromium concentration at the steel–oxide boundary in all three cases is close to 9.5%. These oxidation times agree well with the changes in the Cr/Fe ratio in the oxide film. It is possible that a chromium concentration gradient of 3% per μm is critical for this steel. If the oxidation time is longer, the gradient is reduced, which reduces the flux of chromium atoms to the surface, and therefore the protective film is not restored by incoming chromium when individual parts of the film become detached.

The smaller thickness of the oxide film at the grain boundaries (Fig. 1) is probably due to increase in the chromium content by 4-5%. In particular, the oxidation rate of an Fe–Cr alloy is minimal at about 20% chromium [7]. Recrystallization also influences the formation of oxide at temperature over 1170°K [8].

The lower chromium contents in the outer layers of the oxides are evidently due to evaporation at temperatures above 1070°K in accordance with the reaction

$$2Cr_2O_3 + 3O_2 \leftrightarrows 4CrO_3\uparrow.$$

The formation of the dome parts is evidently due to decomposition of spinel oxides of $(Fe_3O_4)_y$ $(FeCr_2O_4)_{1-y}$ type, detachment of the Fe_2O_3 film, and evaporation of the chromium oxide through the pores and channels in the Fe_2O_3 layer, and the different sizes of the crystals on the inner and outer sides of the oxide film may be responsible for the growth of the Fe_2O_3 crystallites at the expense of the small Fe_2O_3 crystals formed by the decomposition of the spinel.

LITERATURE CITED

1. Physicochemical and Thermophysical Properties of the Chemically Reacting System $N_2O_4 \rightleftarrows 2NO_2 \rightleftarrows 2NO + O_2$ [in Russian], Nauka i Tekhnika, Minsk (1976).
2. H. Yearia, J. Kortright, and R. Langenheim, J. Chem. Phys., 22, 1196 (1954).
3. C. Leygraf, G. Hulquist, and S. Ekelund, Surface Sci., 51, 409 (1975).
4. K. Hay, F. Hicks, and D. Holmes, Werkst. Korros., 21, 917 (1970).
5. D. Whittle and G. Wood, J. Elekrochem. Soc., 115, 133 (1968).
6. A. Seybolt, ibid., 107, 147 (1961).
7. P. Footner, D. Holmes, and D. Mortimer, Nature, 216, 54 (1967).
8. S. Horibe and T. Nakayama, Corros. Sci., 15, 589 (1975).

TWO STAGES IN THE HARDENING OF IRRADIATED METALS

Sh. Sh. Ibragimov, V. F. Reutov, and K. G. Farkhutdinov

UDC 621.039.553

Two stages of hardening have been observed from curves relating the strength of a metal to the radiation damage level [1-5]. In the first stage, which corresponds to a low level of damage (up to about 10^{-2} displacements/atom), the hardening rate is small, whereas in the second, at medium levels of damage (up to about 1 displacement/atom), it increases sharply. An important point is that at each stage the hardening is dependent not only on the damage, but also on the energy spectrum of the primary ejected atoms (PEA). Scientific and practical interest attaches to the effects of the energy spectrum on the hardening and the nature of the hardening defects, particularly in relation to the development of radiation-resistant materials for fusion reactors. This is because information is obtained on the radiation resistance of materials for such reactors by using charged particles of energy at least 10 MeV [3-6], fission fragments [2, 7], and fission neutrons [9], i.e., under conditions when the PEA energy spectra differ substantially from one another and also from the PEA spectrum for neutrons from a fusion reaction.

We have therefore examined the behavior of the hardening and the nature of the hardening defects in copper and nickel as affected by the damage level produced by neutrons from a nuclear reactor and by protons and α particles of energy 28 and 40 MeV, correspondingly. Stretching tests were performed, the microhardness was measured, and the specimens were examined by transmission electron microscopy.

METHODS

The specimens of cooper (99.99%) and nickel (99.98%) were annealed for 1 h under vacuum at $7 \cdot 10^{-3}$ Pa (at 850 and 950°C, correspondingly), and then they were irradiated in a VVR-K reactor and with the isochronous cyclotron at the Institute of Nuclear Physics, Academy of Sciences of the USSR, at temperatures not exceeding 60°C. The fluences were in the ranges $1.7 \cdot 10^{20}$-$5.4 \cdot 10^{21}$ m^{-2} in α-particle irradiation, $5 \cdot 10^{20}$-$2 \cdot 10^{22}$ m^{-2} in proton irradiation, and $1 \cdot 10^{21}$-$1 \cdot 10^{24}$ m^{-2} ($E > 0.1$ MeV) in neutron irradiation.

Translated from Atomnaya Énergiya, Vol. 54, No. 5, pp. 339-342, May, 1983. Original article submitted June 22, 1982.

0038-531X/83/5405-0339$07.50

TABLE 1. Changes in the Yield Point ($\Delta\sigma_{0,2}$) and Microhardness (ΔH_μ) of Copper and Nickel at Various Levels of Radiation Damage Produced by Neutrons from a Nuclear Reactor, Protons (E_p = 28 MeV), and α Particles (E_α = 40 MeV)

Damage level, displacements/atom	$\Delta\sigma_{0,2}$, MPa		ΔH_μ, MPa	
	Cu	Ni	Cu	Ni
VVR-K spectrum neutrons				
$5{,}2\cdot10^{-5}$	9,6	9,8	99,0	116,5
$5{,}2\cdot10^{-4}$	21,3	23,2	137,0	147,1
$1{,}05\cdot10^{-3}$	26,8	50,0	156,2	171,5
$5{,}2\cdot10^{-3}$	78,4	—	203,0	—
$1{,}56\cdot10^{-3}$	93,1	175,4	254,8	235,6
$5{,}2\cdot10^{-2}$	127,2	—	345,9	—
Protons				
$1{,}1\cdot10^{-4}$	11,3	16,7	102,2	—
$4{,}2\cdot10^{-4}$	—	—	118,1	134,9
$5{,}6\cdot10^{-4}$	19,2	—	120,7	147,0
$1{,}3\cdot10^{-3}$	—	40,3	—	166,6
$1{,}8\cdot10^{-3}$	29,4	—	186,6	—
$2{,}5\cdot10^{-3}$	—	—	—	191,6
$3{,}5\cdot10^{-3}$	—	80,4	254,8	—
$7{,}0\cdot10^{-3}$	103,8	—	274,4	245,8
$9{,}2\cdot10^{-3}$	—	—	312,8	288,3
$1{,}2\cdot10^{-2}$	—	—	321,0	—
α-particles				
$5{,}1\cdot10^{-4}$	—	11,8	—	108,3
$7{,}0\cdot10^{-4}$	14,1	—	39,2	—
$1{,}2\cdot10^{-3}$	—	—	58,8	141,6
$2{,}1\cdot10^{-3}$	23,7	61,5	120,1	—
$3{,}5\cdot10^{-3}$	—	—	181,3	205,8
$8{,}1\cdot10^{-3}$	89,6	108,0	263,4	—
$1{,}0\cdot10^{-2}$	—	—	—	316,5
$1{,}2\cdot10^{-2}$	—	—	321,0	—
$1{,}7\cdot10^{-2}$	—	—	343,0	—

The microhardness was measured with a PMT-3 instrument (load on the indentor 0.49 N). The relative error of measurement was ±3%. The stretching tests with a strain rate of $4.5\cdot10^{-4}$ sec^{-1} were performed at room temperature. The relative error in determining the yield point was not more than ±6%.

The electron-microscope studies on the structure change were performed on specimens stretched by 1-1.5%.

The damage level (in displacements/atom) was calculated by computer by means of the Damage program [9].

RESULTS AND DISCUSSION

Table 1 gives the changes in microhardness and yield point for the metals at various damage levels. Identical relationships are obtained [10, 11] for the hardening by radiation on tension testing and microhardness measurement, and so we consider only the microhardness results below, as these were obtained for a somewhat larger number of specimens.

The curves in Fig. 1 show some characteristic features: firstly, no matter what the type of bombarding particle and the material, there are two pronounced stages of hardening; secondly, at identical damage level, the hardening is dependent on the nature of the bombarding particles, particularly in the second stage; and thirdly, the hardening rate in the first stage is appreciably less than that in the second.

The electron micrographs of the stretched specimens showed that in all cases there were clusters and dislocation loops, as well as decoration of the dislocation lines. The mean size and the concentration of the defect groups are dependent on the damage level and the type of bombarding particle.

The D-2-1/2 method was used in identifying the clusters and loops, which are groups of interstitial atoms and vacancies. In the first stage, groups of interstitial type predominate,

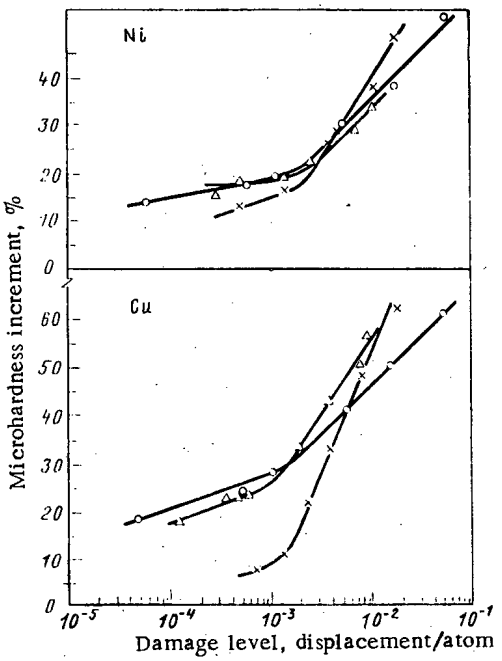

Fig. 1

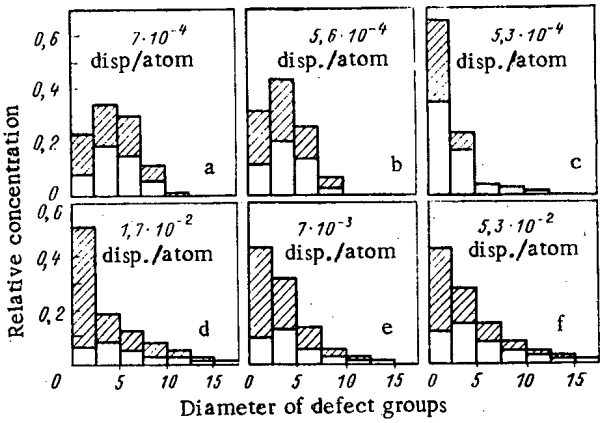

Fig. 2

Fig. 1. Dependence on damage level for the increments in microhardness in copper and nickel on irradiation by neutrons with the VVR-K spectrum (○), protons with E = 28 MeV (Δ), and α particles with E = 40 MeV (×).

Fig. 2. Histograms for the distributions of clusters of vacancy type (hatched region) and interstitial type (open part) in copper and various damage levels produced by α particles of energy 40 MeV (a, d), protons of energy 28 MeV (b, e), and by neutrons from a nuclear reactor (c, f).

TABLE 2. Concentrations and Mean Sizes of Clusters of Interstitial and Vacancy Types in Copper at Various Levels of Radiation Damage Produced by Neutrons from a Nuclear Reactor, Protons (E_p = 28 MeV), and α Particles (E_α = 40 MeV)

Damage level, displacement/atom	Cluster concentration, $\times 10^{21}$ m^{-3}, of various diameters						Mean diameter, nm	
	to 2,5 nm		2,5–5 nm		over 5 nm			
	vacancy	interstitial	vacancy	interstitial	vacancy	interstitial	vacancy	interstitial
Neutrons with the VVR-K spectrum								
$1{,}05\cdot10^{-4}$	1,8	2,2	0,3	1,1	—	0,7	2,8	3,0
$5{,}2\cdot10^{-4}$	3,1	3,7	0,6	2,9	0,1	1,3	3,0	3,2
$5{,}2\cdot10^{-3}$	8,0	5,7	2,0	8,0	2,0	4,4	3,0	4,3
$5{,}2\cdot10^{-2}$	12,6	5,0	5,4	6,0	4,7	8,1	3,6	5,4
Protons								
$5{,}6\cdot10^{-4}$	2,4	1,8	2,6	2,3	1,7	1,8	4,0	4,6
$1{,}8\cdot10^{-3}$	3,45	1,1	2,8	3,1	2,15	2,25	3,8	4,8
$7{,}0\cdot10^{-3}$	8,8	2,6	5,0	4,5	2,8	2,7	3,4	5,6
α-particles								
$7{,}0\cdot10^{-4}$	2,9	1,8	2,0	2,8	0,5	1,6	4,2	4,7
$2{,}1\cdot10^{-3}$	3,15	1,93	4,0	3,5	1,1	2,3	4,3	4,7
$8{,}1\cdot10^{-3}$	6,7	2,2	7,5	4,0	5,8	6,0	3,8	5,8
$1{,}7\cdot10^{-2}$	20,7	2,4	4,5	3,7	6,8	7,6	3,5	7,4

while in the second the vacancy ones do so (Fig. 2 and Table 2), because the concentration of groups of interstitial type remains practically constant in the second stage, although their mean size increases, while the concentration of clusters of vacancy type continues to in-

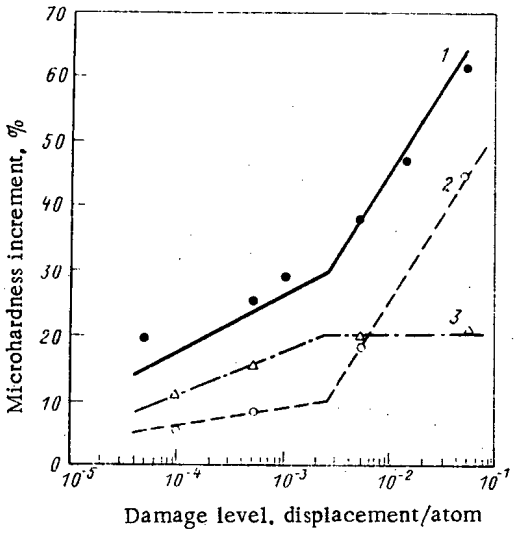

Fig. 3. Dependence of the microhardness increment in copper on damage level upon neutron irradiation: 1) calculation from electron micrographs (● indicates experimental values); 2, 3) contributions from clusters of vacancy and interstitial types ($d \leqslant 5$ nm).

crease, while the mean size decreases, and vacancy groups with size 1.5-5.0 nm becomes predominant. The largest rates of accumulation of vacancy clusters in either stage occur with α particles, while that for clusters of interstitial type (in the first stage) occurs with neutrons.

It has previously been shown [5] that the main contributions to the radiation hardening of copper and nickel irradiated at a temperature close to $0.2T_{mp}$ is made by clusters of size up to 5 nm, whose strength is independent of their type. The approach [5] was applied to the concentrations from the interstitial and vacancy clusters to the overall hardening of copper irradiated by neutrons (Fig. 3), and the calculated degree of hardening differed from the measured value by not more than 7%.

The electron micrographs showed that the two stages are related primarily to the modes of formation and evolution of the two types of cluster. Under these conditions, clusters of interstitial atoms are formed homogeneously and heterogeneously by the migration of displaced atoms produced by all the PEA, while vacancy clusters arise dynamically from vacancies produced by the PEA of fairly high energy [12-14]. It has been found [15-17] that the concentration of interstitial clusters tends to a limit after a short irradiation, and any further increase in the damage level only increases the sizes of these clusters; on the other hand, the concentration of clusters of vacancy type increases monotonically even in the region 10^{-1}-1 displacements/atom. It that case, the rate of accumulation of clusters of interstitial type should be higher than the rate of accumulation of vacancy clusters at low levels of damage, when the trapping of displaced atoms by traps of radiation origin (single vacancies and vacancy clumps) is not too substantial.

The electron micrographs (Table 2 and Fig. 3) show that the concentration of clusters of interstitial type obeys the above laws, whereas the rate of accumulation of vacancy clusters in the first stage is appreciably less than that in the second. There is an appreciable increase in the rate of vacancy cluster accumulation in the second stage on going from neutrons to protons or α particles, i.e., when the hardness of the PEA spectrum increases, so one assumes that the increased number of such defects in this stage is related, in the main, to clusters formed from displacement cascades. This agrees with the views of [1, 4, 14], according to which an increase in the hardness of the PEA spectrum increases the rate of accumulation of vacancy clusters by the production of subcascade regions. There is a lower rate of vacancy cluster accumulation at low levels of damage (in the first stage), which is probably determined by vacancy groups arising by diffusion under the conditions of those experiments, which, e.g., agrees with various other conclusions [18-20].

Therefore, the hardening of metals on irradiation by neutrons, protons, and α particles occurs in two stages, and in the first stage (damage level less than $3 \cdot 10^{-3}$ displacements/atom) the most effect is produced by neutrons and protons, while in the second stage (damage level over $5 \cdot 10^{-3}$ displacements/atom) it is produced by α particles.

LITERATURE CITED

1. J. Mitchell et al., in: Radiation Effects and Tritium Technology for Fusion Reactors, Proc. Int. Conf. V. II USERDA (1976), p. 172.

2. R. Van Konunenburg et al., "Fission fragment simulation of fusion reactor radiation effects on bulk material properties," UCRL-78068 (1976).
3. D. Styris, R. Jones, and E. Bradley, IEEE Trans. Nucl. Sci., NS-26, 1245 (1979).
4. R. Jones et al., J. Nucl. Mater., 85-86, 889 (1979).
5. K. G. Farkhutdinov, "Radiation hardening of copper and nickel on irradiation by neutrons, protons, and alpha particles," Author's Abstract of Candidate's Dissertation, Alma Ata (1980), p. 22.
6. J. Mitchell, C. Logan, and C. Echer, J. Nucl. Mater., 48, 139 (1973).
7. M. Guinan et al., Radiat. Eff., 40, 209 (1979).
8. J. Horak and J. Swanks, Trans. Am. Nucl. Soc., 26, 187 (1977).
9. I. Yu. Abdrashitov et al., "Calculation on radiation damage to materials," Reprint 2-80, Institute of Nuclear Physics, Academy of Sciences of the Kazakh SSR, Alma Ata (1980).
10. Sh. Sh. Ibragimov, V. F. Reutov, and K. G. Farkhutdinov, "Radiation hardening of bcc metals irradiated by α particles and protons at medium energies. Part 1. Radiation hardening of nickel," Reprint 2/78, Institute of Nuclear Physics, Academy of Sciences of the Kazakh SSR, Alma Ata (1978).
11. Sh. Sh. Ibragimov, V. F. Rentov, and K. G. Farkhutdinov, Reprint 3/78, ibid.
12. M. Makin, Atomic Collision Phenomena in Solids, North-Holland, Amsterdam (1970), p. 205.
13. B. Eyre, Inter. Met. Rev., 19, 240 (1974).
14. K. Merkle, "Defect production by energetic particles," ASM Materials Science Seminar on Radiation Damage in Metals, Cincinnati, Ohio (1975).
15. M. Kiritani, in: Fundamental Aspects of Radiation Damage in Metals, Proc. Int. Conf., Vol. 2, USERDA (1976), p. 695.
16. N. Sumida and H. Fujita, J. Phys. Soc. Jpn., 42, No. 4, 1245 (1977).
17. L. Howe, Radiat. Effects, 23, 181 (1974).
18. S. Mantl and W. Triftshäuser, Phys. Rev. Lett., 34, 1554 (1975).
19. M. Kiritani and H. Takata, J. Nucl. Mater., 69-70, 277 (1978).
20. H. Haubold and D. Martinsen, ibid., p. 644.

ABSORPTION OF POINT DEFECTS BY AN EDGE DISLOCATION

A. V. Subbotin

UDC 620.192.53

It is well known that processes of swelling and radiation creep are considered on the basis of so-called balance equations [1]. Analysis of these equations, which are constructed on the basis of certain ideas about microprocesses that occur under radiation, makes it possible to find the rate and absolute values of the swelling and creep, the temperature dependences, etc. Among the main microprocesses underlying the balance equations we can classify the radiation-induced nucleation of point defects (vacancies and interstitial atoms), their recombination, capture by various sorts of traps, and absorption by the surface of developing pores and dislocations. The last mechanism is particularly important. Successive consideration of this mechanism with allowance for the unlike interaction of a vacancy and an interstitial with the elastic field of a dislocation with the assumption of thermodynamic equilibrium in the vicinity of the dislocation core made it possible to introduce [2-4] the concept of "preference," a parameter characterizing the uneven capability of dislocations to capture interstitials and vacancies. The use of this model in the balance equations explains many experimental facts (in particular, the existence of swelling). Recently, however, experiments have yielded results, some of which cannot be explained quantitatively (radiation creep) and some of which do not have a satisfactory qualitative explanation (radiation-induced formation of superlattices). This has led to a number of attempts at a more profound examination of the absorption of point defects by a dislocation [5, 6] on the basis of well-known concepts about the stepped structure of the dislocation core [7-11]. In considering the absorption of point defects with allowance for the structure of the dislocation core, one must take account of the influence of the absorbed point defects on the structure of the core (self-consistent treatment), which was not done in the papers mentioned above. Such a self-

Translated from Atomnaya Énergiya, Vol. 54, No. 5, pp. 342-346, May, 1983. Original article submitted May 28, 1982.

0038-531X/83/5405-0343$07.50

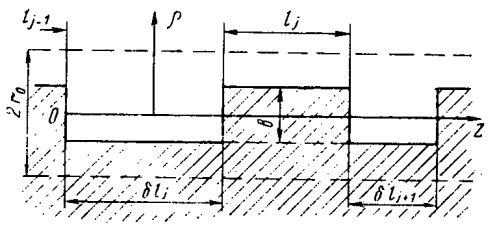

Fig. 1. Core of linear edge dislocation containing incomplete chains of atoms (l_j), forming pairs of steps.

consistent treatment leads to qualitatively new laws: the nonlinearity of the fluxes of point defects toward the dislocation.

Absorption of Point Defects in a Dislocation Core. We consider a linear edge dislocation, representing it as the edge of an atomic half-plane, in which there are incomplete atomic chains of various lengths l_j at distances δl_j from each other, with the edges of the chains forming steps (see Fig. 1). The axis of the dislocation core (Z axis) — a cylinder of radius $r_0 \sim (2\text{-}3)b$, where b is the Burgers vector — will be arbitrarily assumed to pass through the centers of the lateral faces of the steps, with an area $\sim b^2$. Henceforth, for simplicity we shall assume that both the Burgers vector and the lattice constant are equal to b. Absorption of point defects by such a dislocation will be considered with the following assamption.

1. Upon entering the region of a dislocation core far from a step, a point defect is weakly bound to the dislocation ($E_b \ll E^f$, where E_b is the binding energy and E^f is the point defect formation energy) and can leave the region of the core by means of random walk. On approaching a step to a distance $\sim b$, the point defect is undoubtedly absorbed by the step [7].

2. A dislocation core is a region of increased mobility for point defects in the direction along the dislocation line, and the energy E_z^m of migration in this direction is roughly half the energy E^m of migration in an unperturbed lattice. In the direction normal to the dislocation line the mobility in the core and in the unperturbed lattice is the same [7, 8].

3. In regions outside the dislocation core ($\rho \gg r_0$) we take account of the elastic interaction of the point defect with the dislocation:

$$E(\rho, \vartheta) = kT\frac{L\sin\vartheta}{\rho};\ L = \frac{\mu b(1+\nu)\Delta\Omega}{3\pi(1-\nu)kT}, \tag{1}$$

where μ is the shear modulus; ν is Poisson's ratio; $\Delta\Omega$, dilatational volume of the point defect ϑ; angle measured from the glide plane of the dislocation; ρ, distance from the center of the dislocation core; T, temperature; and k, Boltzmann's constant. Over a wide range of temperatures (with $T \geqslant 700°K$), the rate at which quasistationary values of the point-defect concentrations are established (with the external conditions remaining unchanged) is substantially higher than the rate of displacement of the steps as a result of the exchange of the latter by the point defects with the environment. This makes it possible to formulate the quasistationary problem for considering the absorption of point defects, having isolated the region between two neighboring steps which, as a consequence of what has been said above, can be regarded as immobile (see Fig. 1).

The system of equations that describe the migration of point defects toward a dislocation and enable us to determine the rate at which the point defects are absorbed in the region between the steps consists of equations for the point-defect concentration $C(\rho, z, \vartheta)$ in the lattice (2) and in the dislocation core (3), the conditions of the coupling between them (4), (5), and the boundary conditions (6), (7):

$$\Delta C + \frac{1}{kT}\nabla E\nabla C = 0 \text{ for } r_0 \leqslant \rho \leqslant R,\ 0 \leqslant z \leqslant \delta l_j; \tag{2}$$

$$D_\rho\left\{\frac{1}{\rho}\frac{\partial}{\partial\rho}\left(\rho\frac{\partial C}{\partial\rho}\right) + \frac{1}{\rho^2}\frac{\partial^2 C}{\partial\vartheta^2}\right\} + D_z\frac{\partial^2 C}{\partial z^2} = 0, \tag{3}$$

$$0 \leqslant \rho \leqslant r_0,\ 0 \leqslant z \leqslant \delta l_j,$$

where $R = (\pi N_d)^{-1/2}$ and N_d is the dislocation density. We have introduced two diffusion coefficients $D_q = D_{z0}\exp\{-E_z^m/kT\}$ and $D_\rho = D_{\rho 0}\exp\{-E^m/kT\}$ in the longitudinal and transverse directions relative to the dislocation edge because of the need to take account of the influence of tubular diffusion ($D_z \gg D_\rho$).

In the quasistationary case the flux of point defects through the surface of the dislocation core ($\rho = r_0$) is continuous:

$$\left(\frac{DC}{kT}\nabla\mu i_\rho\right)\Big|_{\rho=r_0+0} = D_\rho \frac{\partial C}{\partial \rho}\Big|_{\rho=r_0-0}, \tag{4}$$

where $\mu = kT \ln C/C_0 + E(\rho, \vartheta, z)$ is the chemical potential of the point defect in the lattice; C_0, thermal-equilibrium concentration; i_ρ, unit vector in the direction of ρ; and $D \approx D_\rho$, diffusion coefficient in the unperturbed lattice. One more coupling condition can be written if we bear in mind that the flux of point defects through the surface of the dislocation core along the segment $0 \leqslant z \leqslant \delta l_j$ should be equal to the number of point defects absrobed by the steps:

$$r_0 \int_0^{2\pi}\int_0^{\delta l_j}\left(\frac{DC}{kT}\nabla\mu i_\rho\right)\Big|_{\rho=r_0+0} d\vartheta\, dz = \int_0^{2\pi}\int_0^{r_0} D_z\left\{\frac{\partial C}{\partial z}\Big|_{z=0} - \frac{\partial C}{\partial z}\Big|_{z=\delta l_j}\right\}\rho d\vartheta\, d\rho. \tag{5}$$

The boundary condition determining the concentration of point defects far from the dislocation is in the form

$$C(\rho, z, \vartheta)|_{\rho=R} = \bar{C}. \tag{6}$$

Since steps are capable of absorbing point defects without limit, and since thermodynamic equilibrium manages to be established in their vicinity (at distances $\sim b$) [7], the boundary conditions on the surface of the dislocation core in the vicinity of steps are in the form

$$C(\rho, z, \vartheta)|_{\substack{z=0\\ \rho=r_0+0}} = C(\rho, z, \vartheta)|_{\substack{z=\delta l_j\\ \rho=r_0+0}} = C_0 \exp\left[-\frac{E(r_0, \vartheta)}{kT}\right]. \tag{7}$$

The solution of the system (2)-(7) can be obtained very simply if allowance is made for the fact that the length of a jump by a point defect in the lattice is comparable with the cross section of the dislocation core. This makes it possible to complete the transition from $C(\rho, z, \vartheta)$ to $C(z)$ for $\rho \leqslant r_0$ and to reformulate the system of equations (2)-(7).

The density of the flux of defects leaving the dislocation core is

$$j(z, r_0, \vartheta) = \frac{\nu r_0}{\Omega}\exp\left[-\frac{E(r_0,\vartheta) + E_b}{kT}\right]\left[C(z) - C_0 \exp\left(\frac{E_b}{kT}\right)\right], \tag{8}$$

where $\nu = 4D\rho/r_0^2$ and Ω is the elementary volume. The flux through the lateral surface of a dislocation core of unit length, therefore, is

$$J_1 = \frac{Z_p D_\rho}{\Omega}\left[C(z) - C_0 \exp\left(\frac{E_b}{kT}\right)\right], \tag{9}$$

where $Z_p = 8\pi I_0(L/r_0)\exp(-E_b/kT)$ and $I_0(L/r_0)$ is a Bessel function of an imaginary argument.

In order to determine the defect flux J_2 from the bulk into the dislocation core, it is convenient to consider Eq. (2) with the boundary condition (6) and another condition, viz., the steady state value of the concentration $C(z, \vartheta)$ established on the outer surface of the dislocation core as a result of the absorption and emission of point defects by the core. The concentration $C(\rho, z, \vartheta)$ can be written for $\rho \geq r_0$ as the superposition of two concentrations $C_1(\rho, z, \vartheta) + C_2(\rho, z, \vartheta)$, satisfying Eq. (2) and the boundary conditions.

$$C_1(\rho, z, \vartheta)|_{\rho=R} = 0;\ C_1(\rho, z, \vartheta)|_{\rho=r_0+0} = \tilde{C}(z, \vartheta) - C_0 \exp\left[-\frac{E(r_0, \vartheta)}{kT}\right]; \tag{10}$$

$$C_2(\rho, z, \vartheta)|_{\rho=R} = \bar{C};$$
$$C_2(\rho, z, \vartheta)|_{\rho=r_0+0} = C_0 \exp\left[-\frac{E(r_0, \vartheta)}{kT}\right]. \tag{11}$$

From this we can easily see that the solution for C_1 gives Eq. (9) for the density of the point-defect flux from the dislocation core and that the conditions formulated for C_2 are identical with the formulation of the problem of the flux of point defects toward the dislocation in the case of a diffusion-controlled mechanism. This enables us, using the results of [2-4], to write an expression for the point-defect flux in the dislocation core:

$$J_2 = \frac{Z_d D}{\Omega}(\bar{C} - C_0), \tag{12}$$

where

$$Z_d = \frac{2\pi I_0 (L/2r_0)}{K_0 (L/2R) I_0 (L/2r_0) - K_0 (L/2r_0) I_0 (L/2R)}.$$

Using Eqs. (9) and (12) as well as Eq. (3), we write the reformulated equation for the equation for the concentration of point defects in the dislocation core between two neighboring steps:

$$\frac{d^2}{dz^2} C(z) - \frac{Z_p D_\rho}{\pi r_0^2 D_z} \left[C(z) - C_0 \exp\left(\frac{E_b}{kT}\right) \right] + \frac{Z_d D}{\pi r_0^2 D_z} [\bar{C} - C_0] = 0. \tag{13}$$

From Eqs. (13) it follows that the mean free path of a defect in the dislocation core is

$$l_\tau = r_0 \sqrt{\frac{\pi D_z}{Z_p D_\rho}} = \frac{r_0}{2} \sqrt{\frac{\exp\left(\frac{E_b}{kT}\right)}{2I_0 (L/r_0)} \frac{D_z}{D_\rho}}. \tag{14}$$

Since thermodynamic equilibrium is sustained at the steps, we can find boundary conditions for Eq. (13):

$$C(z)|_{z=0} = C(z)|_{z=\delta l_j} = C_0 \exp\left(\frac{E_b}{kT}\right). \tag{15}$$

From Eq. (13) with the boundary conditions (15) it follows that the equation for the flux of point defects from a segment δl_j to each step (for z = 0 and z = δl_j) is in the form

$$J(\delta l_j) = \frac{Z_d D}{\Omega} (\bar{C} - C_0)\, l_\tau \frac{\mathrm{ch}(\delta l_j / l_\tau) - 1}{\mathrm{sh}(\delta l_j / l_\tau)}. \tag{16}$$

Considering that the segments between the steps δl_j and l_j are absolutely the same as paths for transporting point defects, the complete expression for the flux of point defects to a step, located between δl_j and l_j, can be written as

$$J = J(\delta l_j) + J(l_j). \tag{17}$$

Concentration of Steps. Equation (17) gives the flux per step and, therefore, the rate at which it is displaced along the dislocation. To calculate the total flux of point defects per unit length of dislocations, we must, obviously, determine the concentration of steps in the dislocation core. The concentration of steps is a variable that depends on the ratio of their nucleation and annihilation rates. The rate of annihilation is determined by the velocity of the steps and the direction in which they move. Any absorption of point defects by the steps leads to the growth of atomic chains along the dislocation line and results in their colliding (one chain with a length equal to the total length of all the chains is formed in the collision) or the chains are dissolved. In both cases the pair of steps disappears.

For simplicity, we consider the development of a step structure in a dislocation core in the presence of a flux of only one kind of point defect, interstitial atoms. In this case it is more convenient to consider its development not for chains that form pairs of steps, but for the segments that lie between them, which we shall call collapsed segments. Figure 1 shows the simplest case, that of the edge of a half-plane with one partially filled layer forming a step structure. The configuration of the edge of a half-plane clearly should, in the general case, contain several partially filled layers, whose number depends on the curvature of the dislocations and the ratio of the nucleation and annihilation rates of the steps. For a nonpinned edge dislocation under quasistationary conditions, the formation of a multilayer configuration should lead to curvature of the region of the dislocation core, which is energetically unfavorable. Quantitatively, this is expressed in a drop in the nucleation rate of pairs of steps (with the nucleation of either a chain of atoms or a collapsing segment of minimum viable size) in those regions in which nucleation leads to curvature of the dislocation. Thus, the configuration of the edge of the half-plane should "fit" in the initial linear dislocation "tube," thus enabling us to confine ourselves to consideration of the configuration with one partially filled layer of atoms.

Let us divide the process of absorption of point defects by a dislocation into cycles. The cycle will be assumed to begin with the complete absorption of a row of atoms that comes immediately after the last of the completed rows (the disappearance of the last collapsed segments in it) and to end when the last row has been filled. From the condition of quasistationarity it follows that all the cycles are equivalent. In each cycle the edge of the half-plane all the time contains N_L chains of atoms and the same number of collapsed segments ($2N_L$ steps). The equations for the concentration are found with the assumption that the nuclea-

tion rate K^+ of minimum viable chains, giving rise to pairs of steps, is fairly low: during the lifetime of either a chain of atoms or a collapsed segment no more than one nucleation of the aforementioned type can occur in them. The nucleation of minimum collapsed segments because of the formation of vacancy chains can be neglected, since it leads only to an insignificant overdetermination of the fluxes at the step and does not make any contribution to N_L. Thus, during one cycle only those atoms which are nucleated in collapsed segments give rise to new collapsed segments. With this assumption, for the concentration of the collapsed segments we have

$$K_x^+ \overline{\delta l} N_L + \frac{\overline{V}(\delta l)}{\overline{\delta l}} b N_L = 0, \tag{18}$$

where $\overline{\delta l}$ is the mean length of the collapsed segments; $\overline{V}(\delta l)$, mean rate of disappearance of collapsed segments; and K_x^+, cycle-averaged rate of nucleation of chains in the collapsed segments.

Within the framework of the conditions formulated above, we also consider the nucleation of chains of atoms. Those which are nucleated in chains (unlike those nucleated in collapsed segments) are not annihilated in the given cycle and make a contribution to the concentration of the chains of the next cycle. Considering that the annihilation rate of collapsed segments is at the same time the clllision rate of chains, we can write

$$K_y^+ \overline{l} N_L = -\frac{\overline{V}(\delta l)}{\overline{\delta l}} b N_L, \tag{19}$$

where $\overline{l}$ is the mean chain length and K_y^+ is the cycle-averaged rate of chain nucleation in the chains themselves. The equal sign in Eq. (19), in which the left-hand and right-hand parts have been written for two different cycles, following each other, can be used by virtue of the equivalence of cycles.

An expression for $\overline{V}(\delta l)$ can be obtained by formulating an equation for the distribution function of the collapsed segments δl. An analysis, similar to that used in the nuclearion theory [12-15], gives us

$$\overline{V}(\delta l) \approx -2\left(1+\frac{b}{2\overline{\delta l}}\right)[\overline{J}(\delta l)+\overline{J}(l)]. \tag{20}$$

The condition

$$(\overline{\delta l}+\overline{l})\, N_L = 1 \tag{21}$$

together with Eqs. (18)-(20) forms a closed system.

The cycle-averaged rates of nucleation in the collapsed systems and in chains of atoms and, therefore, $\overline{\delta l}$ and $\overline{l}$ should, obviously, not differ appreciably. Solving the system (18)-(21) with the assumption made above leads to two qualitatively different cases.

1. The mean free path of an interstitial atom in the dislocation core is greater than the mean distance between the steps ($l_\tau > \overline{\delta l}$, $l_\tau > \overline{l}$). Using Eqs. (18)-(21) as well as Eq. (16), we get

$$\overline{\delta l} = \frac{K_y^+}{K_x^+}\overline{l} \approx \frac{b(1+K_x^+/K_y^+)}{\Omega K_x^+} Z_d D(\overline{C}-C_0);$$
$$N_L \approx \frac{\Omega K_x^+}{b(1+K_x^+/K_y^+)^2}\frac{1}{Z_d D(\overline{C}-C_0)}. \tag{22}$$

2. When the mean free path of an intersititial atom in the dislocation core is smaller than the mean distance between the steps ($l_\tau < \overline{\delta l}$, $l_\tau < \overline{l}$), we get

$$\overline{\delta l} = \frac{K_y^+}{K_x^+}\overline{l} \approx \sqrt{\frac{4bl_\tau}{\Omega K_x^+} Z_d D(\overline{C}-C_0)};$$
$$N_L \approx \frac{1}{(1+K_x^+/K_y^+)}\sqrt{\frac{\Omega K_x^+}{4bl_\tau Z_d D(\overline{C}-C_0)}}. \tag{23}$$

Determination of Point-Defect Fluxes in a Dislocation. The flux of point defects per unit length of a dislocation can be written as

$$J_d = -\overline{V}(\delta l)\, N_L. \tag{24}$$

Using Eqs. (22)-(24), we shall show that in the two different cases ($l_\tau > \overline{\delta l}$, $\bar{l}$ and $l_\tau < \overline{\delta l}$, $\bar{l}$) the absorption of defects by a dislocation differs fundamentally.

In the case $l_\tau > \overline{\delta l}$, $\bar{l}$, using Eqs. (20), (22), and (24), we get the following formula for the flux of point defects per unit dislocation length:

$$J_d = \frac{Z_d}{\Omega} D(\bar{C} - C_0). \tag{25}$$

Equation (25) coincides with the expression obtained in [2-4] with the assumption of a diffusion-controlled mechanism of absorption. Thus, when the mean free path of a point defect in the dislocation core exceeds the mean distance between the steps, the absorption of point defects is subject to a diffusion-controlled mechanism and does not depend on the step concentration. Using Eq. (22), we give an estimate of the limit of validity of the diffusion-controlled mechanism ($l_\tau > \overline{\delta l}$, $\bar{l}$) for the flux of interstitial atoms:

$$\frac{K_x^+}{(1+K_x^+/K_y^+)} \frac{l_\tau}{b} > \frac{Z_d}{\Omega} D(\bar{C} - C_0). \tag{26}$$

In the case when $l_\tau > \overline{\delta l}$, $\bar{l}$, using Eqs. (20), (23), and (24), we get an expression for the flux of interstitial atoms per unit dislocation length,

$$J_d \approx \frac{2}{(1+K_x^+/K_y^+)} \sqrt{\frac{K_x^+ l_\tau}{b} \frac{Z_d}{\Omega} D(\bar{C} - C_0)}, \tag{27}$$

which is valid if the condition that is the reverse of Eq. (26) is satisfied. In this case the flux depends essentially on the step concentration which determines the absorptivity of the dislocation.

To illustrate the analysis presented above, we consider a specific mechanism of nucleation of minimum viable chains of atoms. At sufficiently high values of supersaturation, this mechanism can be pairing of interstitial atoms in the dislocation core, both in collapsed segments and in chains of atoms. The expression for the nucleation rate in this case, with allowance for thermal decay, can be written in the form ($K_x^+ \approx K_y^+ \equiv K^+$)

$$K^+ = \frac{\alpha}{\Omega} D_z C(z) \left[C(z) - C_0 \exp\left(\frac{E_b}{kT}\right) \right], \tag{28}$$

where C(z) is the concentration of interstitial atoms in the dislocation core [see Eq. (13)] and α is the number of atomic positions in the core from which pairing takes place. When Eq. (28) is taken into account, the expression (27) for the flux becomes

$$J_d \approx \sqrt{\frac{\alpha l_\tau^3}{\pi b r_0^2 \Omega} \left(\frac{Z_d}{Z_p}\right)} Z_d D(\bar{C} - C_0)^{3/2} \tag{29}$$

with the condition of applicability,

$$\frac{\pi b r_0^2}{\alpha l_\tau^3} \left(\frac{Z_p}{Z_d}\right) > \bar{C} - C_0.$$

The absorption of vacancies by a nonpinned edge dislocation is considered in similar fashion. In this case the formation rate K^- of minimum viable collapsed segments should play a certain role and the chains of atoms and collapsed segments should be interchanged in the entire discussion. The equations obtained are equivalent to Eqs. (23), (27)-(29) with K^+ replaced by K^- and all parameters replaced by those corresponding to vacancies.

CONCLUSIONS

Unlike the diffusion-controlled case of absorption [see Eq. (25)], in which only the elastic interaction of a point defect with the dislocation is important [see Eq. (12)], in the case of surface-controlled absorption [see Eqs. (27), (29)] a more significant role is played by processes inside the dislocation core [see Eqs. (9), (14)].

Let us also point out that the self-consistent treatment of the absorption of point defects by a dislocation leads to nonlinear expressions for the fluxes under certain conditions [see Eqs. (27), (29)]. This result is of fundamental importance for explaining the well-known experimental fact that superlattice (e.g., lattices of pores) are formed in irradiated materials under certain conditions.

The author thanks N. T. Chebotarev and Yu. G. Sokurski for fruitful discussions.

LITERATURE CITED

1. A. Brailsford and R. Bullough, Phil. Trans. R. Soc. A, 302, No. 1465, 87 (1981).
2. I. G. Margvelashvili and Z. K. Saralidze, Fiz. Tverd. Tela (Leningrad), 15, No. 9, 2665 (1973).
3. P. Heald, Philos. Mag., 31, No. 3, 551 (1975).
4. P. Heald and Speight, Acta Metall., 25, 1389 (1975).
5. A. I. Ryazanov and V. A. Borodin, Radiat. Effects, 56, No. 3-4, 179 (1981).
6. É. Ya. Mikhlin and V. V. Nelaev, in: Proc. All-Union Continuing Seminar on Computer Simulation of Radiation and Other Defects [in Russian], Physicotechnical Institute, Academy of Sciences of the USSR, Leningrad (1979), p. 166.
7. J. Lothe, J. Appl. Phys., 31, No. 6, 1077 (1960).
8. R. Thomson and R. Balluffi, J. Appl. Phys., 33, No. 3, 803 (1962).
9. R. Balluffi and R. Thomson, J. Appl. Phys., 33, No. 3, 817 (1962).
10. A. L. Roitburd and L. A. Zil'berman, Fiz. Met. Metalloved., 21, No. 5, 647 (1966).
11. R. Balluffi, Phys. Status Solidi, 31, 443 (1969).
12. Ya. B. Zel'dovich, Fiz. Eksp. Teor. Fiz., 12, No. 11-12, 525 (1942).
13. J. Katz and H. Wiedersich, J. Chem. Phys., 55, No. 3, 1414 (1971).
14. A. V. Subbotin, At. Energ., 45, No. 4, 276 (1978).
15. S. Chandrasekhar, Rev. Mod. Phys., 15, No. 1, 1 (1943).

RADIATION CHEMISTRY OF HYDROCARBON DILUENTS IN SOLVENT-EXTRACTION PROCESSES

G. F. Egorov and O. P. Afanas'ev

UDC 541.15:542.6.1

The two-phase system is subject to ionizing radiation in solvent-extraction reprocessing of spent nuclear power station fuel, which causes irreversible reactions, which interfere with the extraction. In a series of papers on the radiolysis of hydrocarbon solutions of extraction agents [1-7], it has been found that there is a deterioration in selectivity, reextraction of metal salts, and changes in the hydrodynamic characteristics, which are due to the accumulation of diluent radiolysis products.

The scale of the interference is dependent on the structure of the diluent and the character of the impurities [8]. However, the interference is determined only to a certain extent by these factors, and this can be considered by reference to model systems with individual hydrocarbon diluents such as n-octane and n-dodecane.

Here we present results on the compositions of the stable radiolysis products from aliphatic hydrocarbons under conditions of contact with aqueous solutions of nitric acid and on the effects of these products on the extraction behavior of plutonium and zirconium. The radiation sources were ^{60}Co (dose rate $3 \cdot 10^{16}$ eV/ml·sec or about 6 Gy/sec) and a U-12 electron accelerator (dose rate $0.5\text{-}1 \cdot 10^{18}$ eV/ml·sec or about 100-200 Gy/sec, electron energy 3.5 MeV).

Results. The hydrocarbons irradiated in contact with aqueous solutions of HNO_3 acquire the capacity to extract microconcentrations of U, Pu, Zr, Nb, Ru, Pd, and certain other metals. The increase in the distribution coefficients K_d for these elements, such as zirconium (Fig. 1), with the absorbed dose is nonlinear and is dependent on the concentration of the oxygen dissolved in the system.

We used K_d for zirconium in extraction from aqueous solution (10^{-3}-10^{-1} moles/liter) irradiated in contact with 2 mole liter HNO_3 in n-octane to calculate the overall concentrations of the products that bind the zirconium on the basis that the extracted complexes have the form ZrL_4. The kinetic relationships show that some of the products that extract the zirconium are of acid character and are removed from the organic phase during regeneration (washing with alkaline solutions), but the proportion of these products decreases as the dose increases (Fig. 2).

Translated from Atomnaya Énergiya, Vol. 54, No. 5, pp. 347-350, May, 1983. Original article submitted December 18, 1981.

0038-531X/83/5405-0349$07.50

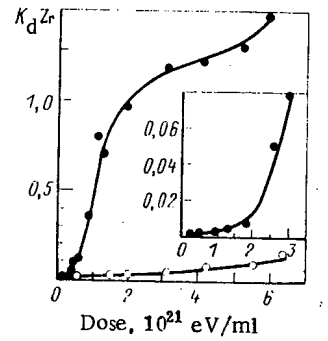

Fig. 1

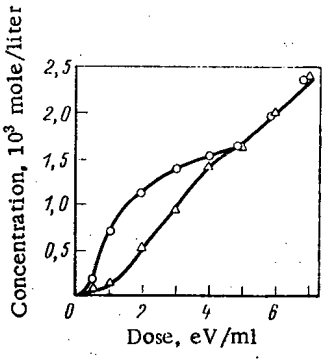

Fig. 2

Fig. 1. Extraction of zirconium by n-octane irradiated on stirring the mixture with 2 mole/liter of nitric acid containing O_2 (○) or without it (●).

Fig. 2. Change in the concentrations of complexing agents that extract zirconium (○) and that retain zirconium in the organic solution on reextraction by soda (Δ) on the irradiation of n-octane in contact with 2 mole/liter nitric acid.

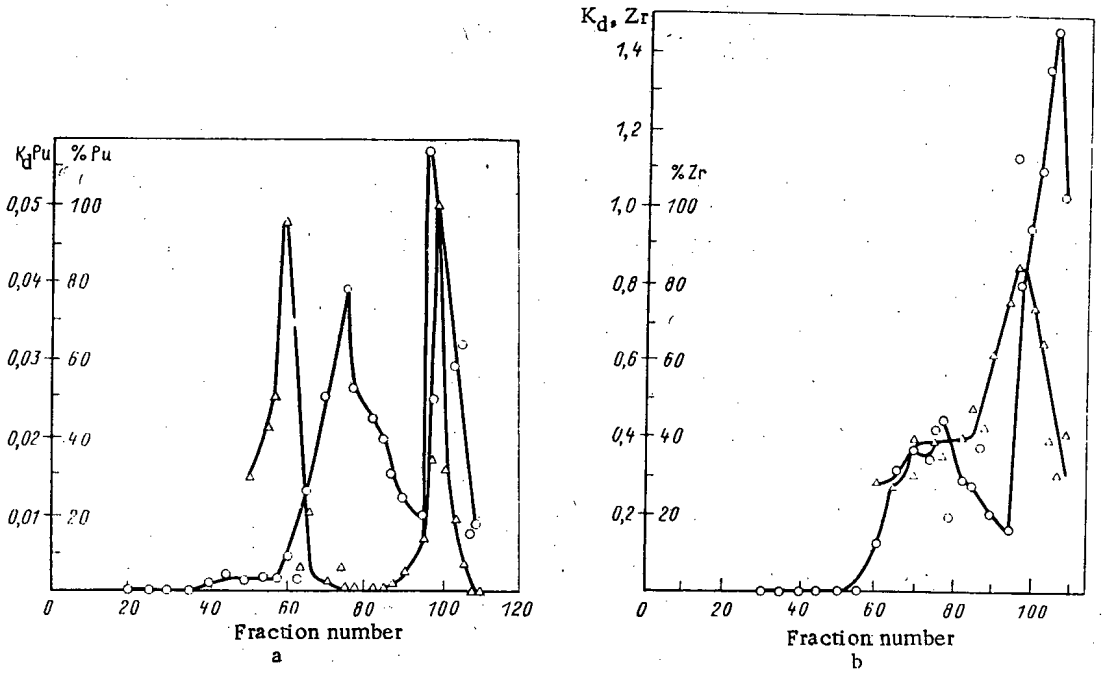

Fig. 3. Extraction and retention of plutonium (a) and zirconium (b) by fractions obtained after chromatographic separation from irradiated n-octane on silica gel: ○) K_d; Δ) % retention on soda reextraction.

It is clear that the products from the radiation nitration and oxidation of hydrocarbons in two-phase systems are complicated, as indicated by the data on the extraction capacity for plutonium and zirconium fractions isolated chromatographically from n-octane irradiated in contact with acid. There are fractions (Fig. 3) that contain substances with elevated and different extraction and retaining powers in relation to plutonium and zirconium.

The radiolysis product concentrations rise because of the prolonged action of the radiation on the recirculating organic solution, and therefore the subsequent conversion to new and more complicated compounds becomes appreciable. Therefore, it is desirable to divide these stable products in organic solutions into two groups in considering the compositions: initial products from the radiolysis of the original components arising from the start of the irradiation, and the secondary products formed by secondary chemical and other reactions.

TABLE 1. Radiation Yields of Products rom the Nitration and Oxidation of n-octane by Nitric Acid Solutions of Various Concentrstions, mole/100 eV

Products	HNO_3 concentration, mole/liter			
	1	2	3	5
Nitro compounds	0,54±0,1	1,2±0,2	2,5±0,3	3,7±0,4
Alkyl nitrites	0,4±0,1	0,8±0,2	1,6±0,2	2,0±0,2
Carbonyl compound	0,01±0,005	0,6±0,1	0,75±0,2	0,9±0,2

TABLE 2. Radiation Yields and Relations of Nitration and Oxidation Products from Hydrocarbons in Two-Phase Systems*

Composition of organic solution (aqueous solution 2 mole/liter HNO_3)	G, mole/100 eV					
	RNO_2	RONO	$RONO_2$	R_2CO	$(-HNO_3)$	η
n-octane	0,4*	—	0,15	1,4	—	0,4
	1,2	0,8	—	0,5	2,0	4,0
n-decane	0,2	—	0,2	0,9	0,8	0,45
	0,5	0,3	—	0,2		4,0
n-dodecane	0,1	—	0,2	0,8	0,3	0,4
	0,2	0,1	—	0,07		4,0
30% TBP + n-octane	0,6	0,1	0,5	1,5	—	0,8
	1,8	1,2	0,2	0,4	—	8,0
30% TBP + n-dodecane	0,4	0,1	0,3	1,2	—	0,75
	1,5	0,3	0,1	0,25	—	7,6

*Irradiation conditions: the first with O_2 bubbling, the second without O_2.

† $\eta = \frac{G(RNO_2) + G(RONO) + G(RONO_2)}{G(R_2CO)}$.

In a two-phase system, the functional compositions of the radiolysis products are the same for different hydrocarbons, while the rates of nitration are limited by the yield of nitrating agents: oxides of nitrogen and nitrous acid produced by the radiolysis of HNO_3. The latter are dependent on the acid concentration and on the solubility of the hydrocarbon in the aqueous phase [8], and therefore the yields of the nitration products increase linearly with the HNO_3 concentration (Table 1) but fall as the molecular mass of the hydrocarbon increases (Table 2). The nitration and oxidation of the diluents are particularly emphasized in the presence of an extraction agent on account of the radiolysis occurring directly in the organic solution (Table 2), where the relation between the nitration and oxidation products is determined by the dissolved oxygen concentration. In the absence of oxygen, the ratio is $\eta = (\Sigma G_{nit.prod}/\Sigma G_{ox.prod.}) \approx 8$, but when O_2 is bubbled through, the value of η decreases to 0.8, i.e., carbonyl compounds accumulate predominantly.

We used n-octane in various systems (Table 3) to examine the compositions of the liquid-phase radiolysis products. In the n-octane + H_2O system, the composition of the radiolysis products was the same as on the irradiation of pure n-octane. In the system n-octane + HNO_3, the composition of the products from nitration and the value of η are dependent on the O_2 concentration. The oxidation and nitration products enumerated in Table 3 consist of mixtures of isomers with the functional groups located on the first, second, third, and fourth carbon atoms in the octane molecule, with the concentrations correspondingly in the ratio 1:3:2.5:2.5. The structures of the initial radiolysis products from n-octane and model studies show [9] that these identified products are formed by the participation of four octyl radicals C_8H_{17} arising by the breakage of C–H bonds in the hydrocarbon molecule. The yields of these were identical for all the systems within the experimental error (from 3.1 to 3.5 mole/100 eV). The final products from the radiolysis of n-octane arise in competing reactions of the radicals with oxygen and oxides of nitrogen [9].

The initial products from the radiation nitration and oxidation of the aliphatic hydrocarbons accumulate in the organic solution in a linear fashion up to doses of $0.5\text{-}1\cdot10^{21}$ eV/ml, after which the rates of accumulation decrease. The variation in K_d for zirconium or plutonium shows two forms (Fig. 1): a slow rise in K_d up to about $0.5\cdot10^{21}$ eV/ml ($\leqslant10^5$ Gy), and a sharp increase at higher doses, when the initial stable radiolysis products attain a certain steady-state concentration (about 10^{-2} mole/liter).

Even this qualitative comparison shows that the initial stable products do not participate directly in extracting the plutonium and zirconium, and that the binding substances arise in the secondary processes. The experiments in model solutions showed that the nitro compounds, organic nitrites, and organic nitrates, and also ketones and aldehydes, do not extract plutonium and zirconium. On the other hand, if we use hydrocarbon solutions of the initial stable products and irradiate them in the absence of oxygen in contact with 2 mole/liter HNO_3, we

TABLE 3. Yields of Radiolysis Products from n-octane on Irradiating Systems of Various Compositions, mole/100 eV

Products	Without O_2			CO_2		
	n-octane	n-octane + H_2O	n-octane + HNO_3*	n-octane	n-octane + H_2O	n-octane + HNO_2*
Simple C_3-C_7 hydrocarbons	0,9±0,1	0,7±0,1	0,3±0,05	0,4±0,1	0,2±0,05	0,2±0,05
Unsaturated hydrocarbons	2,6±0,4	2,5±0,4	—	1,1±0,2	1,1±0,2	—
Intermediate hydrocarbons C_{16}-C_{15}	0,5±0,1	0,45±0,1	0,2±0,05	—	—	—
Dimeric hydrocarbons C_{16}	1,4±0,2	1,3±0,2	0,4±0,1	0,3±0,1	0,3±0,1	0,3±0,1
Carbonyl compounds	—	—	0,4±0,05	1,7±0,1	1,5±0,1	1,3±0,1
Octanols	—	—	0,45±0,05	1,1±0,1	0,9±0,1	0,9±0,1
Octyl nitrites	—	—	0,8±0,1	—	—	—
Octyl nitrates	—	—	—	—	—	0,5±0,05
Nitrooctanes	—	—	0,8±0,1	—	—	0,1±0,01
Octyl radicals C_8H_{17}	3,4±0,4	3,1±0,4	3,5±0,4	3,3±0,4	3,8±0,4	3,3±0,4

*Aqueous solution 2 mole/liter HNO_3.

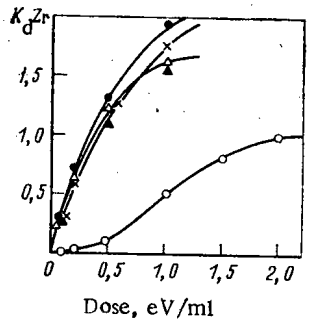

Fig. 4

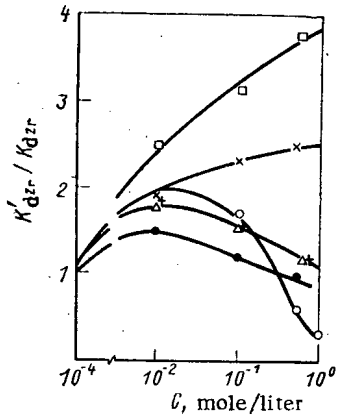

Fig. 5

Fig. 4. Variation of K_d for zirconium on irradiating n-octane in contact with 2 mole/liter HNO_3 and 10^{-2} mole/liter solutions of various substances in n-octane: ○) n-octane with additives; ●) octane-1; ×) 2-nitrooctane; Δ) methyl hexyl ketone; ▲) octyl alcohol.

Fig. 5. Relative change in K_d zirconium in relation to concentrations of substances introduced into n-octane: octene (□); nitrooctane (×); octyl alcohol (○); methyl hexyl ketone and octyl nitrate (Δ, +); octyl nitrite (●); K_dZr, distribution coefficients for mixtures of n-octane with additives; K_dZr, the same, for n-octane.

get (Fig. 4) a rapid rise in K_d for zirconium from the start of the irradiation. The contribution from the conversion of each initial radiolysis product to the extraction of zirconium is more evident when one examines the effects of the concentrations of the substances introduced into the hydrocarbon on the change in the relative K_d for zirconium on irradiating the solution (in contact with acid) to the same dose. Figure 5 shows that the main precursors of the products that extract zirconium are nitro compounds and unsaturated hydrocarbons (olefins).

Identifications have been performed [10] on the radiolysis products from hydrocarbon diluents, and neutral organic compounds have been identified (isomeric alcohols, diketones, oxyketones, pseudonitrols, and oximes), as well as compounds of acid character (carboxylic and dicarboxylic acids, hydroxyacids, ketoacids, and nitrolic and nitrocarboxylic acids, we well as ketoximes and oximes from carboxylic acids). The identification data led to the synthesis of various polyfunctional compounds, and model solutions were used in checking their capacity

TABLE 4. Extraction of Pu, Zr, and Ru by 0.1 mole/liter Solutions of Polyfunctional Compounds in n-octane from 2 mole/liter HNO_3 and Reextraction of These Elements by 10% Na_2CO_3 solution ($V_{org}:V_{wat}$ = 1:1)

Compound	K_dPu	%Pu	K_d Zr	%Zr	K_d Ru	%Pu
Oxime	0	0	0,005	—	0,002	—
Octane-2,4-	0	0	0,09	4,7	0,005	100
2-hydroxynitro-octane	0,002	—	0,03	10,0	0,025	5,0
Pseudonitrol	0,004	—	0,04	—	—	—
Caprenic acid	0,005	—	0,6	60	0,005	—
Subarinic acid	0	0	1,5	30	0,03	8,0
Nitrolic acid	0,01	9,0	0,12	—	—	—
Capriinhydroxamic acid	0	0	130	100	0,1	70
α-nitrocaprylic acid	500	100	50	25	0,04	70
Sum of ketoximes and hydroximina acids	30	100	70	95	0,1	60

to extract and retain Pu(IV), Zr, and Ru (Table 4). The extraction capacities of the compounds enumerated in Table 4 for Pu, Zr, and Ru may be characterized by K_d, while the retaining power is indicated by the proportion of the element remaining in the organic phase after reextraction (in soda regeneration of the extraction agents in percent of the extracted amount). The latter reflects the possibility that the extracted elements can accumulate in the recirculating organic solution.

High extraction capacities for zirconium and particularly plutonium occur for the α-nitrocarboxylic acids. Zirconium is less extracted by dicarboxylic acids, which only partially retain the extracted elements on soda reextraction. The hydroxamic acids have high complexing power for zirconium; however, on our data [10] the concentrations of these in the radiolysis products of hydrocarbons are small, and therefore they make a comparatively small contribution to disrupting the extraction.

Ketoximes and carboxylic-acid oximes (more precisely, hydroxyiminoketones and hydroxyiminoacids) polymerize readily and form strong chelates with plutonium, zirconium, palladium, and various other elements:

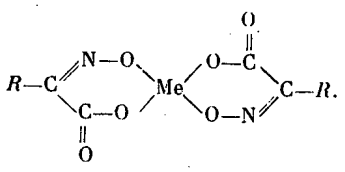

These products evidently make the main contribution to the increase in K_d for plutonium and the fission products at the stage of extraction, and they also contribute to the retention of these elements in the irradiated organic solutions on reextraction.

Therefore, one gets mainly the accumulation of nitration products under the conditions of reprocessing for highly active fuel-rod solutions (i.e., with lack of dissolved oxygen), which cause deterioration in the selectivity of the extraction, while in the reprocessing of low-activity solutions one expects deviations in the hydrodynamic characteristics on account of the preferential formation of oxidation products with surface-active behavior.

LITERATURE CITED

1. J. Good, Nucleonika, 15, 68 (1957).
2. C. Blake, I. Davis, and J. Smith, Nucl. Sci. Eng., 17, 621 (1963).
3. E. Lane, ibid., p. 626.

4. A. Huggard and W. Warner, ibid., p. 638.
5. T. Ishihara and K. Ohwada, Nucl. Sci. Technol., 3, 243, 20 (1966).
6. Z. Nowak, Nucleonika, 16, 133 (1971); 18, 447 (1973).
7. V. A. Medvestovskii et al., in: Proceedings of the Third COMECON Symposium on Research in Reprocessing Irradiated Fuel [in Russian], Ind. KAE Czechslov. Prague (1974), p. 302.
8. G. F. Egorov et al., At. Energ., 47, No. 2, 75 (1979).
9. G. F. Egorov and V. A. Medvestovskii, Khim. Vys. Energ., 5, 78, 551 (1971).
10. O. P. Afanas'ev et al., Extended Annotations on Studies Performed in COMECON Member-Countries within the Framework of Topic 1-6: Reprocessing Irradiated Nuclear Power Station Fuel [in Russian], Prague (1977), p. 50.

POSSIBILITY OF PRODUCING SYNTHETIC STANDARDS FOR INSTRUMENTAL NEUTRON-ACTIVATION ANALYSIS OF BIOLOGICAL MATERIALS

M. A. Kolomiitsev* and V. Yu. Dundua

UDC 539.1.06(088.8)

At the present time the standards used for the neutron-activation analysis of biological materials are prepared from natural biological materials (leaves of plants, beef liver, blood, potato flour) as well as synthetic standards based on glass, etc. Standards made from natural materials have a number of disadvantages: they are powdered (lack a geometric shape), are hygroscopic, have a low thermal and radiation resistance, the quantity of any element in them cannot be varied, they are insufficiently homogeneous, and it is difficult to give specifications for each new batch. Here we discuss the problem of producing synthetic biological standards on the basis of phenol formaldehyde resin (PFR).

The main goal is to produce standard specimens which would have the same physicochemical properties with respect to composition as the biological material to be analyzed. The neutron-activation method is a comparative method, i.e., the quantity of the element (elements) is determined by comparing the induced activity of the sample being analyzed and the standard specimen. In the standard specimen the exact content of an element must be known. In order to determine an element in biological materials, the analyzed and standard specimens are irradiated simultaneously. The content of the element is calculated from the ratio

$$m_a/m_{st} = A_a/A_{st},$$

where m_a and m_{st} are the quantity of the element in the analyzed and standard specimens, respectively, and A_a and A_{st} are the activity of the element in the analyzed and standard specimens, respectively.

A method making it possible to homogenize salts of various chemical elements with PRF was developed earlier by one of us [1]. The low level of intrinsic impurities in the PRF allows pellets of these mixtures to be used as standards for instrumental neutron-activation analysis (INNA) [1, 2]. It has been established that compounds of all elements in the periodic table can be homogenized and multiple-element standards can also be obtained. This method has been used to obtain simulators of the microelement composition of rocks [3, 4] and multiple-element biological standards [5]. The level of development at the present time is such that it is possible to produce synthetic standards constituting a set of various simulators of the atomic composition of biological materials as well as simpler multiple-element standards, containing certain groups of elements, that are convenient for analysis.

Standards based on PFR are undoubtedly appropriate for extensive use for the INNA of biological materials: synthetic standards are simple to prepare, and the concentration of elements in various batches can be easily reproduced [4, 5]. Standards based on PRF, therefore, do not require laborious certification, since the content of the elements is ensured by the technology of the synthesis [3, 4, 5].

Characteristic Features of Homogenization of Some Chemical Elements with PFR. An element is homogenized with PFR by mixing alcohol solutions of compounds of this element with the

*Deceased.

Translated from Atomnaya Énergiya, Vol. 54, No. 5, pp. 354-357, May, 1983. Original article submitted August 7, 1981; revision submitted October 18, 1982.

 0038-531X/83/5405-0354$07.50

resin [1, 3-5]. As compounds of metals it is expedient to use salts of acids that do not contain elements whose activation can give rise to undesirable activity, as well as salts of acids with the lowest molecular mass, in order to avoid disintegration of the resin structure and to obtaim pellets of low mechanical strength. It is less desirable to use powdered standards, because it was shown in [1] that pellets have considerable advantages: they do not have to be weighed after irradiation, they are easily cleansed of surface contaminations, etc. It is best of all to use nitrites obtained by dissolving exact weighed portions of pure metals (high-purity, special-purity) in special-purity nitric acid, since available metals are of a higher purity than commercially produced salts. The dissolution should be carried out in a quartz vessel treated with nitric acid and steamed.

Nonmetallic elements — fluorine, bromine and chlorine — are introduced as part of sodium and potassium halides. If it is necessary to synthesize simulators of tissue with a high chlorine content, e.g., hair, we use m-chlorophenol. It dissolves well in PFR and, moreover, is cross-linked with the resin in ortho and para positions by means of resol methylol-hydroxyls. Sulfur is introduced into the composition of the standard in the form of sulfates of potassium, sodium, or magnesium, and if the content of these metals is lower than the equivalent sulfur content, then sulfur is introduced as part of sulfur-containing aromatic compounds, capable of polycondensation with resol methylol-hydroxyls. A low concentration of phosphorus is provided by introducing sodium and potassium phosphates, while a higher concentration is ensured by introducing ammonium phosphates. If it is necessary to make simulators of bone tissue, in which the content of this element amounts to tens of percent, we can introduce red phosphorus, ensuring homogenization by mechanical mixing. It is advisable, however, to use an organic compound.

The general content of salts introduced into PFR in the form of a dissolved part should not exceed 4-5 mass %. The other elements should be introduced by mechanical homogenization in the form of undissolved powders, except for iron and magnesium. A content of more than 0.5 mass % of these elements in the dissolved part causes coagulation of the resin, which rules out its own homogenization as well as homogenization of other elements. For this reason it is advisable to use organoelemental compounds with a low value of the instability constant.

Gold, silver, mercury, and cooper are easily reduced to the free state by formaldehyde. These elements are homogenized with resol simply by dissolution because their concentration is low while mechanical mixing with a large quantity of PFR cannot ensure homogeneity. It is known that in resol, which is formed during polycondensation of phenol with formaldehyde, the content of the residual formaldehyde may reach several percent. Reduction of gold, silver, mercury, and copper by the residual formaldehyde occurs at a residual formaldehyde content exceeding 0.2 mass %. It has been shown that in order to reduce the concentration of free formaldehyde in resol to 0.1 mass %, it is sufficient to reprecipitate resol from an acetone or alcohol solution four or five times with water. At the same time, the residual concentration of the phenol is lowered to 1 mass %, which raises the radiation resistance of the simulators and reduces the loss of mass under irradiation.

Influence of the Purity of Reagents. As is well known, the concentration of various elements in biological materials may differ by several orders of magnitude. For instance, bone tissue may contain 20 mass % calcium and 10^{-3} mass % strontium. Thus, the introduction into PFR of a pure calcium reagent with a low relative content of strontium impurity can substantially distort the strontium concentration as compared with the specified value. When synthesizing simulators, therefore, one must take account of the fact that the chlorine content is at a level of a few mass %, the bromine content is at a level of 10^{-4} mass %, etc.

If the purity of available reagents does not allow macrocomponents to be introduced into the composition of a simulator based on PFR, therefore, two simulators should be prepared. One of them contains only the microelements, while the other contains only the macroelements. Taken together, the two simulators reproduce the required composition. With this method, the simulators can be measured after irradiation, either together or separately, depending on the problem being solved.

In order to synthesize biological-tissue simulators based on PFR, the content of the intrinsic impurities in the resin should be two to three orders of magnitude lower than the concentration of artificially introduced elements. If the content of the intrinsic impurities in the resin is higher than that, the PFR must be preanalyzed to determine the exact content of these impurities. Then the appropriate corrections are introduced into the certification

in accordance with the values found for the concentrations. It is desirable, correspondingly, to reduce the amount of elements introduced. A technology has been developed for obtaining PFR of sufficient purity for obtaining any biological tissue.

Synthesis of Simulators of the Atomic Composition of Mammalian Tissue and Organs. Mammalian tissue and organs contain sodium, chlorine, phosphorus, sulfur, calcium, potassium, magnesium, iron, and fluorine; these elements should also be incorporated into each individual simulator.

Most of the elements mentioned above are present in tissue and organs in concentrations that exceed the upper limit of solubility in PFR. For this reason, PFR is mixed mechanically with PFR with finely dispersed powders of their compounds. Exclusion of some elements from the general composition so that it can be incorporated into a separate simulator is also advisable from the point of view of the homogenization conditions.

The various tissues and organs are differentiated as to composition. Bones contain up to 26 mass % calcium and up to 12 mass % phosphorus, and hair contains up to 2 mass % chlorine and up to 3.8 mass % sulfur. This is the highest concentration of elements of the base. At the same time, potassium and iron, e.g., are present at the rate of 0.09 and 0.02 mass %, respectively. As a consequence of this, simulators of the main bone tissue should be obtained as complex materials, in which the constituent compounds of elements are homogenized by a combination of dissolution and mechanical mixing. Such simulators constitute a mixture of solid solution of part of the element of the base with a lower concentration and powders of the insoluble compounds of the other parts of elements of the base, whose concentration is above the limit of solubility in PFR. The mechanical strength, homogeneity, and absence of stratification of material are adtained bonding together the powdered components with a viscous polymer material which is a true solution of compounds of a bone-tissue simulator, consisting of two parts (A and B), is given below (in mass %):

Standard A			
Co	$5{,}14\cdot10^{-4}$	Al	$7{,}20\cdot10^{-4}$
Cs	$2{,}06\cdot10^{-5}$	Ag	$5{,}20\cdot10^{-6}$
Cu	$1{,}02\cdot10^{-3}$	Pb	$1{,}03\cdot10^{-3}$
Hg	$5{,}14\cdot10^{-5}$	Sn	$1{,}03\cdot10^{-3}$
I	$5{,}20\cdot10^{-6}$	Tl	$5{,}14\cdot10^{-6}$
Zn	$2{,}06\cdot10^{-2}$	W	$1{,}03\cdot10^{-6}$
Br	$7{,}10\cdot10^{-4}$	Ti	$1{,}02\cdot10^{-6}$
Mn	$3{,}08\cdot10^{-4}$	Cr	$1{,}03\cdot10^{-4}$
As	$1{,}03\cdot10^{-4}$	Se	$5{,}10\cdot10^{-4}$
Ba	$1{,}02\cdot10^{-3}$	La	$5{,}60\cdot10^{-5}$
Mo	$2{,}06\cdot10^{-6}$	Sb	$3{,}15\cdot10^{-5}$
Ni	$5{,}14\cdot10^{-4}$	Pb	$3{,}20\cdot10^{-3}$
Sc	$5{,}20\cdot10^{-7}$		
Sr	$5{,}14\cdot10^{-2}$		
V	$5{,}35\cdot10^{-4}$		
Cd	$1{,}02\cdot10^{-3}$		

Standard B			
Na	0,50	Ca	25,10
Mg	0,42	P	12,15
Fe	0,02	Cl	0,27
		K	0,10
		F	0,15

In weighed portions of 10-25 mg, these simulators are fairly representative as far as atomic composition is concerned.

The use of selective standards for individual elements is not desirable, since the necessary accuracy is not ensured in multiple-element analysis. Each specimen studied must be irradiated along with a large number of standards. When a few tens of elements is to be determined, e.g., the volume of the required standards is ~ 8-10 cm^3. In such a volume the neutron spectrum is distorted substantially, and as a result the individual standards as well as the specimen being analyzed are in fact irradiated under conditions that are not equivalent; consequently, the error of determination increases. Moreover, in order for the neutron spectrum to be the same, the content of the elements in the standards should be as close as possible to their content in the biological materials, since during recording of the induced activity the absorption of γ rays by the matrix of the specimen and the matrix of the standard should be the same. In our case dividing the simulator into two parts does not distort the results of the analysis, since the two simulators are irradiated along with the specimen under study. They can also be used as independent standards, which is very convenient for determining the

concentration of some elements. This does not diminish the accuracy of the analysis, since an individual simulator has the approximate composition of the biological material.

The production of standards simulating the complex atomic composition of biological materials is a problem for scientists the world over. At the request of the IAEA, we developed the SNR-1 multiple-element standard, simulating the atomic composition of biological material. Tests carried out by the IAEA have shown the method of preparing the standards to be correct and these standards are used as reference materials in IAEA member-countries. At the present time these standards have been approved by the USSR State Committee on Standards as state standard specimens and have been entered in the State Register of Measuring Means as No. 2193-81. Below we give the composition of standard SNR-1 with a confidence coefficient of 0.95 (in mass %):

As . . .	$(1{,}10 \pm 0{,}04) \cdot 10^{-5}$
Au . . .	$(5{,}91 \pm 0{,}01) \cdot 10^{-7}$
Br . . .	$(2{,}11 \pm 0{,}08) \cdot 10^{-4}$
Cr . . .	$(6{,}50 \pm 0{,}24) \cdot 10^{-5}$
Cs . . .	$(3{,}30 \pm 0{,}13) \cdot 10^{-5}$
Hg . . .	$(1{,}10 \pm 0{,}10) \cdot 10^{-5}$
La . . .	$(1{,}10 \pm 0{,}11) \cdot 10^{-5}$
Mn . . .	$(6{,}50 \pm 0{,}26) \cdot 10^{-5}$
Rb . . .	$(1{,}31 \pm 0{,}05) \cdot 10^{-3}$
Sb . . .	$(7{,}00 \pm 0{,}81) \cdot 10^{-6}$
Se . . .	$(4{,}40 \pm 0{,}18) \cdot 10^{-5}$
Sr . . .	$(2{,}70 \pm 0{,}11) \cdot 10^{-3}$
Co . . .	$(2{,}16 \pm 1{,}07) \cdot 10^{-5}$
Cu . . .	$(2{,}38 \pm 0{,}12) \cdot 10^{-4}$
Fe . . .	$(8{,}23 \pm 2{,}01) \cdot 10^{-4}$
Ag . . .	$(14{,}26 \pm 5{,}74) \cdot 10^{-7}$
Al . . .	$(1{,}05 \pm 0{,}85) \cdot 10^{-5}$
Cl . . .	$(6{,}22 \pm 0{,}76) \cdot 10^{-4}$
K . . .	$(2{,}43 \pm 0{,}41) \cdot 10^{-4}$
Na . . .	$(1{,}90 \pm 0{,}35) \cdot 10^{-4}$
Zn . . .	$(0{,}37 \pm 0{,}07) \cdot 10^{-4}$

The method of combining different methods of homogenizing elements using PFR as the matrix makes it possible to produce simulators that reproduce the composition of any biological tissue and organs with respect to microelements and macroelements.

The authors express their thanks to N. V. Chikhladze and O. A. Danilova for their assistance in carrying out this work.

LITERATURE CITED

1. M. A. Kolomi'tsev, J. Radioanal. Chem., 20, 549 (1974).
2. M. A. Kolomi'tsev, At. Energ., 35, No. 5, 348 (1973).
3. D. I. Leipunskaya et al., At. Energ., 39, No. 6, 423 (1975).
4. D. I. Leypunskaya et al., J. Radioanal. Chem., 26, 293 (1975).
5. L. M. Mosulishoili et al., J. Radioanal. Chem., 26, 175 (1975).

ACID NUMBER DETERMINED FOR DITOLYMETHANE COOLANT

V. A. Ermakov and N. A. Ogurtsov

UDC 621.039.534:543.257.1+543.852

Ditolylmethane (DTM) is one of the organic coolants and moderators used in nuclear reactors, and the presence of carboxylic acids in this produces appreciable corrosion of materials in contact with the coolant [1]. It is therefore necessary to check the carboxylic acid contents of DTM.

Usually, the concentration of a mixture of acids of unknown composition is expressed as the acid number (AN) [2]. More than 40 different solvents have been used in determining carboxylic acids in various nonaqueous media [3]. For example, in determining the AN of gasoline, ligroin, herosine, and other products [4], use has been made of an 85% aqueous solution of ethanol, while in the pH method of determining AN for oils [5, 6] the solvent is a mixture of ethanol with benzene (3:2), and in determining the AN of crude petroleum and petroleum products and additives [7] one uses a mixture of isopropanol, benzene (toluene), and water (50:49:1), etc. No information has been published on the determination of AN for DTM.

The purpose of the present study was to define the choice of solvent suitable for pH determination of AN of ditolylmethane.

Experiment. We used reactor-grade DTM containing 6.3 mass % of high-boiling products from radiation-chemical transformation of DTM. The following solvent mixtures were used: isopropanol–benzene (1:1), ethanol–benzene (3:2), and ethanol–dimethylformamide (4:1). An electrode cell was fitted with an ÉSL-4V-07 glass electrode* and a silver chloride flow electrode of type ÉVL-1M3, and the cell was flushed with nitrogen before the introduction of 25.0 ml of the solvent for the titrant: an alcoholic solution of potassium hydroxide. At the end of the titration (pH meter type pH-121) the cell was carefully flushed with the corresponding solvent and dried. Then 25.0 ml of the solvent and 1.0-3.0 g of DTM were introduced and the titration was performed again. The method was evaluated on a model solution of benzoic acid in each solvent. The concentrations of the titrant in the various series ranged from 0.0100 to 0.0200 g-eq/liter. The endpoint of the titration was determined from the maximum on the differential titration curve $\Delta pH/\Delta V$ as coordinates (V is the titrant volume). The value of AN was calculated from $AN = (V_K - V_0)T/m$, where V_K is the volume of titrant used in titrating the specimen (solution of DTM in the solvent); V_0, volume of titrant used to titrate the solvent itself; T, titer of the alcoholic KOH solution; and m, sample mass. Most of the measurements were made at room temperature.

Results and Discussion. The best of these solvent mixtures was ethanol and dimethylformamide (4:1). The pH titration curves in this mixture had one titration stepout in the range of pH from 9.0-12.3 (Fig. 1). Table 1 gives the pH data on DTM in this mixture, which shows that the volume of titrant consumed increases in proportion to the mass of the sample.

*Table readings were also obtained in an ÉSL-63-07 electrode.

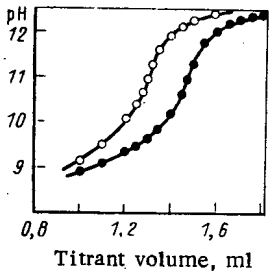

Fig. 1. Curves for pH titration of a mixture of ethanol with dimethylformamide (○) and samples of reactor DTM in this mixture (●); volume of solvent 25.0 ml, mass of DTM sample 1.000 g, titrant 0.0199 N KOH in ethanol, temperature 23 ± 1°C.

Translated from Khimiya Énergiya, Vol. 54, No. 5, pp. 358-359, May, 1983. Original article submitted October 19, 1981.

 0038-531X/83/5405-0358$07.50

TABLE 1. Data from pH Titration of Reaction DTM in an Ethanol–Dimethylformamide Mixture (4:1)*

Sample mass, g	Titrant volume required by sample, ml	AN (mg KOH/g DTM)
1,000	0,095	0,117
1,000	0,095	0,117
2,000	0,167	0,103
2,000	0,220	0,135
2,000	0,146	0,090
2,000	0,145	0,089
3,000	0,270	0,111
3,000	0,290	0,119
3,000	0,250	0,102
3,000	0,235	0,097

*Here the pH is a nominal parameter and is not the true hydrogen-ion activity; titrant 0.0220 N KOH in ethanol, solvent volume 25.0 ml, temperature 23 ± 1°C.

On titrating solutions of the residue after vacuum distillation of the reactor DTM, a precipitate was produced in some cases, but this did not influence the shape of the titration curves or the result. The arithmetic mean AN was 0.108 mg of KOH per 1 g of DTM, with confidence limits (0.95 probability) of ±0.003 mg of KOH/g of DTM. On statistical processing of the data for 20 specimens of solvent (ethanol + dimethylformamide), the relative standard deviation was 2%.

Therefore, a mixture of ethanol with dimethylformamide (4:1) is a good solvent for DTM. The solvent has an equilizing action on the carboxylic acids and therefore is **suitable for** determining the AN of DTM by the pH method.

LITERATURE CITED

1. V. G. Veksel'man and A. I. Il'chenko, Reactors with High-Temperature Organic Coolants [in Russian], Tekhnika, Kiev (1969), p. 9.
2. K. I. **Godovskaya** et al., Technical Analysis [in Russian], Vysshaya Shkola, Moscow (1967), p. 227.
3. I. Denes, Titration in Nonaqueous Media [Russian translation], Mir, Moscow (1971), p. 21.
4. Lubricating Oils and Additives for Them [in Russian], Standartgiz, Moscow (1962).
5. E. P. Sobolev, E. A. Popova, and I. A. Rubinshtein, Khim. Tekhnol. Topliv Masel, No. 2, 56 (1963).
6. E. A. Popova and I. A. Rubinshtein, ibid., No. 4, 57 (1980).
7. B. V. Belyanin and V. N. Erikh, Technical Analysis of Oil Products and Gas [in Russian], Khimiya, Leningrad (1975), p. 84.

INFLUENCE OF ^{232}U UPON THE RADIATION PARAMETERS OF THE PHOTON EMISSION FROM URANIUM FUEL

L. V. Matveev, V. Yu. Rogozhkin, and É. M. Tsenter

UDC 621.039.58

The accumulation of ^{232}U in exhausted uranium fuel poses several problems which must be overcome for a repeated use of regenerated uranium as fuel of nuclear reactors [1]. One of the main problems results from the increased dose of external radiation on the personnel by the high-energy γ radiation of the ^{232}U decay products (^{232}U itself is a weak γ emitter). Some idea of the danger of ^{232}U can be obtained from the comparison of the photon emission parameters of ^{232}U and uranium obtained from natural raw material. The question is which characteristic parameters must be compared.

The simplest characteristic dose parameter of a photon emission is the exposure dose rate at the unit distance from a point source of unit mass:

$$P = K_\gamma Q, \tag{1}$$

where Q is the specific activity of the source; and K_γ is the total γ constant. The total γ constant is the exposure dose activity at unit distance from the source. The γ constant calculated for a certain monoenergetic line of the emission spectrum of a nuclide is termed differential constant. A source can be considered a point source in terms of physics when the maximum dimensions of the source are much smaller than the distance to the point of detection and the free path length in the source material (the absorption of the radiation in the source can be disregarded). Since low-energy photon radiation (first of all, L-shell x rays) significantly contributes to the γ constant, and since the linear absorption coefficients of the low-energy photon emission are large, the concept "point source" can be applied to uranium isotopes as long as the source dimensions do not exceed 0.1-1.0 mm. Thus, in work with uranium one must practically always consider self-absorption in the source material. The self-absorption depends upon the geometrical form of the source and is different for each isotope because of the differences in the energy spectra of the photon emission of the uranium isotopes.

There exist some techniques for expanding the region in which the point-source concept can be employed and, accordingly, the formula indicated above can be used. We can completely exclude from our considerations the low-energy photon emission (e.g., in [2, 3], photon emission with energies below 30 keV is completely disregarded in the calculation of the γ constants) or consider the exposure dose rate and K_γ in Eq. (1) after initial filtering with some absorber material [4]. But these techniques show an important shortcoming: when we disregard low-energy photon emission from the very beginning, we cannot answer the question of

TABLE 1. Exposure Dose Rate (nA/kg) at the Distance 1 m from the Center of Spherical Sources and from a Semiinfinite Radiating Uranium Space

Isotope	Radius of the sphere, cm				Semiinfinite radiating space
	0,01	0,1	1,0	10	
^{232}U	0,072	63	$3{,}2\cdot10^{4}$	$4{,}6\cdot10^{6}$	$9{,}3\cdot10^{8}$
^{233}U	$9{,}2\cdot10^{-8}$	$1{,}1\cdot10^{-5}$	$1{,}2\cdot10^{-3}$	0,12	23
^{234}U	$9{,}3\cdot10^{-8}$	$9{,}4\cdot10^{-6}$	$9{,}4\cdot10^{-4}$	0,094	19
^{235}U	$9{,}8\cdot10^{-10}$	$2{,}5\cdot10^{-7}$	$2{,}7\cdot10^{-5}$	$2{,}7\cdot10^{-3}$	0,53
^{236}U	$9{,}6\cdot10^{-10}$	$1{,}0\cdot10^{-7}$	$1{,}0\cdot10^{-5}$	$1{,}0\cdot10^{-3}$	0,21
^{238}U	$2{,}6\cdot10^{-11}$	$1{,}4\cdot10^{-8}$	$5{,}7\cdot10^{-6}$	$7{,}0\cdot10^{-4}$	0,14

TABLE 2. Equivalent ^{232}U Concentration in Uranium Point Sources, %

Isotope composition of the uranium	Without filter	Behind an initial 5-mm-thick filter		
		Al	Fe	Pb
Natural uranium	$2{,}2\cdot10^{-7}$	$3{,}4\cdot10^{-8}$	$2{,}6\cdot10^{-8}$	$1{,}9\cdot10^{-8}$
4,4% from ^{235}U	$8{,}8\cdot10^{-7}$	$8{,}0\cdot10^{-8}$	$4{,}2\cdot10^{-8}$	$1{,}8\cdot10^{-8}$
90% from ^{235}U	$1{,}8\cdot10^{-5}$	$1{,}2\cdot10^{-6}$	$7{,}4\cdot10^{-7}$	$6{,}2\cdot10^{-9}$

Translated from Atomnaya Énergiya, Vol. 54, No. 5, pp. 359-360, May, 1983. Original article submitted November 3, 1981.

 0038-531X/83/5405-0360$07.50

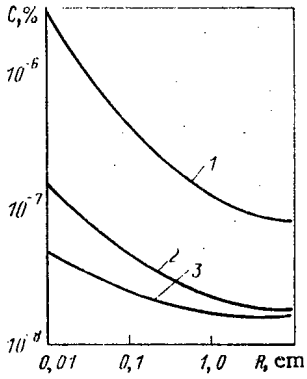

Fig. 1. Equivalent ^{232}U concentration C in spherical uranium sources: 1) uranium enriched with 90% ^{235}U; 2) uranium enriched with 4.4% ^{235}U; 3) natural uranium.

how the low-energy photon emission will contribute to the exposure dose rate produced by volume sources.

In order to bring into account differences in the emisson spectra and the self-absorption in the source materials, we calculated the exposure dose rate at a distance of 1 m from the center of spherical uranium sources of various radii and used as limit case the self-absorption of a semiinfinite emitting uranium space [5]. We assumed in the calculations that the ^{232}U, ^{235}U, and ^{238}U isotopes are in equilibrium with the short-lived decay products. The short-lived decay products are ^{234}Th, ^{234m}Pa, and ^{234}Pa in the case of ^{238}U, and ^{231}Th in the case of ^{235}U. The time after which radioactive equilibrium between ^{238}U and its decay products has been reached is given by the half-life of ^{234}Th ($T_{1/2}$ = 24.1 days) and amounts to about half a year. This time is much shorter in the case of ^{235}U, i.e., the time is several days because the half-life of ^{231}Th is 25.5 h. The radioactive decay chain of ^{232}U and the time dependence of the exposure dose rate produced by a ^{232}U point source have been described in [1, 6]. The maximum exposure dose rate produced by ^{232}U and its decay products is reached after 10.3 yrs. The results of the exposure-dose rate calculation, which is listed in Table 1, allow the comparison of the characteristic parameters of photon emission of various uranium isotopes at various source dimensions.

Let us determine the equivalent ^{232}U concentration in uranium, for which the exposure dose rate produced by ^{232}U is equal to the exposure dose rate of the photon emission from the other uranium isotopes. The equivalent concentration values which we determined for uranium of various isotope compositions are listed in Table 2 and in Fig. 1. The equivalent concentration of ^{232}U decreases when the source dimensions increase, because the radiation of greater penetration (E = 2.61 MeV) originates from ^{208}Tl, i.e., from a decay product of ^{232}U. The maximum energy in the photon emission spectrum of the other uranium isotopes is 2 MeV and is observed in the ^{234}Pa and ^{234m}Pa decay, i.e., in the decay of short-lived decay products of ^{238}U. In the calculations we disregarded multiple scattering and bremsstrahlung produced in the material of the source or the filter. According to the estimates, the exposure dose rate resulting from bremsstrahlung of a semiinfinite radiating ^{238}U space which is in equilibrium with the short-lived decay products exceeds the exposure dose rate determined without the bremsstrahlung by a factor of about 1.5. In the case of ^{232}U and ^{235}U, the contribution of the bremsstrahlung to the exposure dose rate is insignificant and reaches 0.6 and 0.2%, respectively. Thus, the equivalent concentration values listed in the present work are the lower limit and belong to the interval $2 \cdot 10^{-5}$-$6 \cdot 10^{-9}$ %.

Let us note in conclusion that the tolerable ^{232}U concentration in uranium (tolerable in regard to external irradiation of the personnel) cannot coincide with the equivalent concentration, because the main principle of radiation safety is not to exceed the basic dose limit of 5 bohr per year (1 bohr = 0.01 sievert) established in the NBR-76 (Radiation Safety Standard-76) [7]. Therefore, the ^{232}U concentration at which the ^{232}U contribution to the total exposure dose rate is much greater than the contribution of the other uranium isotopes can be considered tolerable.

LITERATURE CITED

1. L. V. Matveev and É. M. Tsenter, At. Tekh. Rubezhom, No. 4, 10 (1980).
2. Yu. V. Khol'nov et al., Characteristic Parameters of the Radiations of Radioactive Nuclides Employed in the National Economy. Fixed Data (Handbook) [in Russian], Atomizdat, Moscow (1980).

3. N. G. Gusev, V. P. Mashkovich, and A. P. Suvorov, Protection against Ionizing Radiation, Vol. 1, Physical Principles of the Protection against Radiation [in Russian], Atomizdat, Moscow (1980).
4. L. V. Matveev, T. K. Ragimov, and É. M. Tsenter, "Gamma constants of actinoids without initial filters and with aluminum, iron, and lead filters," Preprint of VNIINM-5(61), Moscow (1981).
5. L. V. Matveev, V. Yu. Rogozhkin, and É. M. Tsenter, At. Energ., 53, No. 3, 193 (1982).
6. T. S. Zaritskaya et al., At. Energ., 48, No. 2, 67 (1980).
7. Radiation Safety Standards NRB-76 [in Russian], Atomizdat, Moscow (1978).

DEVELOPMENT OF CO PRESSURE IN URANIUM DIOXIDE MICROPINS

Yu. F. Khromov, R. A. Lyutikov, D. E. Svistunov, and A. V. Makeev

UDC 621.039.548:541.123

Relationships previously derived [1] for the equilibrium pressures of O_2 and CO as functions of composition and temperature for uranium dioxide can be used in thermodynamic calculations on the reduction of uranium dioxide by carbon with the release of CO in a closed system without the removal of the gaseous and solid reaction products. An example of such a system is provided by the micropins in a high-temperature gas reactor with pyrocarbon coating and cores made of $UO_{2\pm x}$.

The CO pressure under a gas-tight pin coating is determined by the kinetic factor (the diffusion of oxygen and carbon to the zone of interaction of $UO_{2\pm x}$ and the PyC), the overall porosity, the core size, and the initial fuel composition.

Preliminary x-ray studies have shown that the following equilibrium is set up in a micropin at temperature above 1700°K:

$$UO_2 + 4C = UC_2 + 2CO\uparrow. \quad (1)$$

The coefficients for self-diffusion of oxygen in UO_2 [2] and of carbon in UC_2 [3] in cm^2/sec are such that

$$D^*_{O\to UO_{2.0}} = 1.15\exp(-56\,700/RT); \quad (2)$$

$$D^*_{C\to UC_2} = 132\exp(-89\,700/RT). \quad (3)$$

TABLE 1. Micropin Characteristics

Symbols for points in Fig. 1	V_p, 10^{-4} cm³	$(O/U)_{init}$	Core mass G, 10^{-6} g·mole	Notes
◑	0,5	2,01	2,2	Calculations
○	1,1	2,01	2,2	»
+	1,1	2,005	2,2	»
△	1,1	2,001	2,2	»
□	1,1	2,0005	2,2	»
▲	0,4	2,01	6,9	Conversion of data of [7]
■	0,4	2,005	6,9	The same
●	1,1	2,01	2,2	Conversion of data (◑)
×	1,1	2,001—2,005	2,2	Experiment

TABLE 2. Effects of Burnup and Porosity on CO and Xe Pressures in Micropins at 1873°K with O/U = 2.0000

Burnup mole %	Pressure, MPa: xenon, $V_p = 1{,}1\cdot10^{-4}$ cm³	xenon, $V_p = 0{,}5\cdot10^{-4}$ cm³	carbon monoxide: with allowance for oxides of Ba, Sr, Mo, and Cs, $V_p = 1{,}1\cdot10^{-4}$ cm³	with allowance for oxides of Ba, Sr, Mo, and Cs, $V_p = 0{,}5\cdot10^{-4}$ cm³	without allowance for oxides of Ba, Sr, Mo, and Cs, $V_p = 1{,}1\cdot10^{-4}$ cm³	without allowance for oxides of Ba, Sr, Mo, and Cs, $V_p = 0{,}5\cdot10^{-4}$ cm³
5	3,3	7,5	6,7	15,2	9,6	22,0
25	16,5	37,7	23,8	42,3	37,8	86,5
50	33,0	75,5	48,0 *	110 †	78,0 *	178 ‡

* O/U = 2,0005.
† O/U = 2,0012.
‡ O/U = 2,0020.

Translated from Atomnaya Énergiya, Vol. 54, No. 5, pp. 360-362, May, 1983. Original article submitted May 10, 1982.

 0038-531X/83/5405-0362$07.50

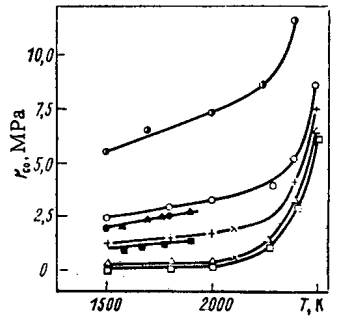

Fig. 1. Temperature dependence of the CO pressure in micropins in comparison with published and experimental data (see Table 1 for symbols).

Oxygen diffusion is not the controlling factor for (1). With allowance for the chemical effect, the diffusion coefficient of oxygen in UO_2 is $D_{UO_2}(chem) = 99\exp(-56{,}900/RT)$ cm^2/sec [4], and Storms [5] has given data on the diffusion of carbon in UC_2 with a thermodynamic factor of $(d/d)(\log a_C/x) = 50$, so that one can assume that the diffusion fluxes of oxygen and carbon to the continuous layer of UC_2 formed on the surface of the UO_2 are approximately equal. This also agrees with the published data [6]. The diffusion mobilities of oxygen and carbon are 10^{-5}-10^{-6} cm^2/sec at 1873°K, and the reduction of the surface layer of dioxide to produce a continuous layer of UC_2 of thickness not more than 1-2 μm will occur within a few seconds or minutes. Because of the high diffusion mobility of oxygen, a constant O/U ratio is set up over the cross section of the core just as rapidly. One can estimate the CO pressure in the micropin by using the limiting equilibrium pressure of CO for the final composition of the core at the set temperature. The CO pressure in a micropin may be calculated from $\log P_{CO} = f(O/U)$ [1] using the parameters characterizing high-temperature gas-cooled reactor pins: UO_2 content $G = 2.2\cdot10^{-6}$ g·mole, overall core volume $V_p = (0.5\text{-}1.1)\cdot10^{-4}$ cm^3, and oxygen coefficient $(O/U)_{init} = 2.0005 - 2.01$. In the range 1500-2000°K, the final O/U ratio for the uranium dioxide in a micropin is $(O/U)_{fin} = 2.0$, and if the temperature is raised to >2000°K it should fall to 0.01-0.001 or less with a porosity of $0.5\cdot10^{-4}$ cm^3.

Figure 1 gives approximate calculations on the CO pressures in micropins and compares them with published data [7], for which purpose reduction coefficients have been introduced, which are directly proportional to the mass of UO_2 in the core and inversely proportional to the overall porosity (Table 1).

A conversion has been performed for the case $V_p = 1.1\cdot10^{-4}$ cm^3 and $G_{core} = 2.2\cdot10^{-6}$ g·mole; here for comparison we also show the experimental values of the CO pressure. According to Fig. 1, the CO pressure in a micropin having a gas-tight covering of PyC and containing $2.2\cdot10^{-6}$ g·mole of uranium dioxide with O/U = 2.01 and overall porosity $0.5\cdot10^{-4}$ cm^3 attains 7 MPa at 1873°K.

To check the calculations, we have made direct measurements of the pressures within pins under static conditions. The heater was a molybdenum capillary of diameter 1.5-2.0 mm attached between current leads in a vacuum chamber. The middle uniformly heated part of the capillary was loaded with 10 micropins. After preliminary outgassing at 2073°K for 1 h, the micropins were broken and simultaneously the pumping system was switched off. The pressure changes in the chamber indicate the CO pressure in the micropins, which at 2073°K and an initial O/U = 2.001 — 2.005 ratio was in the range 0.5-2 MPa, i.e., it agreed with the calculations. The final value of O/U was 2 ± 0.0005.

The burnup of the uranium in the dioxide increases the oxygen activity, because the O_2 is incompletely taken up by the fission products and by oxidation of the core material in accordance with

$$(x/2)\,O_2 + UO_{2.00} = UO_{2\pm x} \qquad (4)$$

with the initial ratio O/U = 2.0005 — 2.01 and a temperature of 1500-2000°K; the fission products determine the O/U ratio corresponding to the irradiated fuel, which can be estimated by means of the $P_{CO} = f(O/U)$ relationship [1].

A thermodynamic analysis was performed on the binding of the oxygen by the fission products on the basis of published data [8, 9]. We considered the oxides SrO, Cs_2O, MoO_2, Sm_2O_3, Ce_2O_3, Nd_2O_3, ZrO_2, Y_2O_3, La_2O_3, Pr_2O_3, and Pm_2O_3, where the amount of cesium was estimated from the relation between Ba and Sr, which was found from the data of [10] for the completely oxidized form. A calculation was also performed on the fission products reacting with carbon to give carbides, which showed that the amount of these was less than 1%, and therefore they

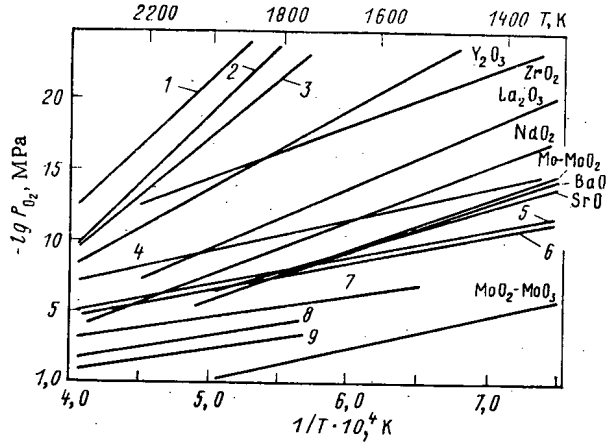

Fig. 2. Dependence of the oxygen partial pressure on temperature for uranium dioxide and a series of fission-product oxides [1, 8, 9]: 1-3) O/U = 1.97; 1.995; 2.00 (min); 4-9) O/U = 2.00 (max); 2.001; 2.003; 2.02; 2.05; 2.10.

were neglected. Here it should be pointed out that the partial free energy of the oxygen in the gas phase plays the principal part in the formation of fission-product oxides, not the ΔG_T^o for the resulting compound.

Figure 2 shows the temperature dependence of the equilibrium oxygen pressure over uranium dioxide and the oxides of uranium fission products. An analysis on the basis of ideal solutions showed that up to 75 mole % of the oxygen released in the fission of the dioxide is bound. Figure 2 also shows that the oxygen binding may be additionally reduced by 10 mole % by the Ba, Sr, Mo, and Cs, which at a certain temperature may not form oxides because of the change in O/U in the core. As a result, the CO pressure and the fuel composition vary considerably as the uranium burns up (Table 2). An estimate of the final composition of the irradiated fuel [10] from the model of [11, 12] at 1873°K and a porosity of $0.5 \cdot 10^{-4}$ cm^3 up to a burnup of 50 mole % gives O/U = 2.0015, which is close to the mean value within the table and which indicates that the apporach is correct. The Xe pressure is 0.5-0.8 of the CO pressure and is substantially dependent on the porosity and burnup. A reduction in the initial O/U ratio, e.g., to 1.98, with the object of reducing the CO pressure in the micropins, is desirable only for a burnup of about 5 mole %, since this method is less effective for higher burnups.

LITERATURE CITED

1. Yu. F. Khromov and R. A. Lyutikov, At. Energ., 49, No. 1, 28 (1980).
2. J. Bell, J. Nucl. Mater., 30, 3 (1969).
3. T. Wallace et al., USAEC-Report LA-DC-8840 (1968).
4. J. Bittel et al., J. Am. Ceram. Soc., 32, 447 (1969).
5. E. Storms, Refractory Carbides, Academic Press (1967).
6. T. Lindemer, M. Allen, and J. Leitnaker, J. Am. Ceram. Soc., 52, 233 (1969).
7. M. Ugajin, T. Arai, and K. Shiba, J. Sci. Technol., 14, 153 (1977).
8. I. S. Kulikov, Thermal Dissociation of Compounds [in Russian], Metallurgiya, Moscow (1965).
9. C. E. Weeks and F. E. Block, Thermodynamic Parameters of 65 Elements and Their Oxides, Halides, Carbides, and Nitrides [Russian translation], Metallurgiya, Moscow (1965).
10. Fortman and A. Naomidis, in: Thermodynam. Nucl. Mater. IAEA, Vienna (1975), p. 147.
11. J. Johnson et al., J. Nucl. Mater., 48, 21 (1973).
12. F. Ewart, ibid., 61, 254 (1976).

A SOURCE OF ERROR IN THERMAL NEUTRON CONVERTERS

A. V. Kondrashov

UDC 621.039.564

Thermal neutron converters are often used in research work on nuclear reactors. Their advantages include simplicity in recording the thermoelectric signal, small size, and short time constant. The main disadvantage is the instability of the calibration characteristics; this is usually explained by burnout of the neutron-sensitive substance.

In this paper we examine one of the surces of error that could have a significant and unpredictable effect on the calibration characteristic of the converters being examined. This possible source, arising during use, is the inhomogeneity of the thermoelectrodes on the section adjacent to the neutron-sensitive element and situated in a temperature gradient field.

There are indications in the literature [1] that the error in measuring the temperature, related to thermal diffusion of nickel out of the nickel base into the thermoelectrodes of the platinum–platinum-hydrogen (10% rhodium) thermocouple, reached 30% within 24 days at a temperature of 950° (Kelvin or Celsius).

We shall examine the mechanism giving rise to this error. Figure 1 shows the schematic diagram of one of the designs of the converter. The thermal electrodes A and B, passing through the thermal insulation I, are in contact with the neutron sensitive element C, which is heated in the neutron radiation field. The heating increases with increasing neutron flux. In addition, a temperature gradient appears along the thermoelectrodes (see Fig. 1b). During initial use, the components of the neutron-sensitive element do not have time to diffuse into the thermoelectrodes and the presence of the temperature gradient is not manifested in the calibration characteristic (see Fig. 1c).

With time, the components of the neutron-sensitive element, in particular, uranium, penetrate into the thermoelectrodes (see Fig. 1d) and the section of the thermoelectrodes with the altered (nonuniform along the length) composition is located in a temperature gradient field. This leads to a progressive change in the calibration characteristic in the converters.

We present below the computed values of the penetration depth of uranium into the nickel thermoelectrode after being held for 180 days at different actual temperatures, which the neutron-sensitive elements have during use:

T, °C	X, mm	T, °C	X, mm
200	$3{,}5\cdot10^{-5}$	500	$3{,}8\cdot10^{-1}$
300	$1{,}6\cdot10^{-3}$	600	2,8
400	$5{,}6\cdot10^{-2}$	700	7,8

In the calculation we used empirical dependences of the diffusion depth of uranium into nickel at different temperatures according to data in [2]. From the results obtained it follows that already at a temperature exceeding 400°C, it may be expected that an error will appear in the measurements due to the thermoelectrical inhomogeneity. In reality, the depth to which uranium diffuses, especially in the low-temperature region, must greatly exceed the value presented due to radiation stimulation of diffusion processes. Thus, it was found in [3] that under the action of a flux with density $6\cdot10^{12}$ neutrons/(cm^2·sec) with energies $E > 1$ MeV, the coefficient of diffusion of gold and aluminum into copper at $T \approx 0.3$ of the melting temperature of copper is approximately 10^6 times higher than the coefficient of diffusion without irradiation. The considerable intensification of diffusion processes with irradiation is also pointed out by others [4, 5], noting that the greatest effect occurs at a relatively low temperature.

Thus, it may be expected that when thermal neutron converters are used in active zones of nuclear reactors even at low temperatures (less than 400°C), depending on the specific con-

Translated from Atomnaya Énergiya, Vol. 54, No. 5, pp. 362-363, May, 1983. Original article submitted July 12, 1982.

0038-531X/83/5405-0365$07.50

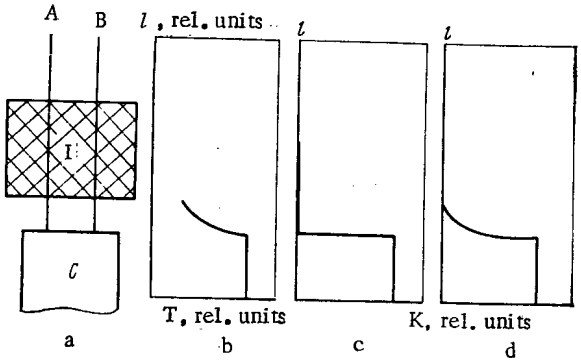

Fig. 1. Schematic diagrams of the construction of a converter (l, distance; I, temperature; K, concentration of the neutron-sensitive composition).

ditions, the limits of error can be very large: from negligibly small to inadmissibly large exceeding tens of percent. This depends on the structure of the converter, the component composition, and the temperature of the neutron-sensitive element, the temperature of the surrounding medium, conditions for heat transfer from the thermoelectrodes, temperature gradient and its constancy along the thermoelectrodes in the zone where they are adjacent to the neutron-sensitive element, distribution of components of the neutron-sensitive element in the thermoelectrodes (due to diffusion, it constantly changes), radiative energy liberation, intensity, fluence, and spectral composition of neutrons, duration of use, etc. Such a complicated dependence on many factors, especially with long operational lifetimes, can lead to large unpredictable errors in measurements and in many cases will cast doubt on the usefulness of thermal neutron converters.

LITERATURE CITED

1. J. Jensen, J. Klebanoff, and G. Haas, Res. Sci. J., 35, No. 12, 1717 (1964).
2. Y. Adda and J. Philiber, La Diffusion dans les Solides, Paris (1966).
3. Denic Acker, These de doctorat science, Universite Paris-Sud (1977), p. 154.
4. Z. Jarzebski, Dyfuzja w metalach., Katowice, Slask (1975).
5. Y. Adda, M. Beyeler, and G. Brebec, Thin Solid Films, 25, No. 1, 107 (1975).

EFFECT OF RESIDUAL CHARGE ON FORMATION OF RADIATION-INDUCED CURRENT IN A COMPTON DETECTOR

A. P. Elokhin, N. I. Filatov, and S. N. Makeev

UDC 539.1.074.8

The analysis of the formation of radiation-induced current (RIC) in a Compton detector is usually restricted to the current density of Compton electrons in the dielectric of the detector [1]. In this paper we take into account near-electrode effects in the spatial distribution of the dosage and current density of secondary charged particles arising in the dielectric at the metal–dielectric interface [2], as well as the surface density of charge on the electrodes, in the formation of RIC in a detector subjected to the action of pulsed ionizing radiation.

When a Compton detector is irradiated with γ rays, an electric field arises in the dielectric due to the passage of Compton electrons in it, free charge carriers with thermal energy, and residual charge (electrons captured by traps, positive ions), as well as the surface charge density arising on the electrodes of the detector due to the difference in the current density of electrons leaving the detectors and incident on them. Determining the intensity of the electric field due to each of the components separately, we find the total field, the potential difference corresponding to it, and, finally, the RIC in the irradiated detector.

When the condition

Translated from Atomnaya Énergiya, Vol. 54, No. 5, pp. 363-364, May, 1983. Original article submitted July 16, 1982.

 0038-531X/83/5405-0366$07.50

$$\sum_{i=1}^{3} \mu_i (E_\gamma) H_i \ll 1 \tag{1}$$

is satisfied (here $\mu_i(E_\gamma)$ is the linear attenuation coefficient of γ rays in the i-th medium, H_i is the thickness of the i-th medium), the rate at which a positive ion density is generated is practically constant. For a dielectric with thickness $H_2 > R_c$ (R_c is the free path of secondary electrons in the dielectric), the spatial distribution of the dosage is nonuniform (Fig. 1). In this distribution, in the region of the plateau, the condition of electronic equilibrium is satisfied, while the total density of residual charge equals zero. On the other hand, in the region of the first electrode, the charge is positive, while near the second electrode, it is negative [3]. The rate of generation of residual charge, taking into account the constancy of the rate of generation of positive ion density in the dielectric when condition (1) is satisfied, $\tau_T < 10^{-10}$ sec, and $\tau \approx 10^{-10}$ sec, is described by the expression

$$\varphi(x) = eq_p \left[1 - \frac{g(x)}{g(\bar{x})}\right], \tag{2}$$

where e is the electron charge; q_p, rate of generation of a positive charge density, $cm^{-3} \cdot sec^{-1}$; g(x), spatial distribution of the dosage; $\bar{x}$, point in the region of the plateau where $\varphi(\bar{x}) = 0$; τ_T, thermalization time of a Compton electron; and, τ, lifetime of a free charge carrier.

The kinetic processes, characterizing the change in the residual charge, reduce to its generation, recombination with free charge carriers, and relaxation. The time dependence of the residual charge density in the dielectric $\rho_{res}(x, t)$ with the initial (electret [4]) charge distribution $\rho_0(x) \neq 0$ and pulsed γ irradiation ($1/K_3 \gg \tau_p \gg \tau$) is determined from the solution of the equation

$$\frac{d\rho_{res}}{dt} = \varphi(x) f(t) - K_2 \rho_{res} n - K_3 \rho_{res}, \tag{3}$$

where f(t) is the function describing the temporal variation of the γ-ray flux; n, density of free charge carriers, cm^{-3}; K_2, rate of recombination of free carriers with the residual charge, $cm^3 \cdot sec^{-1}$; K_3, inverse lifetime of the residual charge, sec^{-1}; and τ_p, duration of the radiation pulse. The density n(t) is found from the equation [5]

$$n \approx G\bar{g} f(t)/2K_1 N_0,$$

where G is the radiation yield of free charge carriers; $\bar{g} = \frac{1}{H_2}\int_{x_1}^{x_2} g(x)\,dx$; K_1, rate of capture of charge carriers by a trap; and N_0, density of traps in the dielectric. We found the spatial distribution of dosage g(x) and current density of secondary charged particles j(x) from a solution of the transport equation for fast electrons [6]. It was found experimentally that if the absorbed dose with single or repeated irradiation of the detector does not exceed $5 \cdot 10^5$ rad, then the effect of the residual charge on the distribution of fast electrons can be neglected. The surface charge density for each of the electrodes is defined by the expressions

$$\sigma_1(t) = [j(x_1) - j(0)]\,\Phi(t);$$
$$\sigma_2(t) = [j(x_3) - j(x_2)]\,\Phi(t), \tag{4}$$

(5)

where $\Phi(t) = \int_0^t f(t')\,dt'$; $j(0)$; $j(x_1)$; $j(x_2)$; $j(x_3)$ is the value of the current density of secondary electrons at the interface of the media A-B, B-C, C-D, D-A, respectively (see Fig. 1). When the i-th electrode is grounded, $\sigma_i = 0$ ($i = 1, 2$). We further assume that $\sigma_1 = 0$. The intensity of the electric field, due to the surface charge density σ_2, equals $E_f = ([j(x_3) - j(x_2)]/\varepsilon\varepsilon_0)\Phi$, while the potential difference is determined by the equation $V_0 = ([j(x_3) - j(x_2)]/\varepsilon\varepsilon_0)\Phi H_2$. We find the intensity of the electric field due to the charge density of fast electrons ρ_f and the residual charge density ρ_{res} from Poisson's equation

$$E_2(x, t) = E_2(x_2, t) - \frac{1}{\varepsilon\varepsilon_0}\int_x^{x_2} \rho_\Sigma(x', t)\,dx', \tag{6}$$

where $\rho_\Sigma = \rho_{res}(x, t) - \rho_f(x, t)$. The quantity $\rho_f(x, t)$ can be determined from the continuity equation, while the potential difference created by the field $E_2(x, t)$ can be determined from the expressions

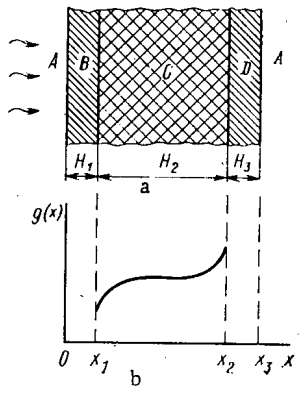

Fig. 1

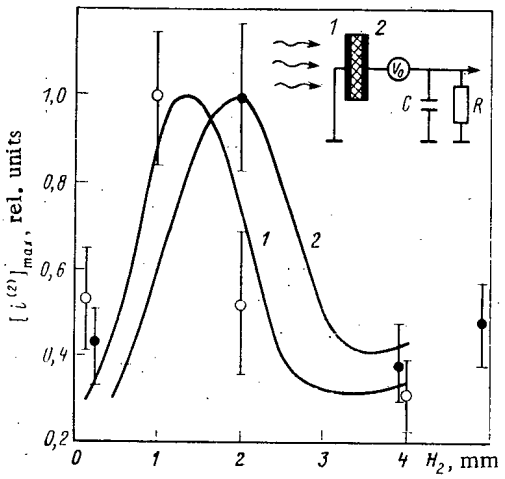

Fig. 2

Fig. 1. Conditions of irradiation of a flat heterogeneous target (a) and spatial distribution of dosage in the dielectric (medium C) with $H_2 > R_C$ (b).

Fig. 2. Amplitude of RIC as a function of the thickness of the dielectric with pulsed action of γ-ray flux in aluminum–polyethylene–aluminum (1) and copper–polyethylene–copper (2) targets: $\bar{E}_\gamma$ = 1 MeV, $H_1 = H_3 << R_{B,D}$; —) calculation; ○, ●) experiment. A diagram showing the RIC detector is shown in the upper right-hand corner.

$$V(t) = H_2 E_2(x_2, t) - \varkappa(t); \tag{7}$$

$$\varkappa(t) = \frac{1}{\varepsilon\varepsilon_0}\int_{x_1}^{x_2}\int_{x'}^{x_2} \rho_{res}(x'', t)\, dx''\, dx' + \frac{\Phi}{\varepsilon\varepsilon_0}\left[H_2 j(x_2) - \int_{x_1}^{x_2} j(x)\, dx\right]. \tag{8}$$

We shall find the sought potential difference V(t) by using Kirchhoff's equation for the RIC detection circuit (Fig. 2):

$$i = C\frac{dV_R}{dt} + \frac{V_R}{R}; \tag{9}$$

$$V = V_0 - V_R, \tag{10}$$

where C is the equivalent capacitance of the circuit; R, resistance of the load; V_R, potential difference on the load resistance; and i, current going into the external circuit. Using Eqs. (7) and (10), we find

$$E_2(x_2, t) = [V_0(t) + \varkappa(t) - V_R]/H_2. \tag{11}$$

For $j \geqslant 10^{-2}$ particles/(cm²·sec·γ-quanta), the conduction current density, due to drift of free charge carriers, is two orders of magnitude smaller, which is what permits neglecting it in the equation for the total current. In this case we have $j_{total}(x, t) = \varepsilon\varepsilon_0(\partial/\partial t)\cdot E_2(x, t)$. Since $j_{total} \equiv 0$, using (8), (9), and (11), we find the current in the Compton detector:

$$i^{(2)} = \frac{S}{H_2}\left\{f(t)\left[j(x_3)H_2 - \int_{x_1}^{x_2} j(x)\, dx\right] + \frac{d}{dt}\int_{x_1}^{x_2}\int_{x'}^{x_2} \rho_{res}(x'', t)\, dx''\, dx'\right\}, \tag{12}$$

where S is the area of the electrodes. Reasoning analogously and taking into account the fact that in calculating RIC at the first electrode (with the second electrode grounded), the direction of the current density of secondary electrons reverses, it is easy to obtain

$$i^{(1)} = \frac{S}{H_2}\left\{f(t)\left[\int_{x_1}^{x_2} j(x)\, dx - j(0)H_2\right] - \frac{d}{dt}\int_{x_1}^{x_2}\int_{x_1}^{x'} \rho_{res}(x'', t)\, dx''\, dx'\right\}. \tag{13}$$

As follows from the expressions presented, the RIC is greatly affected by the current density of electrons incident on the detector $j(0)$ or leaving it $j(x_3)$. We found from a calculation of the quantity i, taking into account the current density of electrons incident on the detector from the external medium, that the polarity of the RIC changed in contrast to the case $j(0) = 0$.

The decrease in the initial charge in the dielectric with repeated pulsed irradiation of the detector is due to its radiation annealing, and this is what was found in [7]. The thickness of the dielectric for which an extremum (maximum) was observed in the distribution $[i]_{max}(H_2)$, while calculating the maximum sensitivity of the detector $[i]_{max}(H_2)$ with pulsed γ irradiation, was determined. A comparison of the calculation and the measurements, performed with the help of a pulsed γ-ray source ($\bar{E}_\gamma$ = 1 MeV, $\tau_p \approx 100$ μsec) with detectors differing by the thickness of the dielectric (H_2 = 0.1-4 mm), showed satisfactory agreement (see Fig. 2). The value of H_2 at which an extremum is observed in the indicated dependence, if $i^{(2)}$ ($i^{(1)}$) is viewed as a function of the variable upper limit, is determined from the condition $(d[i^{(2)}]_{max})/dH_2 = 0$. Using this condition, we obtain the equation

$$H_2^2 \frac{d\rho_{res}}{dt}(H_2, t) - H_2 f(t) j(H_2) + f(t) \int_0^{H_2} j(x)\,dx - \int_0^{H_2} \int_{x'}^{H_2} \frac{d\rho_{res}}{dt}(x'', t)\,dx''\,dx' = 0. \quad (14)$$

Equation (14) can be solved numerically if the solution of (3) and the distributions $j(x)$, $g(x)$ obtained for different H_2 are known. As a rough estimate of the value of H_2 at which the extremum is observed, assuming $d\rho_{res}/dt \approx 0$ in (14), we find $H_2 \approx \int_0^{H_2} j(x)\,dx/j(H_2)$. From here it follows that an extremum in the distribution of $[i^{(2)}]_{max}(H_2)$ with nonuniform distribution of the Compton-electron current density in the dielectric is observed when the boundary value of the current density $j(H_2)$ is comparable to the average value of the current density over the entire thickness of the dielectric.

The value of H_2 at which the extremum is observed depends on the atomic number of the dielectric material, the material of the electrodes (see Fig. 2), and on the energy of the γ rays, since $j(x)$ and $g(x)$ depend implicitly on these quantities.

LITERATURE CITED

1. B. Gross, Rad. Res., 14, 117 (1961).
2. J. Wall and E. Burke, IEEE Trans. Nucl. Sci., NS-17, No. 6, 305 (1970).
3. A. F. Adadurov et al., At. Energ., 50, No. 5, 344 (1981).
4. G. A. Lushcheikin, Polymeric Electrets [in Russian], Khimiya, Moscow (1976).
5. E. L. Frankevich, Khim. Vys. Energ., 1, No. 6, 567 (1967).
6. A. A. Shkurpelov, A. P. Elokhin, and V. P. Veselov, At. Energ., 52, No. 6, 433 (1982).
7. V. M. Gorbachev et al., ibid., 33, No. 1, 576 (1972).

MEASUREMENTS OF THE REACTIVITY OF NUCLEAR REACTORS

V. A. Kachalin and V. N. Pridachin

UDC 539.125.503:621.039.515

Measurement of the reactivity is one of the standard problems in the monitoring and control of power reactors and in the investigation of nuclear physics facilities. Various specialized devices based on the analog or digital principle of calculating reactivity are applied to this end. High metrological characteristics and great functional possibilities are characteristic of digital reactivity meters [1]. However, until recently, the practical utilization of digital reactivity meters was restrained by the limited choice of computers. The appearance of accessible and reliable mini- and microcomputers with sufficiently large possibilities for processing information is causing justified interest in their application for measurement of reactivity in the real-time mode.

The purpose of the research performed consisted of the development of a portable digital reactivity meter based on commercially manufactured computers satisfying a wide range of requirements of research and engineering problems on nuclear power facilities.

Procedure for Measurement of Reactivity. One can write an expression for the reactivity from the kinetics equations of a nuclear reactor [2] in the form

$$\rho/\beta = l\left(dN/dt + \sum_{i=1}^{6} dC_i/dt\right)\beta\left[N + \left(dN/dt + \sum_{i=1}^{6} dC_i/dt\right)\right], \quad (1)$$

where ρ is the reactivity; l, lifetime of the prompt neutrons; N, neutron density; C_i, concentration of the precursors of the i-th group of delayed neutrons; and β, effective yield of delayed neutrons.

Equation (1) is directly simulated by an analog reactivity meter, but it can also be used to calculate the reactivity with a digital device. Actually, the main functional element of analog reactivity meters [3] is a series R_iC_i-circuit in which the current is the analog of dC_i/dt. Using the transfer function of an R_iC_i-circuit [$h(t) = \exp(-t/R_iC_i)$], where R_iC_i is a quantity which is the inverse of the decay constant λ_i of the precursors of the i-th group of delayed neutrons, and having specified the time step Δt and the variation law of an input quantity corresponding to the neutron density, one can calculate with the necessary accuracy the instantaneous values of the current in the circuit and, consequently $l\,dC_i/dt$. For a linear variation on the section Δt the relation between the reactivity and the neutron density is written as:

TABLE 1. Relative Computational Error of the Reactivity, %*

Δt, sec	t_Φ, sec	0,01	0,05	0,1	0,5	−0,01	−0,05	−0,1	−0,5	−1	−5
0,1	0,01	1,91 / 0,78	1,90 / 0,77	1,90 / 0,75	1,82 / 0,56	1,91 / 0,79	1,91 / 0,79	1,91 / 0,81	1,93 / 0,87	1,95 / 0,92	1,98 / 1,02
	0,5	−0,02 / 0,00	−0,02 / −0,01	−0,03 / −0,01	−0,09 / −0,06	−0,01 / 0,00	0,00 / 0,00	0,00 / 0,00	0,05 / 0,03	0,12 / 0,05	0,49 / 0,21
0,5	0,01	7,51 / 1,16	7,45 / 1,11	7,37 / 1,04	6,22 / 0,26	7,53 / 1,19	7,59 / 1,24	7,64 / 1,29	7,98 / 1,65	8,21 / 1,92	8,69 / 2,53
	0,5	−0,29 / −0,01	−0,42 / −0,03	−0,60 / −0,05	−2,45 / −0,18	−0,23 / 0,00	−0,10 / −0,02	0,05 / 0,04	1,04 / 0,24	1,94 / 0,46	4,91 / 1,41

*The numerators give the error in the first step of the calculation; the denominators give the error in the tenth step.

Translated from Atomnaya Énergiya, Vol. 54, No. 5, pp. 365-367, May, 1983. Original article submitted July 26, 1982.

0038-531X/83/5405-0370$07.50

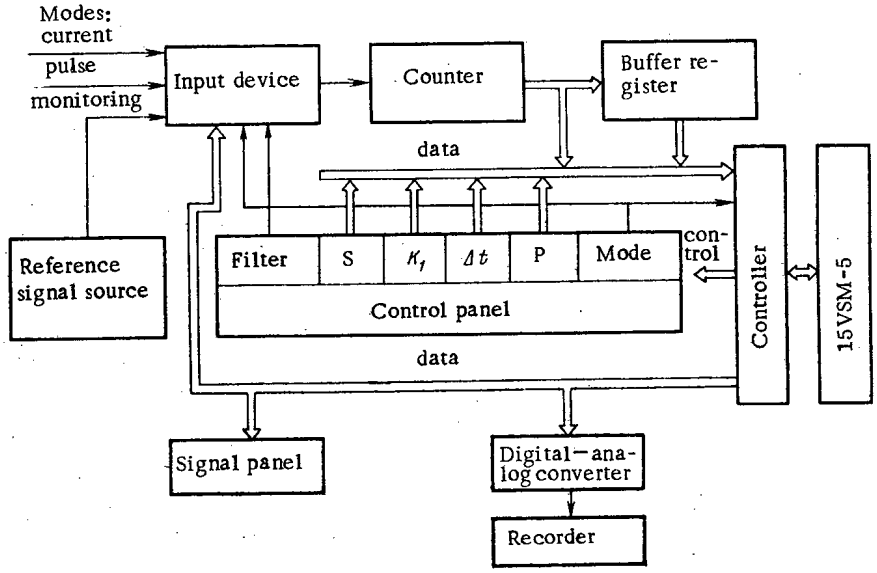

Fig. 1. Structural layout of the reactivity meter.

$$\rho/\beta = \sum_{i=1}^{6} I_{i,m}/N_m, \qquad (2)$$

$$I_{i,m} = I_{i,m-1}E_i + (N_m - N_{m-1})F_i,$$

where $I_i = (l\,dC_i/dt)\cdot\beta^{-1}$; $E_i = \exp(-\lambda_i\Delta t)$; $F_i = (\beta_i/\beta)[(1 - E_i)/\lambda_i\Delta t]$; $\Delta t = t_m - t_{m-1}$; $I_{i,0} = 0$; $i = 1, \ldots, 6$. Neglect of the term dN/dt is justified by the fact that it makes an insignificant contribution to the reactivity, and taking it into account intensifies the effect of reactor noise on the output of the measuring circuit [4]. When necessary, one can take the term dN/dt, as also $\sum_{i=1}^{6} dC_i/dt$ in the denominator of the expression (1), into account in calculating the reactivity.

The values of the neutron density for reactivity discontinuities different in magnitude, sign, and rise time t_ϕ were calculated for a qualitative estimate of the algorithm (2) on the basis of a solution of the kinetics equations of a reactor. The calculated values of the neutron density were used to calculate the reactivity by a program implementing the algorithm (2) for two values of the step Δt (0.1 and 0.5 sec). The results of the calculations of the relative errors in computing the reactivity are given in Table 1.

Structural Layout of the Reactivity Meter. The algorithm (2) has been realized in a reactivity meter (see Fig. 1) created on the basis of a 15VSM-5 specialized computer, which belongs to the class of desk-type minicomputers and is a modification of the Élektronika-50 minicomputers [5]. The advantages of the 15VSM-5 are its high computational accuracy (the significance of the mantissas of numbers is 12, and of the order — two decimal digits) and simplicity of programming.

One of the main requirements of a reactivity meter is the provision for measurement of the reactivity over a wide dynamic range of neutron flux density which encompasses the start-up and operating regimes of a reactor. Since it is necessary to work with pulse and current detectors, it is necessary to have two conversion channels — pulse and current. In the reactivity meter which has been developed, the integrating method of measurement has been implemented, due to the use in the input device of a voltage-to-tracking frequency converter (VFC) with preliminary amplification of the input signal by a programmable amplifier. Thus, the input device outputs a unified signal — the pulse tracking frequency, independent of the type of detector. In order to eliminate the component of the error in calculating the reactivity caused by the presence and drift of the zero-level shift of the amplifier–VFC channel, the measurement is performed in two stages in each step of the calculation: in the first stage the shift with the input signal disconnected is measured, and in the second stage the composite signal and shift are measured with subsequent algebraic subtraction of the value of the shift in the computer. The input of data into the computer is accordingly accomplished from the buffer register and the input counter. The programmable amplifier is constructed on the basis of a 701ML18 micromodulator constant-current amplifier.

The reactivity meter is controlled with the help of switches located on a control panel. The operator specifies the operating mode (current, pulse, monitoring), the transfer coefficient K_1 of the constant-current amplifier (automatically or manually), the value of the recorder scale S in reactivity units (automatically or manually), the parameter P, whose instantaneous value it is necessary to output from the computer to the digital signal panel, and the value of the reactivity computation step.

The calculated reactivity values are output through a three-decade digital–analog converter to a recorder, and can be output to the digital signal panel. A decimal indicator signal panel is accomplished with AL304V light-emitting units. The format of a number is: sign of the mantissa, three digits of the mantissa, sign of the order, and two digits of the order. If the operator wishes, the values of an input quantity or the scale of the recorder in reactivity units can be output to the signal panel.

In order to calibrate the current channel and to perform a complex check of the instrument, the monitoring regime is implemented, in which the input of the programmable amplifier is connected to the output of the reference signal source. In calibration a specified constant-current signal is fed to the amplifier input, and for complex checking – a current signal which simulates a stepwise change of 0.1β in the reactivity.

Operating Characteristics of the Instrument. The reactivity meter has been used successfully for more than a year on a VK-50 boiling reactor and a BOR-60 fast reactor. Checking of the reactivity meter on a Spectrum-1 critical assembly for the purpose of an experimental evaluation of the characteristics of the instrument and comparison with calculation preceded the reactor tests. Two kinds of perturbations of the reactivity were realized: slow (t_ϕ = 60 sec) input–output and fast (t_ϕ = 0.3 sec) dropping of the absorbing rods. With slow manipulations by the rods (0.225, 0.120β), the measured values of reactivity are within the limits of error of the results obtained for a steady-state period (1.5%). With rapid dropping of the rods, the final value of the step Δt has a significant effect on the computational error. For a "heavy" rod (β) the error in the first step amounts to ∿10% with Δt = 1 sec in calculating the reactivity.

The principal technical characteristics of the instrument are: range of input currents from 10^{-10} to 10^{-4} A (five conversion ranges); permissible counting rate 10^5 pulses/sec; reactivity computational step from 0.5 to 4.5 sec with a discreteness of 0.5 sec; and the number of scale values for the recorder in reactivity units is seven values specifiable by the operator prior to the start of measurements.

LITERATURE CITED

1. V. N. Sarylov et al., At. Tekh. Rubezhom, No. 11, 19 (1979).
2. J. Kipin, Physical Principles of the Kinetics of Nuclear Reactors [in Russian], Atomizdat, Moscow (1967).
3. I. B. Karasev et al., Vorp. Nauki i Tekh., Ser. Yad. Priborostr., No. 36, 59 (1978).
4. W. Lehto and C. Cohut, Reactor Techn., Winter 1971-1972, 14, No. 4, 345.
5. V. I. Grubov and V. S. Kirdan, Handbook on Computers and Analog Devices [in Russian], Naukova Dumka, Kiev (1977).

SPATIAL EFFECTS IN THE MEASUREMENT OF SMALL REACTIVITY

I. P. Matveenko, V. A. Lititskii,
A. G. Kostromin, O. I. Makarov,
and V. I. Shikina

UDC 621.039.54

The use of reactivity meters realizing the inverse solution of the point kinetics equations (ISKE) of a reactor to measure reactivity in large reactors necessitates taking account of the error due to spatial effects. At the present time several methods are available for correcting these effects either by calculation [1, 2] or by special technical methods [3]. In [2] an efficient method is proposed for taking account of spatial effects in measurements of reactivity up to $(1.5\text{-}3)\beta_{ef}$ within the limits of the experiment. In the development of this method it turned out to be very useful to assume that for an abrupt change in reactivity of the reactor, the neutron detector efficiency, defined as the ratio of its counting rate to the rate of production of neutrons (taking account of importance), is also changed abruptly. This assumption corresponds to a space–time rearrangement of the prompt neutron distribution after the reactivity change, and is realized in practice for reactivities up to $(3\text{-}4)\beta_{ef}$ in the whole volume of the reactor, except near the perturbed region [4].

If the calculational corrections to the change in neutron detector efficiency are used in the ISKE method, it is convenient to introduce a coefficient which describes the sensitivity of the measured value of the reactivity to the change in detector efficiency, defined as

$$\eta(\rho, t) \equiv \frac{1}{\rho} \frac{\partial \rho}{\partial \omega(\rho, t)}, \tag{1}$$

where ω is the ratio of the detector efficiency after and before the reactivity introduction; $t > 0$, time after the reactivity introduction; and ρ, reactivity of the reactor. It is clear that in this case the relative error of the reactivity measurement is

$$\frac{\Delta\rho(t)}{\rho} = \eta(\rho, t)\,\Delta\omega, \tag{2}$$

where $\Delta\rho(t)$ is the correction due to the spatial effect, and $\Delta\omega$ is the relative change in detector efficiency. Using the above approximation concerning $\omega(t)$, it is easy to show that

$$\eta(\rho, t) = \frac{\beta n_0}{\rho h(t)} \sum_i a_i \exp(-\lambda_i t),$$

which is plotted in Fig. 1 for various values of ρ. It is assumed that before the reactivity change (rod drop) the reactor was in the critical state.

In designing an experiment to minimize error, it is of interest to compare the sensitivity coefficient $\eta(\rho, t)$ for the ISKE method with the analogous sensitivity coefficient for the inverse multiplication method, whose value η_0 obviously does not depend on time, and is equal to unity. With an increase in the absolute value of the reactivity ($|\rho/\beta| \gg 1$), $\eta(\rho, t)$ approaches η_0, which corresponds to the assumption that the delayed neutrons are mainly stored up until the reactivity is changed. It can be shown that at $t = 0$, i.e., immediately after the introduction of negative reactivity, the sensitivity coefficient is

$$\eta(\rho, 0) = \frac{\beta - \rho}{\rho}, \tag{3}$$

so that at $t = 0$ the "sensitivity" to a change of the neutron detector efficiency is greater for small than for large absolute values of the reactivity, and for $|\rho| \gg \beta_{ef}$ the sensitivity coefficient $\eta(\rho, t) \to 1$. Therefore, in measuring a large reactivity the ISKE method has no advantage over the inverse multiplication method as regards sensitivity to spatial effects.

Translated from Atomnaya Énergiya, Vol. 54, No. 5, pp. 367-368, May, 1983. Original article submitted August 2, 1982.

0038-531X/83/5405-0373$07.50

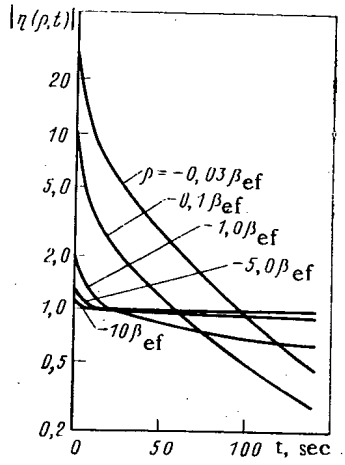

Fig. 1

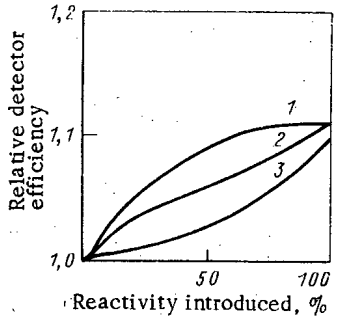

Fig. 2

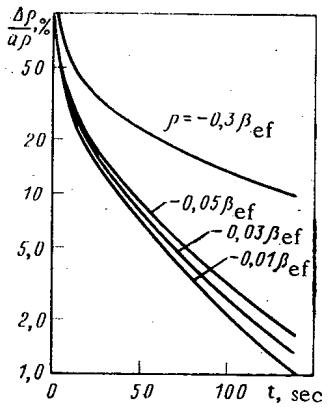

Fig. 3

Fig. 1. Time dependence of sensitivity coefficient for various values of the reactivity.

Fig. 2. Calculated dependence of the relative change in neutron detector efficiency on reactivity for the detector at: 1) 0.25h; 2) 0.50h; 3) 0.75h; where h is the height of the core allowing for end shields.

Fig. 3. Time dependence of standard error of the measurement of small reactivity perturbations.

For a reactivity $|\rho| \leqslant \beta_{ef}$ the sensitivity coefficient $\eta(\rho, t)$, which has a rather large value at $t = 0$, decreases to unity in ∿10–20 sec, and continues to decrease, the more rapidly the smaller the absolute value of the reactivity.

In general, the change $\Delta\omega$ in neutron detector efficiency depends both on the magnitude of the reactivity and the place it is introduced, and on the location of the neutron detector. It is customary to assume that spatial effects can be neglected for a small perturbation of the reactivity ($|\rho| \ll \beta_{ef}$). Assuming that the relative change in detector efficiency is porportional to the reactivity, which is practically realizable in any case for small values of the reactivity, it can be shown that in a number of experiments spatial effects cannot be neglected even for small reactivity changes. Figure 2 shows the calculated dependence of $\Delta\omega$ on the reactivity introduced by the compensation system calculated by the DHESTR program, which is a two-dimensional program for calculating reactor transients in the multigroup approximation, taking account of delayed neutrons, for various locations of the neutron detectors along the height of the latent surface of the BN-600 reactor vessel. In most cases $\Delta\omega$ is proportional to ρ, i.e., $\Delta\omega = \alpha\rho$, over limited parts of the motion of the compensation system.

Then it follows from Eqs. (2) and (3) that

$$\frac{\Delta\rho(t)}{\rho} = \frac{\eta(\rho, t)}{\eta(\rho, 0)} \text{ const}, \qquad (4)$$

i.e., in this case $\Delta\rho(0)/\rho(0)$ does not depend on the absolute value of the reactivity introduced. This relation is plotted in Fig. 3. The relative error of the reactivity measurement is maximum at $t = 0$ and decreases more rapidly for small values of the reactivity than for large. If an experiment to measure small reactivity perturbations is arranged in such a way that the result is recorded a long time after the perturbation, spatial effects can clearly be neglected. However, in a number of experiments, e.g., in measuring components of the power reactivity coefficient by the small perturbation method, or in oscillator measurements, the time of measurement is determined by the experimental conditions. In this case the error of the reactivity measurement can be appreciable, and spatial effects must be taken into account just as for the introduction of a large reactivity.

The results obtained may be useful in minimizing errors in the study of rapid processes in a reactor which lead to small reactivity changes.

LITERATURE CITED

1. J. Allen et al., Trans. Am. Nucl. Soc., 19, 417 (1974).
2. Yu. A. Kazanskii et al., At. Energ., 51, 387 (1981).
3. K. Ferguson et al., Nucl. Technol., 29, 37 (1976).
4. V. E. Kolesov et al., Preprint FÉI-1162, Obninsk (1981).

CALCULATION OF THE OPTIMAL ENERGY DISTRIBUTION IN A REACTOR

A. M. Afanas'ev

UDC 621.039.562

It is necessary, when developing a method for calculating the optimal energy distribution in a reactor, to take account of the large dimensionality of the original system of equations and a minimum computation time. The first one follows from the requirements of not exceeding the specified capacity of each fuel channel, and the second one is associated with the use of optimization results in operational control of a reactor. Out of the algorithms published for domestic reactors [1-3], the method for calculation of high-powered water-cooled channel reactors (RBMI) proposed in [3] best corresponds to these conditions. A reduction of the required operational computer memory and a decrease in the computation time has been achieved in [3] with the help of heuristic methods — the selection of potentially "dangerous" channels with subsequent checking of the correctness of the choice and correction of it. The selection method takes into account the multilattice structure of an RBMK. It is advisable to use other selection rules in a reactor without a multicellular structure.

The optimization is performed in this paper for the most loaded channels, whose number is somewhat larger than the number of control rods which have not reached the end. The numbers of these channels are determined in the course of solving the problem. A linear model has been used in [1-3] for description from the initial one is not "small," this leads to a noticeable imbalance in the reactivity and in errors in the optimal layout. An iterative procedure is proposed in this paper for taking account of the dependence of the effectiveness of rods on the neutron field.

The problem has ben formulated as follows. A reactor is operating in the steady regime. One can represent the equation of state of the reactor in the form

$$\hat{H}(\mathbf{r})\,N_0(\mathbf{r})=0, \qquad \int N_0(\mathbf{r})\,d\mathbf{r}=Q, \tag{1}$$

where $\hat{H}$ is a specified operator; N_0, steady neutron field; and Q, quantity which characterizes the reactor power. It is necessary to find at the points with the coordinates r_j those variations of the controls ρ_j which satisfy the equation

$$\hat{H}(\mathbf{r})\,N(\mathbf{r})+\sum_{j=1}^{M}\rho_j F_j(\mathbf{r})\,N(\mathbf{r})=0 \quad \text{and} \quad \int N(\mathbf{r})\,d\mathbf{r}=Q, \tag{2}$$

and the constraints

$$\alpha_j\leqslant\rho_j\leqslant\beta_j, \quad j=1, 2, \ldots, M \tag{3}$$

for which the condition

$$\min_{r_i}[(1-N(r_i)/\Pi_i)/\sigma_i]=\max, \quad i=1, 2, \ldots, K \tag{4}$$

would be satisfied. Here, according to [3], Π_i is the threshold value for which the i-th channel is damaged; σ_i, error with which the margin until damage is known; r_i, coordinate of the i-th channel; F_j, spatial localization function of the j-th control; $F_j(r) = \delta(r - r_j)$; α_j, β_j, specified quantities; M, number of controls; and K, number of channels in the active zone of the reactor.

Let us represent the solution of Eqs. (2) in the form

$$N(\mathbf{r})=N_0(\mathbf{r})+\sum_{j=1}^{M}\rho_j G_j(N)\,\Psi_j(\mathbf{r}), \tag{5}$$

Translated from Atomnaya Énergiya, Vol. 54, No. 5, pp. 368-370, May, 1983. Original article submitted August 9, 1982.

0038-531X/83/5405-0375$07.50

where G_j is a function whose form will be determined below and Ψ_j is the influence function of the j-th control at the point $\mathbf{r}$.

With the fact that the operator $\hat{H}$ is singular taken into account, we shall determine Ψ_j from the solution of the equation

$$\hat{H}(\mathbf{r})\Psi_j(\mathbf{r}) = -F_j(\mathbf{r})N_0(\mathbf{r}) + \nu_j \mathcal{F}(\mathbf{r})N_0(\mathbf{r}), \tag{6}$$

where $\int \Psi_j(\mathbf{r})\,d\mathbf{r} = 0$, and $\mathcal{F}(\mathbf{r})$ is a specified weighting function; the value of ν_j is calculated from the condition of orthogonality of the right-hand side of Eq. (6) to $N_0^+(\mathbf{r})$:

$$\nu_j = N_0(\mathbf{r}_j)N_0^+(\mathbf{r}_j) \Big/ \int \mathcal{F}(\mathbf{r})N_0(\mathbf{r})N_0^+(\mathbf{r})\,d\mathbf{r}, \tag{7}$$

where N_0^+ is the solution of the equation conjugate to (1).

With $\mathcal{F}(\mathbf{r}) \equiv \text{const} = 1$, ν_j^{-1} characterizes the variation of the criticality of the reactor upon a change of the j-th control by unity. When the spatial localization function of the automatic regulation (AR) system $F_{AR}(\mathbf{r})$ is selected as $\mathcal{F}(\mathbf{r})$, ν_j will characterize the displacement of the AR rods for maintaining criticality. After substitution of Eq. (5) into the expression (2), we obtain with (1) and (6) taken into account that the solution of Eq. (5) makes Eqβ (2) vanish identically when the conditions

$$G_j(N) = N(\mathbf{r}_j)/N_0(\mathbf{r}_j); \tag{8}$$

$$\sum_{j=1}^{M} \rho_j G_j(N)\nu_j = 0 \tag{9}$$

are satisfied. With the expressions (7) and (8) taken into account, Eq. (9) is transformed to the form

$$\sum_{j=1}^{M} \rho_j N(\mathbf{r}_j)N_0^+(\mathbf{r}_j) = 0. \tag{10}$$

When $|N(\mathbf{r}_j) - N(\mathbf{r}_j)| \ll N_0(\mathbf{r}_j)$, the expressions (5)-(10) coincide with the corresponding ones from [3], and the assumptions of additiveness and linearity taken as the basis of the method for calculation of the optimal energy distribution developed in [1] are also satisfied. We note that the equating of G_j to unity leads to a second-order error in $N(\mathbf{r})$ and a first-order error in the reactivity balance condition (10).

After substitution of Eq. (5) into the expression (4) and discretization over space, we shall solve the obtained system of equations by the iteration method according to the following scheme:

$$\max Z^{(n)}; \tag{11}$$

$$Z^{(n)} + \frac{1}{\Pi_i \sigma_i} \sum_{j=1}^{M} \tilde{\rho}_j^{(n)} \Psi_{ji} \leqslant Z_{0,i}; \quad i = 1, 2, \ldots, K; \tag{12}$$

$$\sum_{j=1}^{M} \tilde{\rho}_j^{(n)} \nu_j = 0; \tag{13}$$

$$\alpha_j G_j(N^{(n-1)}) \leqslant \tilde{\rho}_j^{(n)} \leqslant \beta_j G_j(N^{(n-1)}); \quad j = 1, 2, \ldots, M; \tag{14}$$

$$N_i^{(n-1)} = N_{0,i} + \sum_{j=1}^{M} \tilde{\rho}_j^{(n-1)} \Psi_{ji} \text{ and } N_i^{(0)} = N_{0,i}. \tag{15}$$

where n is the iteration numbers, $Z = \min\ [(1 - N_i/\Pi_i)/\sigma_i]$; $Z_{0,i} = (1 - N_{0,i}/\Pi_i)/\sigma_i$; $\tilde{\rho}_j = \rho_j G_j(N)$; $\Psi_{ji} = \Psi_j(\mathbf{r}_i)$; $N_i = N_i(\mathbf{r}_i)$. The iterations are concluded when the values $N_i^{(n)}$ and $N_i^{(n-1)}$ agree to within the accuracy of a specified number ε for i = 1, 2, ..., K. Convergence of the iterative process should be expected because $\Psi_j(\mathbf{r})$ does not vary during the entire iterative procedure and the effectiveness of the j-th control, which is corrected at each iteration by virtue of a change in the field profile, cannot be greater than some number. The size of the matrix $\hat{\Psi}$ is large; therefore, when solving the problem its elements Ψ_{ji} are placed in an external memory device (EMD) and are read into the operational memory of the

TABLE 1. Basic Parameters Adopted in the Optimization of Reactors

Parameter	[1]	[2]	[3]	This paper
M	90	40	90	57
M_w	40	40	40	27
K	120	424	1500	975

machine only when necessary. The optimal state at the n-th iteration is determined as a result of the successive solution of problems with a number of constraints L somewhat larger than the number of "working" (rods which have not reached the end) controls at the $(n-1)$-th iteration $M_w^{(n-1)}$. The transition from one problem to another can be schematically represented as follows. Let the solution obtained with expressions (13) and (14) and the set of channel numbers $\{i_m\}$ taken into account not satisfy certain inequalities (12). Then the numbers $\{i_j\}$ (where $j = 1, 2, \ldots, J$; J is a specified number) corresponding to the maximum discrepancies are determined and a new set of conditions (12) is formed, with respect to which the following optimization problem is solved, etc.* The process is continued until those L constraints are selected for which the solution of the problem satisfies all the conditions (12)-(14). After the conclusion of the n-th iteraction for channels whose numbers have entered the list of "dangerous" ones $O^{(n)}$ [the inequalities (12) have been rewritten into equations], the value of $\varepsilon_{max}^{(n)}$ is calculated:

$$\varepsilon_{max}^{(n)} = \max_{l \in O^{(n)}} \varepsilon_l \text{ and } \varepsilon_l = |(Z^{(n)} + N_l/\Pi_i \sigma_i) - 1|.$$

If $\varepsilon_{max}^{(n)}$ is greater than the specified ε_1, calculation of the n-th iteraction is repeated with a new initial set of constraints (12). This has been undertaken in connection with the fact that passage through a "bad" vertex with corresponding loss of accuracy is possible in the process of sorting the vertices of the polyhedron formed from the constraints. The calculation of each partial optimization is performed according to the algorithm of the double simplex method [4]. The latter is more economical than the simplex method algorithm (since the coefficients of the goal function are positive) and permits calculating a new solution very efficiently on the basis of the optimal solution obtained earlier when changing the constraints (14) and adding new inequalities of the type (12).

A program OPTIMA has been written in FORTRAN for a BÉSM-6 using the algorithms given above. Depending on the initial choice of channel numbers in the first iteration, the time necessary for optimization of the energy distribution of a reactor with $K \approx 1000$, $M \approx 60$, and $\Pi_i \equiv$ const and $\sigma_i \equiv 1$ oscillated from 40 sec to 2 min (~30% of the time was expanded on exchanges with the EMD disk). Solution of the problem in the linear approximation (after the first iteration) with a decrease of the nonuniformity coefficient of the energy distribution from 1.8 to 1.3 led to subcriticality of the reactor by approximately 0.5% and some inaccuracies in the determination of the "dangerous" channels and the "working" controls (their numbers are situated closer to the periphery of the active zone in the subsequent iterations). For compensation of the reactivity excess in this case, separation of approximately two rods located on the lower end would be required.

In calculating with the OPTIMA program, an amount of operational computer memory S in kilobytes can be estimated from the formula

$$S = 4\,|(M \times M + 22M + K) \cdot 10^{-3} + 1|. \quad (17)$$

With a total number of controls M, S increases quadratically with an increase in the "working" controls M_w and depends only linearly on the number of constraints K. The amount of operational computer memory necessary for optimization of the energy distribution by the OPTIMA program is 27 [1], 16 [2], 32 [3], and 19 kilobytes [this paper] in accordance with the data of [1-3] and this paper (see Table 1).

*A new set is formed from the numbers $\{i_j\}$ and $\{i_m\}$ so that the total number of constraints does not exceed L. When necessary, the part of the numbers from $\{i_m\}$ corresponding to channels with the least capacity is excluded.

Thus, when solving problems for domestic reactors using the OPTIMA program, a volume of operational computer memory of class SM-2 is sufficient.

The author extends his gratitude to B. Z. Torlin and V. N. Konev for a useful discussion of the paper and for help in calculating the influence functions.

LITERATURE CITED

1. I. Ya. Emel'yanov et al., At. Energ., 44, No. 4, 310 (1978).
2. O. L. Bozhenkov et al., At. Energ., 51, No. 2, 91 (1981).
3. A. A. Anikin and Ya. V. Shevelev, in: Vopr. At. Nauki i Tekh., Ser. Fiz. Tekh. Yad. Reaktorov, No. 3(12), 35 (1980).
4. A. I. Zukhovitskii and L. I. Avdeeva, Linear and Convex Programming [in Russian], Fizmatgiz, Moscow (1967).

REPRESENTATIVENESS IN SAMPLING COOLANT SODIUM

P. S. Otstavnov, I. A. Efimov, V. I. Ivanov, S. E. Lavrov, L. A. Stabenova, and I. G. Sheinker

UDC 621.039.526:621.039.58

Safe operation of a nuclear reactor requires constant monitoring of the radioactive impurities in the coolant and the protective gas in the first loop. There are several methods of measuring the radioactivity of nuclides in a sodium coolant. Here we report several observed phenomena that influence the representativeness of the activity measurements for the first loop of a sodium-cooled fast reactor.

There are two basic disadvantages in operating with special bypass pipes in the first loop of the reactor in order to measure the activities of the fission and corrosion products in sodium and on the walls of the pipes by measuring the γ-ray spectra: the method is not operational, since it requires a delay in order to reduce the γ background from the ^{24}Na, and it is impossible to measure the activities of nuclides that do not give γ radiation (tritium and ^{90}Sr) or of α-active nuclides (uranium, plutonium, etc.). Therefore, regular measurements are made on the activities of samples of coolant taken from the loop in a fast reactor, along with other systems for monitoring the sealing of the fuel-rod sheaths as indicated by the delayed-neutron activity in the coolant and the activity of the gaseous fission products in the protective gas, as well as γ spectrometry of the pipelines in the first loop.

A deficiency of a tubular sampler resembles that of the nonsampling method of radioactivity measurement in that it is difficult to monitor the deposition of impurities on the inner walls of the tube. It is found that fission and corrosion products are deposited on the inner and outer surfaces of the vessel on pumping the sodium through a sampler. Evidently, this explains the excess of about 10% or so in the specific activities of certain nuclides such as ^{137}Cs in the sodium samples taken into metal vessels through the sampling device relative to the specific activities in the main pipeline.

We have made measurements on the radionuclide concentrations by reference to the volumes of sodium samples taken into metal vessels, and we have found that the main contribution to the uncertainty over impurities in the coolant arises from the redistribution of the impurities over the sample volume during cooling.

The BR-10 reactor was used in testing a sampler devised for the BN-600 apparatus (Arkhipov, V. M., et al., in: Proc. 2nd Intern. Conf. on Liquid Metal Technology in Energy Production, Richland, Washington, April 1980, p. 16(69), Conf. 800491-P1). In this sampler, the circulating sodium flushes four vessels in a cassette and fills them. Then the cassette with the vessels containing the frozen sodium in an inert medium is transferred to a container and sent for analysis.

Figures 1 and 2 show the distributions of the radionuclides in a sample of sodium cooled under natural conditions in the sampler. The sample was taken into a nickel vessel of diam-

Translated from Atomnaya Énergiya, Vol. 54, No. 5, pp. 370-371, May, 1983. Original article submitted August 9, 1982.

 0038-531X/83/5405-0378$07.50

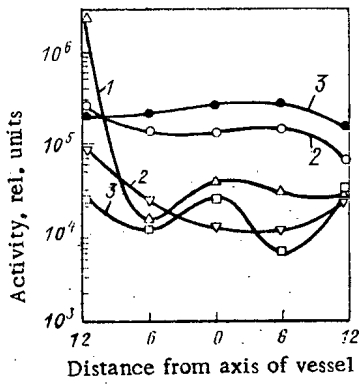

Fig. 1

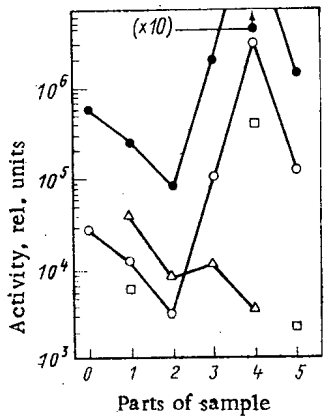

Fig. 2

Fig. 1. Distributions of concentrations of ^{137}Cs (△, ▽, □) and ^{125}Sb (○, ●) in layers from sodium (1-3).

Fig. 2. Concentrations of ^{137}Cs (●), ^{134}Cs (○), nuclear fuel (Δ), and ^{90}Sr (□).

eter 24 mm, height 20 mm, and wall thickness 1 mm. After filling with the sodium, the vessel stayed in the sampling device in an argon atmosphere for 10 days to reduce the ^{24}Na activity. Then the sample was kept in air for several days at room temperature. A layer of oxidation products was formed at the top on account of the contact with the air.

The radionuclide concentrations were measured at points ranging over the diameter of the vessel and along the height, and material washed from the walls and bottom was also examined. The sample was divided along the height into four parts: 0, oxidation products (upper layer) and 1, 2, and 3, layers for sodium (thickness about 5 mm). The washing from the walls and the bottom is denoted by the number 4 in Fig. 2, while the results for measurement on the sodium all taken together is denoted by 5.

Figure 1 shows the concentrations of ^{137}Cs and ^{125}Sb along the diameter for the three layers of sodium on a semilogarithmic scale. For clarity the experimental points have been joined by a smooth curve. The error of measurement was up to 30%. Figure 1 shows that the cesium concentrations can vary by factors of hundreds over the diameter and over the height; ^{125}Sb was observed only in layers 2 and 3, and the distribution of this over the diameter and height and of these layers was more uniform than that for ^{137}Sc. The observed concentrations did not differ by more than factors of 5-7. Anitmony was not observed in layer 1 on measuring the concentrations at points along the diameter, or else the concentrations at these points were less by about a factor of 10 than those in layer 2. However, ^{125}Sb was observed on examining an average specimen of layer 1, and the concentration was close to the concentrations at points in layer 2.

Figure 2 gives the concentrations for ^{137}Cs, ^{134}Cs, nuclear fuel (plutonium), and ^{90}Sr in average specimens of the sodium (0, 1, 2, 3) and in the sodium flushed from the inner surface of the vessel (4), as well as the mean concentrations of cesium and strontium obtained by measuring the entire mass of sodium (5). The concentration differences for cesium are by factors of 100 or more, while those of the nuclear fuel differ by factors of 10 or more, and those of strontium by up to factors of 50. It is possible that the concentrations for strontium, antimony, and nuclear fuel varied so widely because the measured threshold for the concentrations of these elements is limited by the sensitivity of the recording apparatus.

^{22}Na was observed in all the specimens, and the amount was proportional to the mass taken within the error of measurement. The concentrations of the nuclides with respect to the volume of the sodium as referred to unit decay of ^{22}Na are analogous to those shown in Figs. 1, 2.

There was skewness in the nuclide distribution over the diameter and over the height. The skewness and the concentration variations in the volume are due primarily to convection and diffusion, whose direction and rate are dependent on the temperature and temperature gradient. The deviations of the nuclide concentrations from equilibrium as occurring in the initial system are dependent on the cooling time to the solidification point of sodium. Diffusion after the solidification of the sodium can be neglected. It may be that the concen-

trations of the nuclides in the sodium (at one or two points) are influenced by the possible presence of microparticles that adsorb the impurities strongly. There may also be a slight effect on the impurity distribution from hydrodyanmic process at the time of filling.

Therefore, to obtain reliable information on the impurity distribution over the volume of the sodium cooled in the vessel, it is necessary to measure the entire sample mass.

GEOMETRIC PARAMETER OF REGULAR POLYGONAL PRISMS

I. É. Isakas, V. V. Kuz'minov, Yu. V. Petrov,
É. G. Sakhnovskii, and V. A. Shustov

UDC 621.039.51

The exact values of the geometric parameter for homogeneous critical reactors without reflectors (i.e., the exact values of the leading eigenvalue of the Dirichlet problem for Helmholtz's equation) are known only for the simplest geometries [1, 2]. A knowledge of the exact solutions permits estimating the error of approximate methods used in solving problems with a complicated boundary geometry. Most often, the Wigner–Seitz approximation is used, in which the real lateral boundary is modeled by the surface of a circular cylinder with an equivalent volume. This approximation was chosen in [3, 4] as the zeroth-order approximation for perturbation theory for the form of a cylindrical reactor. The following theorem is also proved therein: the first-order correction to the radial geometric parameter in the zeroth-order approximation, linear with respect to the deviation of the boundary of the cylinder cross section from a circle and the derivative with respect to this deviation, equals zero. The second-order correction can be found by Rayleigh's method [5], representing the equation of the directrix of the cylinder, as in [3, 4], as a Fourier series expansion. Then, for regular polygonal prisms with a number of lateral faces $k \geqslant 3$, the following equation can be used for the ratio of the radial geometric parameter B^2 to the radial geometric parameter B_0^2 in the zeroth approximation:

$$\frac{B^2}{B_0^2}=\zeta\left\{1+16\gamma^2\sum_{m=1}^{\infty}\left[\frac{\nu_{01}J'_{km}(\nu_{01})}{J_{km}(\nu_{01})}-1\right](m^2k^2-4)^{-2}\right\},$$

where $\zeta=\frac{k}{2(1-\gamma)\pi}\operatorname{tg}\frac{\pi}{2k}$; $\gamma=\frac{k}{2\pi}\sin\frac{2\pi}{k}\Big/\left(1+\frac{k}{2\pi}\sin\frac{2\pi}{k}\right)$; ν_{01} is the first root of the Bessel function $J_0(x)$. The results of calculations using this equation for k = 3-8, presented in the second column of Table 1, can be compared with numerical calculations.

It is convenient to find a more accurate numerical value of the geometric parameter using the method of finite elements [6]. In these calculations, we used triangular finite elements with **polynomial** trial functions of first, second, and third degree [7]. We found the error in the computed value of B_h^2 using the equation for the convergence of the approximate solution to the exact value of B^2: $|B^2 - B_h^2| \leqslant ch^k$, where h is the grid spacing; c is a constant; and k is determined by the degree of the finite-element polynomial. To compare the numerical methods, we calculated the geometric parameter of regular triangular and hexagonal prisms using the HEXA program as well [8], with whose help Helmholtz's equation is solved by

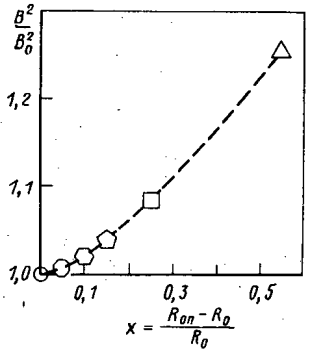

Fig. 1. Geometric parameters of regular polygonal prisms.

Translated from Atomnaya Énergiya, Vol. 54, No. 5, pp. 371-372, May, 1983. Original article submitted September 21, 1982.

 0038-531X/83/5405-0380$07.50

TABLE 1. Estimate of the Geometric Parameter of Regular Polygonal Prisms

No. of faces	B^2/B_0^2		
	second approx. of perturbation theory	method of finite elements	error in the 2nd-order approx. of perturbation theory, %
3	1,2583 (1)	1,2545323 (4) *	0,31
4	1,0913 (1)	1,08645738 (4) †	0,45
5	1,0442 (1)	1,041318 (1)	0,28
6	1,0249 (1)	1,023211 (4) ‡	0,17
7	1,0154 (1)	1,014398 (1)	0,10
8	1,0102 (1)	1,00956 (1) **	0,06

*Value calculated using the HEXA program, $B^2/B_0^2 = 1.2544$ (1).

†Exact value $B^2/B_0^2 = 2\pi/\nu_{01}$, where $\nu_{01} = 2.404825558$ (see [9]).

‡Value calculated using the HEXA program, $B^2/B_0^2 = 1.0232$ (1). The value used previously in [3, 4], $B^2/B_0^2 = 1.026$, calculated in [10] using Ritz's method, is not accurate enough.

** In [11], for an octagonal prism, $B^2/B_0^2 = 1.009$.

a finite difference method in a hexagonal geometry. The results of numerical calculations using the finite element method are presented in the third column of Table 1 (the error of the calculation — the error in the last digit of the number presented — is indicated in parentheses).

As is evident from Table 1, even for the largest deviation from a circle with an equivalent area (regular triangle), the error of the Wigner–Seitz approximation is not larger than 25%, while the second-order perturbation theory decreases the maximum error of 0.45%. Figure 1 shows the dependence of B^2/B_0^2 for polygonal prisms on the parameter $x = (R_{os} - R_o)/R_o$ (R_{os} is the radius of the circumscribed circle), characterizing the maximum deviation of the cross-section of the prism from an equivalent-area circle with radius R_o.

After writing this paper, we learned about [12], wherein the value of the geometrical parameter for regular polygons with a number of edges k = 3-20 was obtained by a numerical-analytical method by replacing the continuous boundary of the region by a discrete approximation. The results agree with the calculation using the finite element method within the limits of error in rounding off the sixth digit.

We thank L. M. Kotov for help in the calculations.

LITERATURE CITED

1. H. Sudék, in: Nuclear Reactors, Physics of Nuclear Reactors [Russian translation], Vol. 1, IL, Moscow (1956), p. 179.
2. V. N. Babich et al., Linear Equations of Mathematical Physics [in Russian], Nauka, Moscow (1964).
3. Yu. V. Petrov and É. G. Sakhnovskii, At. Energ., 49, No. 2, 127 (1980).
4. Yu. V. Petrov and É. G. Sakhnovskii, Problems in Nuclear Power and Engineering. Series in Physics and Engineering of Nuclear Reactors [in Russian], No. 5(18) (1981), p. 54.
5. B. Rayleigh, The Theory of Sound, Vol. 2, Peter Smith.
6. W. G. Strang and G. J. Fix. An Analysis of the Finite Element Method, Prentice-Hall (1973).
7. V. V. Kuz'minov and I. S. Slesarev, Preprint IAÉ-3450/5, Moscow (1981).
8. I. É. Isakas and V. A. Shustov, Preprint LIYaF-490, Leningrad (1979).
9. Handbook on Special Functions [in Russian], Nauka, Moscow (1979), p. 227.
10. G. N. Plindov, in: Physics of Nuclear Reactors [in Russian], Vol. 1, Izd. ONTI FÉI, Obninsk (1966), p. 374.

11. Reactor Physics Constants, ANL-5800 (1963), p. 542.
12. R. Murray et al., J. Nucl. Sci. Eng., 34, 86 (1968).

A TECHNIQUE OF MEASURING NEUTRON SPECTRA OF POWERFUL SOURCES

G. V. Anikin and I. I. Kotukhov

UDC 539.125.5.164

Measuring the neutron spectra of a powerful source, e.g., of a reactor, is not a simple experimental problem. Such measurements are usually made with the aid of scintillation detectors with γ suppression [1] and at a small power rate of the reactor so that neutron spectra at energies $E_n \geqslant 0.5$ MeV can be determined. When the spectrum must be determined during the time of reactor operation at a high power rate, the neutron flux and the γ radiation must be preliminarily attenuated in the beam under inspection which exists through a channel in the reactor shield. Two techniques of attenuating the flux have been suggested in, e.g., [2]: initially passing the beam through filters of materials with a known total neutron interaction cross section, and scattering the beam with some (e.g., iron) object and thereafter measuring the spectrum of the scattered neutrons under an angle of about 90° relative to the initial beam. Since the attenuating filters must be rather thick ($\sim$10-30 cm), the first technique makes it necessary to know the total neutron cross sections σ_{tot} with high accuracy, which is not always possible. Furthermore, multiple neutron scattering in the filter must be brought into account. Information on the angular distributions of the elastically and inelastically scattered neutrons could be used in the second technique, yet such information is very limited, and the authors of [2] have suggested to simply calibrate the detector through preliminary measurements of a known spectrum differing only slightly from one energy to another by inelastic scattering can be properly assessed only under the above conditions.

In order to avoid the above difficulties, the authors of the present work have proposed a technique of determining the neutron spectrum of a powerful source by scattering neutrons at a sample with a large Z under very small ($\sim$1-3°) angles. In the angular interval below 3°, the scattering cross section increases sharply and has the angular dependence

$$\sigma(\theta) = \gamma^2 \operatorname{ctg}^2 \theta/2,$$

which results from the electromagnetic interaction of the neutrons with nuclei and had been predicted by Schwinger as early as in 1948 [3]. In this formula the constant γ is proportional to the charge Z of the nucleus and does not depend upon the neutron energy. The above angular dependence was experimentally confirmed in, e.g., [4].

The detector count varies from one energy group to another, e.g., in the transition from the scattering angle 3° to the angle 1°, and is in this transition proportional to the neutron flux in the same energy group of the source spectrum (reactor beam) and to the change in the Schwinger scattering cross section $\Delta\delta_{Schw}$. All other scattering effects, such as elastic and inelastic scattering by the short-range nuclear potential and multiple scattering, hardly change when the angle is changed only very slightly. Since $\Delta\delta_{Schw}$ is a quantity known from the theory, the relative number of neutrons in the energy groups of the initial spectrum

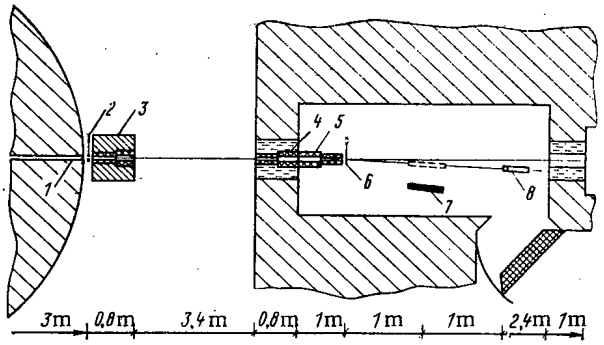

Fig. 1. Scheme of the experiment: 1) channel in the reactor shield; 2) equivalent attenuator of the direct flux; 3) additional shield; 4) collimator in the wall of the measuring box; 5) additional collimator in the box; 6) scatterer; 7) cone for background measurements; 8) scinillation detector.

Translated from Atomnaya Énergiya, Vol. 54, No. 5, pp. 372-374, May, 1983. Original article submitted October 21, 1982.

 0038-531X/83/5405-0382$07.50

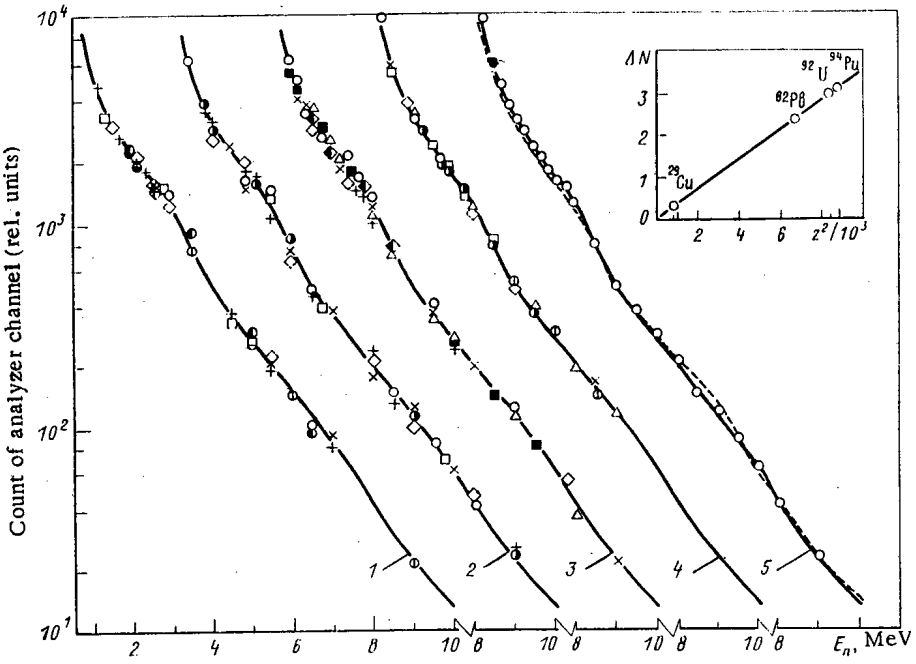

Fig. 2. Comparison of the difference spectra of various scatterers with the reactor spectrum: 1) ^{92}Cu scattered; 2) ^{82}Pb scatterer; 3) ^{92}U scatterer; 4) ^{94}Pu scatterer; 5) averaged difference spectrum for the four elements (the insert displays the Z^2 dependence of the integrals of the difference spectra normalized to the atomic number of the sample).

can be easily obtained from the energy dependence of the difference in the scintillation detector counts at a certain two scattering angles. This technique has an additional advantage insofar as the Schwinger scattering is the same for all neutron energies. This conclusion, which was obtained in the Born approximation, to date has not been experimentally confirmed, but, if the conclusion is correct, the determination of the source spectrum will be greatly simplified: the difference between the spectra measured under different angles (e.g., 1.5° and 3°) must have the same shape as the source spectrum. The results of our measurements confirm these conclusions. We found it necessary to introduce small corrections for the difference in the scattering under the angles 1.5° and 3° by a purely nuclear potential; the difference was assessed with the optical model of the nucleus.

Measurement Procedure. The energy dependence of the Schwinger scattering was studied on the fast neutron beam of the BR-10 reactor (Fig. 1). The total flight path of the neutrons from the surface of the reactor core through the channels in the reactor shield, in the additional shield, and in the wall of a special measuring box to the scattering sample was about 9 m. The intrinsic divergence of the primary beam did not exceed 10' and a total angular resolution of the setup amounted to ∿20' when the dimensions of the stilbene crystal were brought into account (half-width on half the maximum height of the angular resolution curve).

We measured the spectra of the scattered neutrons for each of the scattering samples (plutonium, uranium, lead, and copper) at detector positions corresponding to the angles 1.5 and 3° relative to the primary beam. Each spectrum was obtained as the difference of two measurements: with the particular sample in the beam, and with a sample of equivalent thickness in the beam and the particular working sample outside the beam. The isotropic background of the site, the background produced by the exit of the last collimator, and the background produced in the air in the direct beam close to the crystal were properly subtracted. The bakcground produced by the sample proper and reflected by the box walls toward the stilbene crystal was disregarded. Additional measurements were made with samples and shielding cones inserted between the crystal and a particular sample to assess the latter type of background. The spectrum of this background is very "soft." In the energy interval 1-1.5 MeV the contribution of this background to the total detector count was about 25%. This background was measured for the angle 3°. The same background level was assumed for the angle 1.5°.

No particular measures for stabilizing the photomultiplier gain were taken. The closed concrete box served as a natural thermostat which provided for adequate stability of the detector operation during a series of experiments. The linearity of both the spectrometer scale and the circuits of neutron and γ radiation splitting was checked by measuring the well-known spectrum of the neutrons from the spontaneous fission from ^{252}Cf in angular measurements between the series.

Results of the Measurements. Figure 2 shows the difference of the experimental spectra measured at the scattering angles 1.5 and 3°. The spectra has been obtained with the four elements as scatterers. The difference spectra (the various points refer to individual series of measurements) were normalized to the integral reactor spectrum, which we measured in the direct beam at low power rates. The solid curves of Fig. 2 depict the shape of the reactor spectrum.

Curve 5 illustrates good agreement (to within 3-5%) of the difference spectrum averaged over the four scatterers with the reactor spectrum. The dashed line refers to a preceding measurement of the BR-10 spectrum by L. A. Trykov et al. [5].

Possible Normalization of the Neutron Cross Sections. Since the Schwinger cross section is known from the theory (the constant γ in the above formula is proportional to the nuclear charge Z and amounts to $1.347 \cdot 10^{-14}$ cm for uranium), the integral of the difference spectrum can be compared with a certain magnitude of the neutron flux, and the ratio of the integral difference spectrum and the indicated integral of the spectrum of neutrons scattered under, e.g., 3° allows the determination not only of the energy dependence, but also of the absolute value of the scattering cross section at the particular angle and for the corresponding element.

The insert of Fig. 2 illustrates the dependence of the integrals of the difference spectra for the four elements in accordance with the formula indicated above, the dependence being quadratic in Z. The absolute values of the scattering cross section (and also of the cross section of other reactions) for elements with small Z can be obtained after normalizing the neutron flux with the aid of the Schwinger scattering by a sample of a heavy element.

This technique of cross-section normalization is advantageous insofar as the experimenter need not place the detector in the direct neutron beam for determining the beam intensity, in which case the influence of both the spectrometer load characteristic and the dependence upon the angles under which the neutrons intersect the detector crystal in the direct and the scattered flux must be taken into consideration.

We may assume at the present time that we confirmed that the experimentally observed bump of the cross section at small scattering angles (as predicted by Schwinger) agrees with the calculation made with the above formula or with the optical model including an addition to the potential of the neutron-nuclear interaction. This correspondence exists in regard to the absolute value with an accuracy of 5-10% [5]. The accuracy of the cross sections normalized to the Schwinger scattering cannot be better. However, when special measurements of the Schwinger scattering are made at low neutron energies ($\lesssim 0.5$ MeV), where the angular dependence according to the above formula can be easily separated from the background of the hardly changing "purely nuclear" scattering, the accuracy in the determination of $\delta_{Schw}(\theta)$ can be substantially increased.

In conclusion, the authors thank G. N. Smirenkin and L. A. Trykov for discussing several problems related particularly to the spectrometry of fast neutrons, N. E. Fedorova for help in the initial evaluation of the experimental data, and V. M. Kupriyanov for helping in the compilation of the computer programs.

LITERATURE CITED

1. Ya. A. Egorov, The Scintillation Technique in the Spectrometry of Gamma Radiation and Fast Neutrons [in Russian], Gosatomizdat, Moscow (1963).
2. V. I. Kukhtevich, L. A. Trykov, and O. A. Trykov, A Single-Crystal Scintillation Spectrometer [in Russian], Atomizdat, Moscow (1971).
3. J. Schwinger, Phys. Rev., 73, No. 4, 407 (1948).
4. Yu. A. Aleksandrov, in: Nuclear Reactions at Low and Medium Energies [in Russian], Izd. Akad. Nauk SSSR, Moscow (1958), p. 206.
5. L. A. Trykov, V. P. Semenov, and A. N. Nikolaev, At. Energ., 39, No. 1, 56 (1975).

THE SOLUBILITY OF OXYGEN IN SODIUM

F. A. Kozlov and P. S. Kozub

UDC 621.039.534

Oxygen is one of the chief impurities present in a coolant. There are abundant data on the solubility of oxygen in sodium [1-12], but they differ substantially, for the following most-probable reasons: first, errors in the experimental method which lead to further contamination of the sodium in the process of analysis of the samples, or to an incorrect determination of the saturation temperature; second, the influence of other impurities — e.g., hydrogen — on the solubility of the oxygen in the sodium. In the present study we took special precautions to exclude these errors in the experimental determination of the solubility of the oxygen.

The tests were carried out on a test stand with circulating sodium. The oxygen concentration was determined by means of a universal sampler-distiller [13], usually on four parallel samples.

After determining the saturation temperature t_s by means of a plug indicator, we measured the clogging temperature t_c and the washout temperature t_w. At t_c the flow through the plug indicator begins to decrease as a result of the formation and growth of a plug as the sodium flowing through the openings of the disk cools, and at t_w the flow begins to increase as a result of the dissolution of the plug as the sodium temperature rises.

We placed two cold traps on the stand; one was used for cleansing the sodium of the oxygen (the oxygen concentration in the purified coolant did not exceed 0.1 ppm), and the other was used to purify sodium that had been contaminated with hydrogen.

The oxygen concentration C_O in the sodium was given both by the amount dosed into the loop and by the amount washed out, from a cold trap contaminated with oxygen. The oxygen concentration in the sodium did not exceed 0.1 ppm in any of the tests.

The test results are shown in Table 1. Processing of these data by the method of least squares yields the relation

$$\lg C_O \text{ (ppm)} = 6.02 - 2320/T, \tag{1}$$

where t_s is taken to be equal to the temperature at which we fixed the beginning of the elution of the plug in the openings of the plug indicator. The choice of this as the determining temperature was made on the basis of an analysis which showed that the following relation holds:

$$\frac{\Delta t_c}{\Delta t_w} = \frac{t_s - t_c}{t_w - t_s} = \sqrt{\left(\frac{d_{0c}}{d_{0w}}\right)^{1.125} \frac{\psi_c}{\psi_w} \frac{1 - \left[1 - \frac{1}{2}\left(1 - \sqrt{\left(\frac{\xi_2}{\xi_1}\right)_c a}\right)\right]^{1/1.78}}{1 + \frac{1}{2}\left[\sqrt{\left(\frac{\xi_2}{\xi_1}\right)_w \frac{1}{a}} - 1\right]^{1/1.78}}} > 1, \tag{2}$$

TABLE 1. Solubility of Oxygen in Sodium

$t_s = t_w$ °C	$\Delta t = t_w - t_c$, °C	C_O, ppm
185	55	9
213	37	15,3
218	32	20,6
247	22	31
255	15	36,1
260	15	51
270	5—7	59,3
288	14	70,5
282	13	71,4
281	17	74

Translated from Atomnaya Énergiya, Vol. 54, No. 5, pp. 374-375, May, 1983. Original article submitted October 21, 1982.

0038-531X/83/5405-0385$07.50

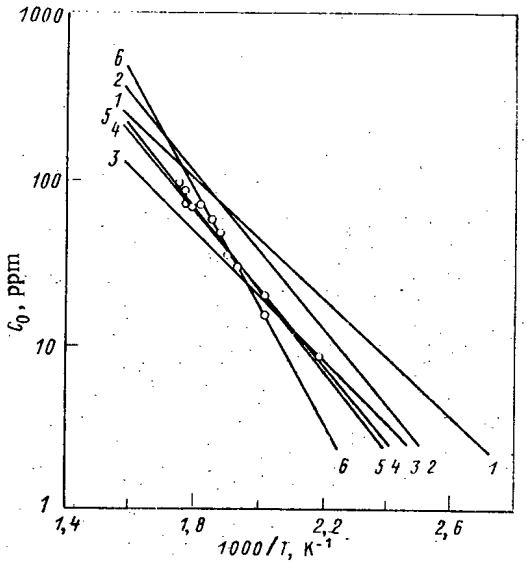

Fig. 1. Solubility of oxygen in sodium: 1) Claxton [2]; 2) Ilinchev [2]; 3) our data from 1060 [4]; 4) the present study (○); 5) Noden [1]; 6) Rutkauskas [12].

where d_0 is the initial dimension of the disk openings; $\varphi > 1$, coefficient for taking account of the hydrodynamic resistance of the plug indicator outside of the opening (heat exchanger, etc.); a, coefficient characterizing the variation of the flow rate through the plug indicator at which we fixed t_c (t_w); and ξ_2, ξ_1, resistance coefficient of the disk of the plug indicator at the beginning of the test and at the moment when we determined t_c (t_s). Since in our tests with the plug indicator all three of the factors in Eq. (2) are greater than unity, it follows from this expression that although the temperature measured at the time when the plug is washed out is greater than t_s, it is closer to t_s than is the temperature measured at the time of formation of the plug in the openings.

A comparison of the results (see Fig. 1) shows that our data agree with the equation obtained by a critical generalization of practically all the previously available information [1], which indictes the realibility of the experiments conducted in this study.

LITERATURE CITED

1. J. Noden, J. Brit. Nucl. Eng. Soc., 12, No. 3, 329 (1973).
2. G. Ilinchev, in: Proceedings of the CMEA Symposium "Status and Prospects of Work on the Construction of Atomic Power Stations with Fast Reactors" [in Russian], Vol. 2, Izd. FÉI, Obninsk (1973), p. 223.
3. K. Claxton, Preprint AERE-R 4897, Harwell (1965).
4. I. B. Dmitrieva, F. A. Kozlov, and É. K. Kuznetsov, in: Liquid Metals [in Russian], Atomizdat, Moscow (1967), p. 319.
5. J. Gray, K. Neal, and B. Voorhees, Nucleonics, 14, No. 10, 34 (1956).
6. Z. S. Bannykh and I. F. Fefelova, in: Proceedings of the Ural Chemical Institute [in Russian], No. 5, Goskhimizdat, Leningrad (1957), p. 110.
7. J. Allen, Nucl. Eng., 7, No. 76, 352 (1962).
8. R. Hinze, ibid., 5, No. 48, 225 (1960).
9. T. Trocky, W. Bruggeman, and F. Gever, in: Proceedings of the Geneva Conference. Selected Reports of Non-Soviet Scientists, Vol. 9: Reactor Technology and Chemical Processing [in Russian], Goskhimizdat, Leningrad (1958), p. 297.
10. A. McIntosh and K. Bagley, J. Brit. Nucl. Energy Conf., 4, No. 35, 59 (1958).
11. J. Evans, Nucl. Eng., 4, No. 35, 59 (1959).
12. V. Rutkauskas, in: Int. Symp. on the Alkali Metals, Nottingham, July, 1966.
13. F. A. Kozlov et al., Inventor's Certificate No. 355534, Byull. Izobret., No. 31, 151 (1972).

MEASUREMENTS OF ^{90}Sr IN A SODIUM COOLANT

P. S. Otstavnov and L. A. Stabenova

UDC 621.039.526:539.124

The radionuclide ^{90}Sr belongs to the group of biologically most dangerous and most hard-to-detect nuclides which are formed in the process of operation of nuclear reactors. Therefore, the extensive experimental information on fission products in nuclear reactors contains very little information on strontium. The half-life of ^{90}Sr is about 28 yrs; upon decaying, it emits β-particles with an energy of 0.55 MeV. In media ^{90}Sr is usually accompanied by its daughter nuclide ^{90}Y, with a half-life of 60.5 h and a β-particle energy of 2.27 MeV. Thanks to the higher energy of the β-particles emitted by ^{90}Y during its transition into ^{90}Zr, it is possible to measure the strontium content of investigated naterials on the basis of the yttrium in equilibrium with ^{90}Sr. Since the mean free paths of the β-particles emitted by ^{90}Sr and ^{90}Y in a substance are short and their energy spectrum is continuous, it is very difficult to measure these nuclides in investigated substances, especially in the case of substances which are themselves radioactive.

In the usual method of determining the strontium content in the sodium coolant of the first loop of a reactor, chemical methods are used to separate the ^{90}Sr from the extracted sample of sodium; the strontium is applied as an aliquot to a backing and subjected to radiometric analysis. This method has the following important shortcomings:

in the process of the chemical operations for the preparation of an aliquot there may be losses of the investigated nuclides both with the gaseous products and with the precipitants. As a result, the aliquot is depleted in the nuclide under investigation;

as was shown by the investigations in [1], the strontium concentration per volume of the extracted sample of sodium coolant cooled under the natural conditions of the sampler may differ by almost two orders of magnitude; much of the strontium is on the inner walls of the cup in which the sample was extracted;

the amount of ^{90}Sr is usually determined by measuring the ^{90}Y content of the aliquot, since it is assumed that the ^{90}Y, which has a relatively short half-life, will always be in radioactive equilibrium with the ^{90}Sr. Yttrium and strontium belong to different groups of the periodic system of the elements and have different chemical properties. If in the process of separating the strontium during the preparation of the aliquot the yttrium was removed and the concentration of strontium was determined on the basis of the yttrium shortly after the aliquot was prepared, the results extrapolated to strontium may be much too low.

In order to obtain reliable results, it is desirable to determine the ^{90}Sr content directly in the extracted sample of sodium coolant, including the wall layer. In the present study the ^{90}Sr content was measured directly in the sample of sodium coolant taken in a metal cup in the sampling apparatus. The principle of determination of the strontium concentration is described in [2]. The ^{90}Sr concentration was determined with a β-spectrometer. The spectrometer was calibrated on the basis of the hard components of the β-radiation of the nuclides ^{106}Rh (3.54 MeV), ^{144}Pr (2.99 MeV), ^{90}Y (2.27 MeV), and ^{91}Y (1.54 MeV) of known intensity. For each energy range we found the recording coefficient $K = A_0/A$, where A_0 and A are the intensity of the nuclide measured with a 4π counter and with a beta spectrometer in the energy range under consideration. We took into account the relative contribution of the other elements in the region of the spectrum determining the ^{90}Y.

Since the medium investigated contains several nuclides, e.g., ^{106}Ru–^{106}Rh, ^{144}Ce–^{144}Pr, and ^{90}Sr–^{90}Y, we first determine the intensity of the harder component of energy and subtract it from the apparatus spectrum, then determine the intensity of the next-hardest component and again subtract it from the remaining portion of the spectrum, etc. The problem is made easier by the fact that usually the qualitative composition of the radionuclides in the coolant sample is known: the radionuclides formed during the operation of an atomic power station have been studied fairly thoroughly, both theoretically and experimentally, and their char-

Translated from Atomnaya Énergiya, Vol. 54, No. 5, pp. 375-376, May, 1983. Original article submitted November 22, 1982.

0038-531X/83/5405-0387$07.50

TABLE 1. Activity of Nuclides in Coolant Samples, Bq

Nuclide	Method of the present study	Radiochemical method	Gamma spectrometry
^{22}Na	$21,8 \cdot 10^3$	$22,2 \cdot 10^3$	—
^{137}Cs	$8,3 \cdot 10^4$	—	$7,7 \cdot 10^4$
^{90}Sr	44	<4	—

acteristics are given in the reference literature. The effect of γ-emitting nuclides (^{137}Cs, ^{22}Na) is excluded on the β-spectrometer by the discrimination threshold. For reliable measurements of the ^{90}Sr, the activity of the nuclides with radiation harder than that of ^{90}Y must be comparable to or less than the activity of the ^{90}Sr. Experience has shown that this condition is always satisfied in practice.

The method of this study was used for investigating samples of sodium coolant taken from the first loop of a reactor and specimens of the installation walls. In the investigation of "thick" layers of sodium, we introduced a correction for self-absorption. The total error of the measurement was ±25%.

The results of measurements of the ^{22}Na and ^{137}Cs values in the investigated samples by the method of this study and by other methods (chemical and γ spectrometric) are in good agreement within the limits of error of the measurement (see Table 1). The results for ^{90}Sr diverge widely. As an analysis of the reasons for this divergence showed, almost all the strontium was on the walls of the investigated segment and practically no strontium was present in the prepared aliquot.

LITERATURE CITED

1. P. S. Otstavnov et al., 54, No. 5, 370 (1983).
2. V. V. Ovechkin and I. A. Pirkin, in: Collection of Studies on Some Problems of Dosimetry and Radiometry of Ionizing Radiation [in Russian], No. II, Gosatomizdat, Moscow (1961), p. 44.

MEASUREMENT TECHNIQUES
Izmeritel'naya Tekhnika
Vol. 25, 1982 (12 issues) $400

MECHANICS OF COMPOSITE MATERIALS
Mekhanika Kompozitnykh Materialov
Vol. 18, 1982 (6 issues) $330

METAL SCIENCE AND HEAT TREATMENT
Metallovedenie i Termicheskaya Obrabotka Metallov
Vol. 24, 1982 (12 issues) $420

METALLURGIST
Metallurg
Vol. 26, 1982 (12 issues) $435

PROBLEMS OF INFORMATION TRANSMISSION
Problemy Peredachi Informatsii
Vol. 18, 1982 (4 issues) $320

PROGRAMMING AND COMPUTER SOFTWARE
Programmirovanie
Vol. 8, 1982 (6 issues) $135

PROTECTION OF METALS
Zashchita Metallov
Vol. 18, 1982 (6 issues) $380

RADIOPHYSICS AND QUANTUM ELECTRONICS
Izvestiya Vysshikh Uchebnykh Zavedenii, Radiofizika
Vol. 25, 1982 (12 issues) $400

REFRACTORIES
Ogneupory
Vol. 23, 1982 (12 issues) $380

SIBERIAN MATHEMATICAL JOURNAL
Sibirskii Matematicheskii Zhurnal
Vol. 23, 1982 (6 issues) $495

SOIL MECHANICS AND FOUNDATION ENGINEERING
Osnovaniya, Fundamenty i Mekhanika Gruntov
Vol. 19, 1982 (6 issues) $380

SOLAR SYSTEM RESEARCH
Astronomicheskii Vestnik
Vol. 16, 1982 (4 issues) $275

SOVIET APPLIED MECHANICS
Prikladnaya Mekhanika
Vol. 18, 1982 (12 issues) $400

SOVIET ATOMIC ENERGY
Atomnaya Energiya
Vols. 52–53 (12 issues) $440

SOVIET JOURNAL OF GLASS PHYSICS AND CHEMISTRY
Fizika i Khimiya Stekla
Vol. 8, 1982 (6 issues) $175

SOVIET JOURNAL OF NONDESTRUCTIVE TESTING
Defektoskopiya
Vol. 18, 1982 (12 issues) $485

SOVIET MATERIALS SCIENCE
Fiziko-khimicheskaya Mekhanika Materialov
Vol. 18, 1982 (6 issues) $345

SOVIET MICROELECTRONICS
Mikroelektronika
Vol. 11, 1982 (6 issues) $195

SOVIET MINING SCIENCE
Fiziko-tekhnicheskie Problemy Razrabotki Poleznykh Iskopaemykh
Vol. 18, 1982 (6 issues) $420

SOVIET PHYSICS JOURNAL
Izvestiya Vysshikh Uchebnykh Zavedenii, Fizika
Vol. 25, 1982 (12 issues) $400

SOVIET POWDER METALLURGY AND METAL CERAMICS
Poroshkovaya Metallurgiya
Vol. 21, 1982 (12 issues) $435

STRENGTH OF MATERIALS
Problemy Prochnosti
Vol. 14, 1982 (12 issues) $495

THEORETICAL AND MATHEMATICAL PHYSICS
Teoreticheskaya i Matematicheskaya Fizika
Vols. 50–53, 1982 (12 issues) $380

UKRAINIAN MATHEMATICAL JOURNAL
Ukrainskii Matematicheskii Zhurnal
Vol. 34, 1982 (6 issues) $380

Send for Your Free Examination Copy

Plenum Publishing Corporation, 233 Spring St., New York, N.Y. 10013
In United Kingdom: 88/90 Middlesex St., London E1 7EZ, England

Prices slightly higher outside the U.S. Prices subject to change without notice.

RUSSIAN JOURNALS IN THE PHYSICAL AND MATHEMATICAL SCIENCES

AVAILABLE IN ENGLISH TRANSLATION

ALGEBRA AND LOGIC
Algebra i Logika
Vol. 21, 1982 (6 issues) $270

ASTROPHYSICS
Astrofizika
Vol. 18, 1982 (4 issues) $320

AUTOMATION AND REMOTE CONTROL
Avtomatika i Telemekhanika
Vol. 43, 1982 (24 issues) issues) $495

COMBUSTION, EXPLOSION, AND SHOCK WAVES
Fizika Goreniya i Vzryva
Vol. 18, 1982 (6 issues) $345

COSMIC RESEARCH
Kosmicheskie Issledovaniya
Vol. 20, 1982 (6 issues) $425

CYBERNETICS
Kibernetika
Vol. 18, 1982 (6 issues) $345

DIFFERENTIAL EQUATIONS
Differentsial'nye Uravneniya
Vol. 18, 1982 (12 issues) $395

DOKLADY BIOPHYSICS
Doklady Akademii Nauk SSSR
Vols. 262–267, 1982 (2 issues) $145

FLUID DYNAMICS
Izvestiya Akademii Nauk SSSR, Mekhanika Zhidkosti i Gaza
Vol. 17, 1982 (6 issues) $380

FUNCTIONAL ANALYSIS AND ITS APPLICATIONS
Funktsional'nyi Analiz i Ego Prilozheniya
Vol. 16, 1982 (4 issues) $320

GLASS AND CERAMICS
Steklo i Keramika
Vol. 39, 1982 (6 issues) $460

HIGH TEMPERATURE
Teplofizika Vysokikh Temperatur
Vol. 20, 1982 (6 issues) $400

HYDROTECHNICAL CONSTRUCTION
Gidrotekhnicheskoe Stroitel'stvo
Vol. 16, 1982 (12 issues) $305

INDUSTRIAL LABORATORY
Zavodskaya Laboratoriya
Vol. 48, 1982 (12 issues) $400

INSTRUMENTS AND EXPERIMENTAL TECHNIQUES
Pribory i Tekhnika Eksperimenta
Vol. 25, 1982 (12 issues) $460

JOURNAL OF APPLIED MECHANICS AND TECHNICAL PHYSICS
Zhurnal Prikladnoi Mekhaniki i Tekhnicheskoi Fiziki
Vol. 23, 1982 (6 issues) $420

JOURNAL OF APPLIED SPECTROSCOPY
Zhurnal Prikladnoi Spektroskopii
Vols. 36–37 (12 issues) $420

JOURNAL OF ENGINEERING PHYSICS
Inzhenerno-fizicheskii Zhurnal
Vols. 42–43, 1982 (12 issues) $420

JOURNAL OF SOVIET LASER RESEARCH
A translation of articles based on the best Soviet research in the field of lasers
Vol. 3, 1982 (4 issues) $95

JOURNAL OF SOVIET MATHEMATICS
A translation of Itogi Nauki i Tekhniki and *Zapiski Nauchnykh Seminarov Leningradskogo Otdeleniya Matematicheskogo Instituta im. V. A. Steklova AN SSSR*
Vols. 18–20, 1982 (18 issues) $680

LITHOLOGY AND MINERAL RESOURCES
Litologiya i Poleznye Iskopaemye
Vol. 17, 1982 (6 issues) $420

LITHUANIAN MATHEMATICAL JOURNAL
Litovskii Matematicheskii Sbornik
Vol. 22, 1982 (4 issues) $205

MAGNETOHYDRODYNAMICS
Magnitnaya Gidrodinamika
Vol. 18, 1982 (4 issues) $325

MATHEMATICAL NOTES
Matematicheskie Zametki
Vols. 31–32, 1982 (12 issues) $400

continued on inside back cover

Declassified and Approved For Release 2013/02/06 : CIA-RDP10-02196R000300020005-5